AN ITERATIVE INVERSION METHOD FOR TRANSMISSION LINE FAULT LOCATION

by

Shang Chieh Wu

A dissertation submitted to the faculty of
The University of Utah
in partial fulfillment of the requirements for the degree of

Doctor of Philosophy

Department of Electrical and Computer Engineering

The University of Utah

August 2011

The University of Utah Graduate School

STATEMENT OF DISSERTATION APPROVAL

The dissertation of **Shang Chieh Wu**

has been approved by the following supervisory committee members:

Cynthia Furse	, Chair	**05/16/2011** Date Approved
Rong-Rong Chen	, Member	**05/16/2011** Date Approved
Faisal Khan	, Member	**05/16/2011** Date Approved
Neal Patwari	, Member	**05/16/2011** Date Approved
Wayne Springer	, Member	**05/16/2011** Date Approved

and by **Gianluca Lazzi** , Chair of

the Department of **Electrical and Computer Engineering**

and by Charles A. Wight, Dean of The Graduate School.

ABSTRACT

This dissertation discusses various transmission line forward modeling techniques in both time and frequency domains. Although time domain methods offer simplicity in most cases, the computational inefficiency and lack of fidelity make these methods less attractive. Therefore, the more efficient frequency domain technique is emphasized - a modified transmission matrix (also known as ABCD) method.

One of the most difficult problems in electrical wire fault location nowadays is detecting and locating frayed wiring, where the wire is only partially damaged. This type of fault can be very small and extremely difficult to detect. Most inversion schemes used to locate faults require forward models that accurately represent detailed reflections. Resolving these very small faults requires an especially accurate forward model where not only the fault but also all the other very small changes caused by normal aspects of the wiring system are included.

A very high resolution Finite Difference Time Domain (FDTD) method can be used to simulate this type of fault and details of the surrounding wiring system with enough fidelity to distinguish the small fault. However, this is very costly in terms of computational resources. This dissertation demonstrates a quick way of building the fray profile that significantly reduces the simulation time.

Finally, the ultimate goal of the highly realistic forward modeling is the inversion, in which a set of measured data is given and the inversion algorithm interprets the

location and the nature of fault on the wire. Multiple iterations are typically required, and thus, high efficiency is necessary. A new method introduced in this dissertation is capable of identifying multiple unknown parameters in just a few steps.

TABLE OF CONTENTS

CHAPTER 1

INTRODUCTION

1.1 Background

Electrical wires are to instruments and equipment as the nerves and veins are to human body. Signals, commands and power are delivered to their destinations via these wires. In critical applications, such as spacecraft or aircraft, faulty wires can cause total loss of investment, catastrophic damage to the equipment, injuries and loss of human lives. Many of these tragedies could be preventable if we understand what the wiring system is telling us. The system constantly signals us where the problems are, but not in ordinary human language. In the past, these messages have been overlooked, since it is too costly either in time or money or simply just too difficult to understand, until the catastrophe happens.

Studies indicate that the crashes of both TWA 800 off New York's Long Island in 1996 and Swissair 111 near Nova Scotia in 1998 were strongly correlated to the faulty wiring systems onboard [1]. With an average age of more than 22 years [2], the United States Air Force fleet is suffering from readiness problems. Many of the aircraft and spacecraft have served well beyond the age they were designed for, which is typically 15 to 20 years. The virtually invisible wire faults make these aged work horses prone to disasters. Although wire faults are found more frequently in aging aircraft, newer

designs are not immune to wiring problems. Airbus's flagship A380, for example, had to delay its delivery schedule due to wiring problems [3] and the price tag for that incidence was six billion dollars [4]. Fortunately the problem was discovered before hitting the market. In May of 1986, a NASA Delta 3925 rocket booster carrying a GOES (Geostationary Operational Environmental Satellite) weather satellite failed due to a momentary short caused by a chafed wire. An Air Force Titan 4B broke up when a short circuit occurred, and 13 years earlier, the failure of another Delta was also due to a chafed wire that caused short circuits [5]. Numerous incidents like these have happened and billions of dollars have been wasted. It was not until the TWA tragedy in 1996 that the government and industry started seriously looking for solutions to this problem. The wiring fault is an old problem, one that needs new solutions.

Hard faults, in which the wire is short circuited or completely break apart, are relative easy to detect and locate. The impedance (either near zero or very high) is beyond the tolerance of the system. Capacitance sensing or various types of reflectometry can locate this type of fault quite precisely. For smaller faults; however, the change in characteristic impedance is often not measurable easily. Traditionally, wire fault troubleshooting relies on experienced technicians to inspect the suspected areas visually. In addition to the inability of inspecting hidden spots, physically searching through bundles of already bridled wires on an aged aircraft can often cause even more unintended damages. That is on top of the cost of grounding the aircraft. Therefore, newer methods are needed to mitigate these problems.

Reflectometry has become a popular technology that provides effective and reliable results if properly understood. The measured results are often difficult to

interpret, and computational algorithms are often required to interpret the results. These algorithms need two types of simulation. Forward modeling is used to simulate the transmission line and predict the outcome of the reflectometry response. Inverse modeling takes these forward simulations, often runs with many different parameters, compares them in some way to the measured data, and determines the most likely forward model that matches the measured data, thus determining the wiring system and location and severity of the wiring fault.

Time domain transmission line modeling has been one of the main techniques for the existing forward simulation methods. The simplicity of programming makes many of the simple transmission line simulations possible. However, the demand of computational resources makes these methods less valuable in more complex scenarios and inverse simulations. This is especially true for those algorithms that synthesize the result with three-dimensional models (i.e., some types of FDTD simulations). Additionally, existing methods are often inflexible and need much reprogramming for different configurations. A more efficient simulation method in time domain is needed. This dissertation introduces a new time domain method that does the reconfiguration processes graphically and with very little reprogramming.

In addition to its inefficiency, pure time domain methods are difficult to use to model nonlinear behavior and frequency dependent parameters such as characteristic impedances and complex propagation constants. Most of the time domain simulation methods idealize these parameters in order to simplify the process. The simplification often loses the fidelity that is critically needed in more realistic models. A work around to this problem is to simulate the transmission line in the time domain, transform the

result from time domain to frequency domain in order to apply frequency domain parameters and then convert it back to time domain. Although this can be very inefficient, it is probably one of the better solutions available. The drawback is that the frequency domain process is typically a blanket solution in which the algorithm applies to the entire transmission line system. In the real word, the transmission line systems are rarely identical in every section. Therefore, this method also has its limitations.

In order to solve these problems, this dissertation demonstrates several methods in the frequency domain that do not require back and forth time/frequency domain conversions. Instead, they simulate the transmission lines directly in the frequency domain. The ABCD method in particular, can simulate realistic results within seconds and each section can have its own frequency properties. The simulation time of this method is independent of the wire length, since it is an analytical solution. Therefore, it does not have the common numerical method problems, in which the simulation time can grow linearly or even exponentially with the length and complexity of the transmission line.

Most of results in this dissertation will be demonstrated with time domain reflectometer (TDR). This is the primary tool that our sponsors (Boeing Co. and NASA) use, and it provides a recognizable baseline for anyone working in reflectometry. However, the application is not limited to TDR. It works for STDR, SSTDR [6] and other types of reflectometry, as well.

Finally, one of the most difficult tasks is the inversion, in which we need to interpret a set of given or measured data into a possible configuration or a fault. One approach is to compare the data against a library of data from known models. To

generate this library, a common approach is to measure all the interested fault scenarios. This is very commonly used in the military radar industry, in which the model airplane or even real airplane is constantly being measured, and the signatures are recorded and stored in a huge library for target recognition. Given enough data gathered, a pattern of an object may be revealed. Even with abundant financial and technical resources, the military radar industry often has to rely on some type of simulation to assist on the building of the library. Thus, radar target generators (RTG) are frequently used to simulate reflected radar signals for calibration and training purposes. This is similar to what could be required for wire fault location. However, the faults on a transmission line do not have a fixed size, shape or location, and every wiring system is different. Therefore, creating such an inclusive library by measurement is nearly impossible. In order to identify the nature of a fault on a transmission line, an efficient and realistic forward method is needed, and a systematic inversion algorithm is also required.

1.2 Overview

The objective of this dissertation is to develop forward simulations and inversion algorithms to locate small faults in electrical wiring systems. This required efficient forward simulations of high fidelity, and very accurate inversion algorithms. Several novel methods were developed and compared, and the best combination of methods was selected.

Chapter 2 reviews and discusses various existing forward modeling techniques. These techniques are categorized into three generations. The first generation methods can be represented by the bounce/lattice diagram and the Bergeron method [7]. These

methods typically provide quick estimations where accuracy is not required. They are also used in textbooks frequently due to their intuitivism.

The second generation methods rely on numerical techniques and are mostly accomplished in the time domain. These methods trace the waveform propagation numerically. FDTD and Generalized Bounce Diagram (GBD) [8], [9] are often used to model simple transmission lines.

The third generation method is led by the well-known microwave technique, the scattering parameters, or S-parameters. Various high profile publications [10] - [13] have used this method as the foundation for solving transmission line or geophysical forward problems.

Chapter 3 discusses the problems of the existing methods. Additionally, this dissertation demonstrates a few techniques that can mitigate some of these problems. Signal flow diagram (SFG) and the extended signal flow diagram (ESFG) are introduced to provide a systematic way of solving cascading transmission line modeling problems. With proper configurations, using these methods can be as easy as building Lego® blocks. Thus, the simplicity makes this technique very attractive for those who need to analyze transmission lines in the field.

Most of the second generation methods are capable of producing decent results; however, are not sufficient for small fault inversion purposes. Additionally, the speed of these numerical methods is often too slow for real world applications. Therefore, the third generation methods are introduced to mitigate the problems. The ABCD parameter method [14] , [15] is discussed in this chapter. It is capable of modeling frequency dependent parameters and components such as characteristic such as characteristic

impedances, complex propagation constants and reactive loads. Furthermore, this method is very computationally efficient and suitable for inversion purposes.

Chapter 4 introduces a quick way of estimating chafe profiles using commercial software packages [16]. CST's Microwave Studio was chosen due to its capability of simulating three-dimensional bodies. Like most of the similar 3D products, CST Microwave Studio does a great job simulating the electromagnetic models, but suffers from slow performance and heavy computational resource requirements. We overcome this limitation by interpolating only a few simulated results, so the profile of a chafe can be quickly formed. This fault profile can further be represented with an analytical equation using curve fitting method. Thus, the nature of the fault can be determined by a simple search on the profile. The fault signatures and probing techniques are also discussed.

Chapter 5 demonstrates a few different approaches for inversion, all of which rely heavily on the forward method. For simple structures, the analytical inverse solution was derived and can be applied. However, this method often fails on many of the real world situations, such as multisection configurations or noisy environments. The second inversion approach utilizes scanning algorithms that can often find the fault, but at the cost of computational time. For complex structures, this method can be extremely inefficient. An iterative inversion method [17], [18] is introduced as the third approach. With the assistance of realistic forward model and optimization techniques, the inverse result can be determined with only a few iteration steps.

Chapter 6 summarizes this dissertation and comments on possible future research effort, and hence to improve the capability and performance of transmission line

modeling. The major technical contributions of this dissertation are the development of highly efficient forward models with sufficient fidelity to model small, frequency dependent faults, and the development of associated inverse models to determine the location of small faults in wiring systems. These methods are significant improvements over previously available methods, and can provided far better resolution for small faults than ever before. However, they are still limited by the basic stability of the wiring system. If a fault signature and the signature of normal variation on the wire (due to moisture, vibration, etc.), these two may not be distinguishable. Hence, if the system is set with sufficiently low tolerance to locate the fault, it will also suffer from false positives caused by the ordinary changes. This limits the faults that can be found to those above the noise margin of the system.

CHAPTER 2

WIRE FAULT LOCATION TECHNIQUES

2.1 Overview

The objective of this dissertation is to develop forward simulation models and inversion algorithms to locate small faults in electrical wiring systems. This requires efficient forward simulations of high fidelity, and very accurate inversion algorithms. This chapter reviews the methods that have previously been used, and ways in which they may be modified for our application.

Numerous transmission modeling techniques have been used. In general, these techniques can be categorized into three different approaches. The first generation modeling techniques utilize graphical approaches to trace the wave propagation. These methods are able to perform quick estimation graphically with little training. Therefore, they are presented in many of the textbooks to teach students and engineers about signal propagation in wiring systems. However, the capabilities of these graphical methods are limited to very simple cases. Additionally, the idealized wave propagations rarely provide sufficient fidelity to match real world measurement results with the level of detail needed to locate small faults.

The second generation techniques enhance the wave tracing capabilities by logically dividing the transmission lines into a number of small sections or grids. With

the assistance of modern computing power, these methods can model much more complicated fault scenarios such as multisections and branched networks. One of the biggest drawbacks for these methods is inefficiency. Since the wires are divided into many small subsections, increasing resolution to model small faults increases the computational burden substantially and slows the process dramatically. This is especially serious for long wires with very small faults where high resolution is needed. Another problem for these second generation methods is that the modeling is often performed in time domain, so many of the frequency dependent parameters are not properly represented. Although time domain methods have frequently been used for simulation purposes [19] - [21], these methods are rarely used for inversion purposes, in which high fidelity and high efficiency are both needed.

The third generation modeling methods are generally performed in the frequency domain. The result may be later transformed back into the time domain. Since the modeling is performed in the frequency domain, the frequency dependent parameters are taken into account. Without having to divide the wires into many small sections or meshes, the resolution has less impact on the overall efficiency of the method. Therefore, the third generation methods are typically much more efficient and the results come much closer to the detailed measurement data.

The three generations of the forward modeling methods are discussed in this chapter. Table 2.1 summarizes the various techniques that are applied to these forwarding modeling methods.

Table 2.1 Forward Modeling Techniques

Forward Modeling Techniques		
Generation	**Method**	**Applied Techniques**
First	Bounce/Lattice Diagram	Graphical
	Bergeron Diagram Method	Graphical
Second	Finite Difference Time Domain (FDTD)	Discrete, Time Domain
	Generalized Bounce Diagram (GBD)	Discrete, Time Domain
	Signal Flow Graph (SFG)	Analytical & Graphical in Time Domain
	Extended SFG	Analytical & Graphical in Time Domain
Third	S-Parameters	Discrete, Frequency Domain
	ABCD Parameters	Discrete, Frequency Domain

2.2 Transmission Line Basics

The main difference between circuit theory and transmission line theory is the electrical length, in which the physical length of the medium is expressed in number of wavelengths. When the physical length of a medium is much smaller than the electrical wavelength, the transmission line effects may be ignored. However, once the signal frequency increases or the wavelength shortens, the transmission line effects need to be accounted for. In general, when the ratio of physical length to the wavelength is greater than 0.01 [22], the transmission line effect cannot be ignored.

Most of the common transmission lines operate in Transverse ElectroMagnetic (TEM) mode, where the electric field and the magnetic field are transverse, or perpendicular, to the direction of wave propagation. There are transmission lines, such as hollow waveguides and optical fibers that operate in higher order modes; however, they are beyond the scope of this dissertation.

A TEM transmission line can be represented with the lumped element circuit model [22] as shown in Figure 2.1, where R' is the combined resistance per unit length (Δz), L' is the combined inductance per unit length, G' is the combined conductance per unit length and C' is the combined capacitance per unit length. These basic elements are often called the transmission line parameters and the equivalent circuit model built using these basic parameters are called lumped element circuit.

The complex propagation constant (γ) of a transmission line is defined as (2–1), where real part (α) is the attenuation constant with the unit of Neper/m and imaginary part (β) is the phase constant with the unit of rad/m. The characteristic impedance (Z_0) is defined as (2–2).

$$\gamma = \sqrt{(R' + j\omega L')(G' + j\omega C')} = \alpha + j\beta \tag{2–1}$$

$$Z_0 = \sqrt{\frac{R' + j\omega L'}{G' + j\omega C'}} \tag{2–2}$$

At very high frequencies, where ω dominates, or lossless conditions, where R' and G' can be neglected, (2–2) can be simplified to (2–3).

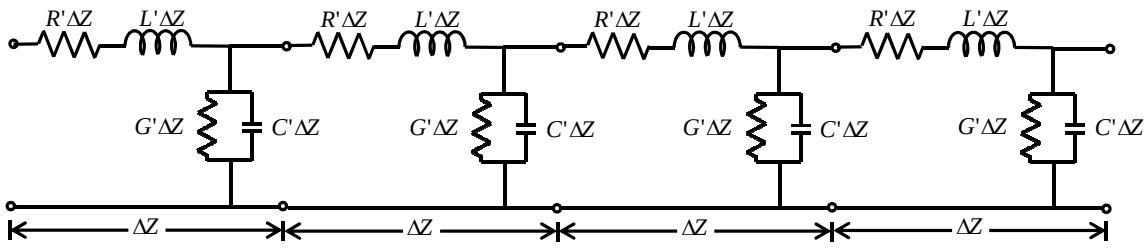

Figure 2.1 Transmission line lumped element circuit model.

$$Z_0 = \sqrt{\frac{L'}{C'}} \tag{2–3}$$

Unlike steady state, the transient response of an electrical signal on a transmission line bounces back and forth between the sending and receiving ends. If there is an impedance mismatch on the transmission line, a portion of the energy transmits through and the rest reflects back off the impedance mismatch. Thus, multiple reflections occur and the wave propagates in different directions simultaneously. Unless the impedances of the signal source, the transmission line, and the load are all perfectly matched, the transitional signal bouncing behavior is inevitable. It is this transient behavior that brings back the information on the wire health condition to where the test source is. Although this transient behavior can be observed using either current or voltage signals/pulses, most applications use voltage since it is easier to measure and interpret. Therefore, reflectometry is also often referred to as voltage reflectometry.

Figure 2.2 shows an incidental signal propagating along a transmission line with the characteristic impedance of Z_0 and a load with characteristic impedance of Z_L. The magnitude of the signal that is being reflected and transmitted can be calculated with the voltage reflection coefficient (Γ) and voltage transmission coefficient (T), which are defined in (2–4) and (2–5).

The main task of reflectometry is to track the propagation of the waves as they bounce back and forth on the transmission line. Without a proper method, this task can be tedious and yet complex on a multisection configuration. The next section of this dissertation introduces various forward modeling techniques.

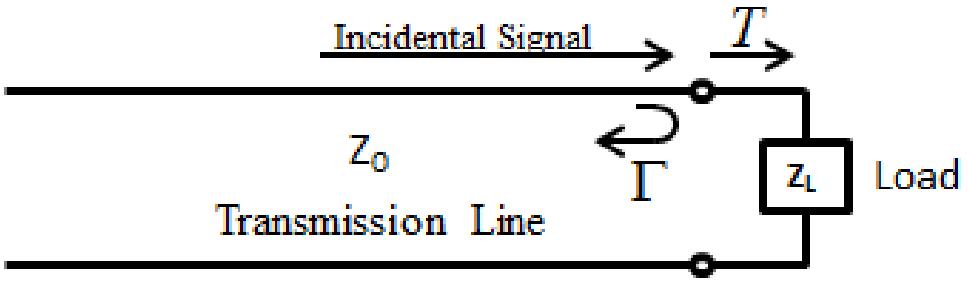

Figure 2.2 Reflection coefficient and transmission coefficient on a transmission line with load

$$\Gamma = \frac{Z_L - Z_0}{Z_L + Z_0} \tag{2–4}$$

$$T = 1 + \Gamma \tag{2–5}$$

2.3 Time Domain Reflectometer

A typical TDR includes two essential elements: a signal generator and a high speed data sampler. The type of signal generator may vary depending on the manufacturers. 3M Advanced System Tester - 900AST for example, uses pulses with various widths as the signal source. Campbell Scientific TDR100 as shown in Figure 2.3, on the other hand, utilizes a sharp rising step function as its signal source. For simplicity, this dissertation has chosen TDR100 as the primary equipment for the data measurement.

A typical TDR internal circuit is displayed in Figure 2.4 [23]. A step signal source with $50\,\Omega$ impedance is connected to a high speed data sampler with $1\mathrm{M}\,\Omega$ impedance in parallel. Since the $1\mathrm{M}\,\Omega$ data sampler has much higher impedance than the $50\,\Omega$ source impedance, it is essentially an open to the signal source and the load effect can be ignored. The equivalent circuit is displayed in Figure 2.5.

Figure 2.3 Campbell Scientific TDR100 time domain reflectometer.

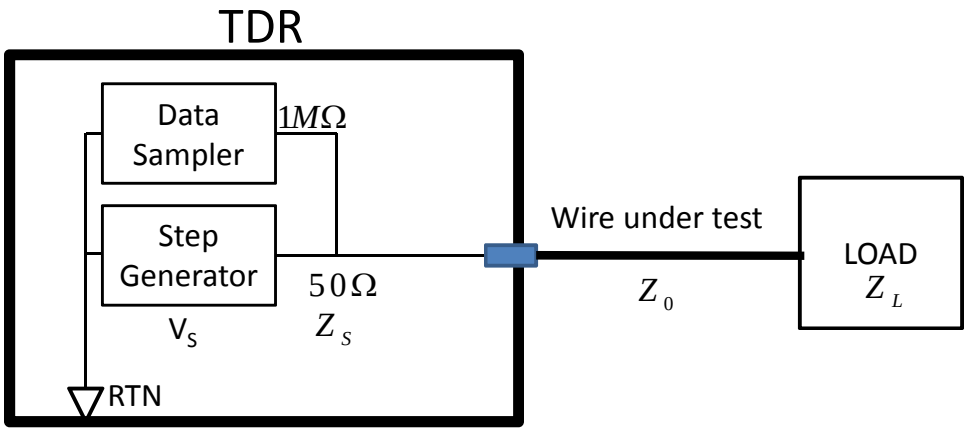

Figure 2.4 A typical TDR circuit with a load (Z_L) at the end of wire under test (Z_0). The data sampler with 1MΩ impedance acts like an open to the step generator.

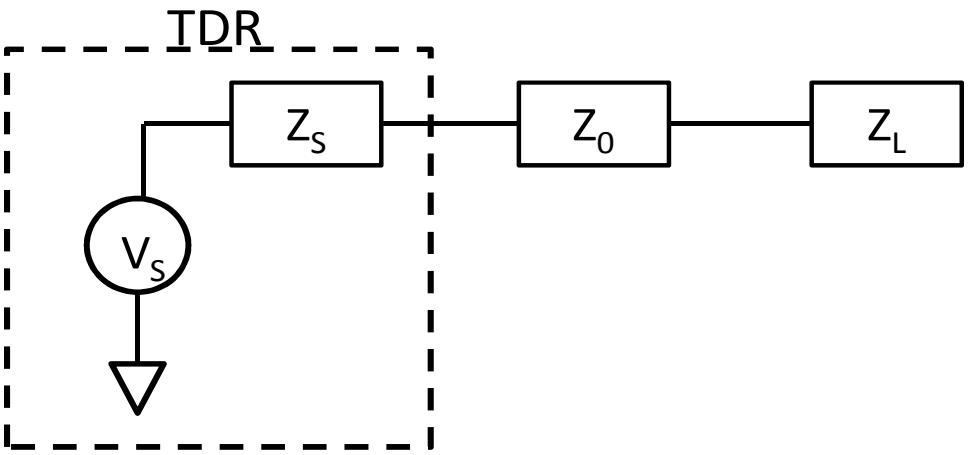

Figure 2.5 The equivalent circuit of the TDR with wire under test (Z_0) and load impedance of Z_L.

2.4 First Generation Forward Methods

2.4.1 Bounce/Lattice Diagram

The bounce diagram, also known as the lattice diagram, provides a systematic way of tracing the wave propagation on a transmission line in a graphical manner. This methodology is called the bounce diagram since it represents the electromagnetic waves that bounce back and forth at the impedance discontinuities of the transmission line. Figure 2.6 shows the typical voltage bounce diagram [22] that represents the transient voltage at a quarter ($l / 4$) of the total wire length with an incidental voltage signal of V^+.

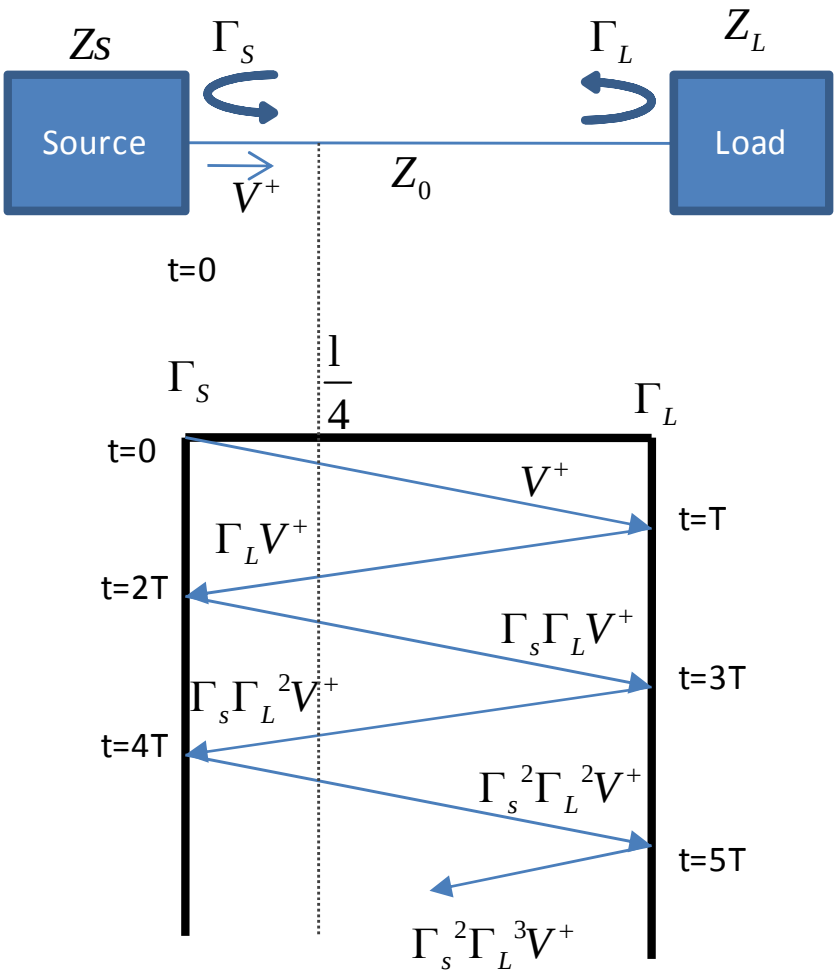

Figure 2.6 An example of a single section bounce diagram at length $L = \frac{l}{4}$

Both voltage and current of the electromagnetic wave bounces off the discontinuities, but we are more interested in the voltage since it is easier to measure. There is a voltage reflection coefficient at each end of the transmission line, Γ_S at the source and Γ_L at the load. The source and load reflection coefficients can be calculated as (2–6) and (2–7), where Z_0 represents the transmission line characteristic impedance, Z_S denotes the source characteristic impedance and Z_L is the characteristic impedance of the load. The zigzag segments represent the transient voltages at $l/4$ on the transmission line, in which the amplitudes of the voltages change by a factor of the reflection coefficient at either end of the transmission line. The vertical axis of the voltage bounce diagram is the time it takes to travel, with a normalized unit of period (T). T shows the time it takes the signal to propagate from one end of the transmission line to the other.

$$\Gamma_S = \frac{Z_S - Z_0}{Z_S + Z_0} \tag{2–6}$$

$$\Gamma_L = \frac{Z_L - Z_0}{Z_L + Z_0} \tag{2–7}$$

At the point of interest on the transmission line, in this example, a quarter of the total length, draw a vertical line from the point of interest on the transmission line to the bounce diagram and sum up all the transient voltages that intersect with the vertical dashed line in Figure 2.6. This way the total transient voltage response can be obtained.

Consider sending a sharp rising step voltage signal down the line, the result of time domain wave propagation observed at $l/4$ can be displayed in Figure 2.7. This step function response is the signal that would be measured with so-called time domain reflectometry (TDR).

This graphical representation of wave tracking method is very intuitive and it is often used in textbooks. However, most of the practical applications are much more complicated than just a single section of wire. Instead, it can be many cascaded sections or networks. Tracking the wave in these configurations with bounce diagrams may be possible, but is a daunting task. Thus, the simple bounce diagram method is rarely used in real world problems.

$$(a) = V^+$$
$$(b) = (1+\Gamma_L)V^+$$
$$(c) = 1+\Gamma_L+\Gamma_S\Gamma_L)V^+$$
$$(d) = (1+\Gamma_L+\Gamma_S\Gamma_L+\Gamma_S{\Gamma_L}^2)V^+$$
$$(e) = (1+\Gamma_L+\Gamma_S\Gamma_L+\Gamma_S{\Gamma_L}^2+{\Gamma_S}^2{\Gamma_L}^2)V^+$$

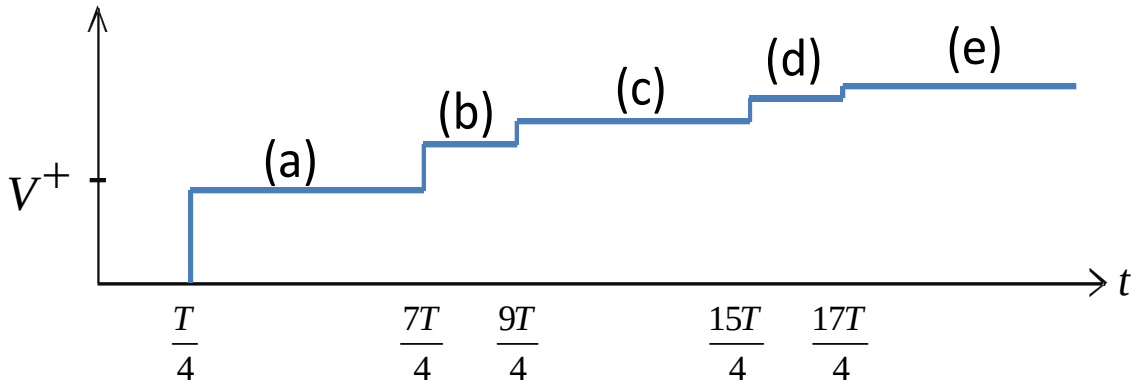

Figure 2.7 TDR response at $l/4$ using the simple bounce diagram method

2.4.2 The Bergeron Diagram Method

In a system where the load is not linear, that is, the relationship between the current and voltage at the source or load is not linear, the simple bounce diagram method no longer works since it uses the superposition methodology to track the wave propagation.

The Bergeron diagram method [7] is another graphical way of tracking the wave propagations. Figure 2.8 shows a single section transmission line terminated with a load (Z_L). At t=0, the switch closes and the voltage source (V_S) with an internal impedance (Z_S) induces a voltage signal down the transmission line.

The Bergeron diagram method starts with the steady-state ($t = \infty$), and thus the characteristics of the transmission line can be ignored temporarily and circuit theory can be used. The next step is to derive the receiver (load) input characteristic or the load line equation, which is displayed as (2–8).

$$V_B = i_B Z_L \tag{2–8}$$

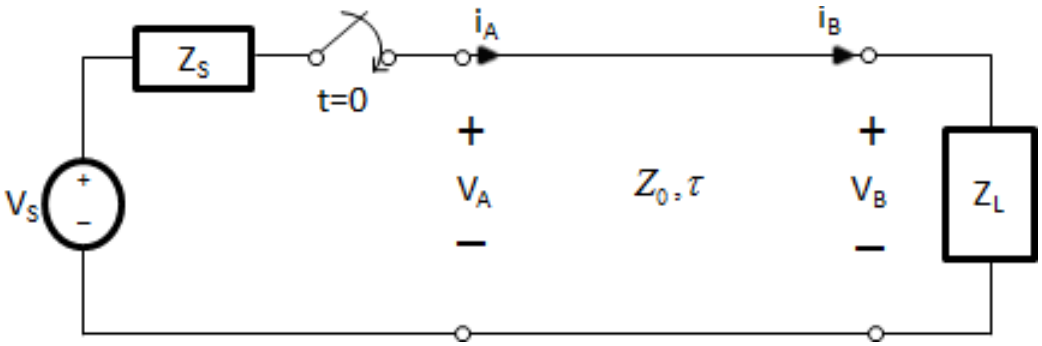

Figure 2.8 A step voltage source is induced to the single section transmission line with a load of Z_L.

The load line slope of (2–8) is Z_L. Similarly, the characteristic of the output of the driver (source) can be written as (2–9) with a slope of $-Z_S$.

$$V_A = V_S - i_A Z_S \tag{2–9}$$

The next step is to plot the lines derived in (2–8) and (2–9) on a voltage-current diagram as shown in Figure 2.9. Since the slope of (2–8) and (2–9) are different in polarity, the two lines will intersect at a point Q. When $t \to \infty$, a steady-steady condition is reached. Thus, the voltages at A and B are the same as the source V_S. Likewise, the current at the source is the same as at A, B and the load (Z_L). Therefore, the intersection point of Q is called the quiescent point.

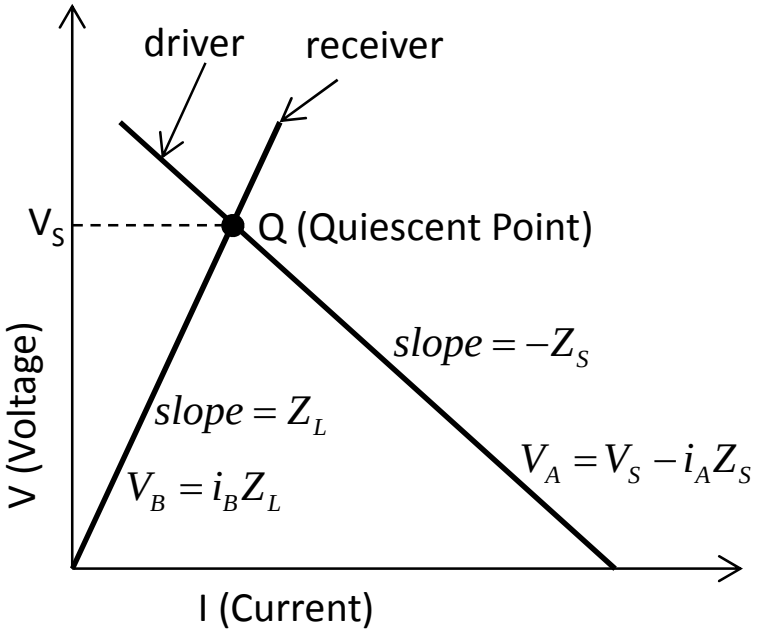

Figure 2.9 The driver output characteristic equation ($V_A = V_S - i_A Z_S$), receiver input characteristic equation ($V_B = i_B Z_L$), quiescent point intersection (Q) under steady-state condition

By starting at (V,I) = (0,0), plotting the wave propagation in a fashion of Z_L and $-Z_S$ in slopes, a zig-zag Bergeron Diagram is developed as shown in Figure 2.10. To find the transient voltage response at the load (Z_L), we can extend the intersections between the zig-zag pattern and V_B using (2–8). The TDR response at the load is demonstrated in Figure 2.10. Similarly, the TDR response at the source can be found by extending the intersections between the zig-zag pattern and V_A with (2–9). The result is displayed in Figure 2.11.

For transmission line configurations that are not linear, the simple bounce diagram typically fails. However, with the Bergeron diagram method, the process is similar to what have been described, except that the limiting lines are curved rather than straight. One can simply plot the nonlinear receiver and driver equations to replace (2–8) and (2–9). The rest of the steps remain the same as demonstrated. An example of nonlinear load transmission line analysis using the Bergeron's diagram method is displayed in Figure 2.12.

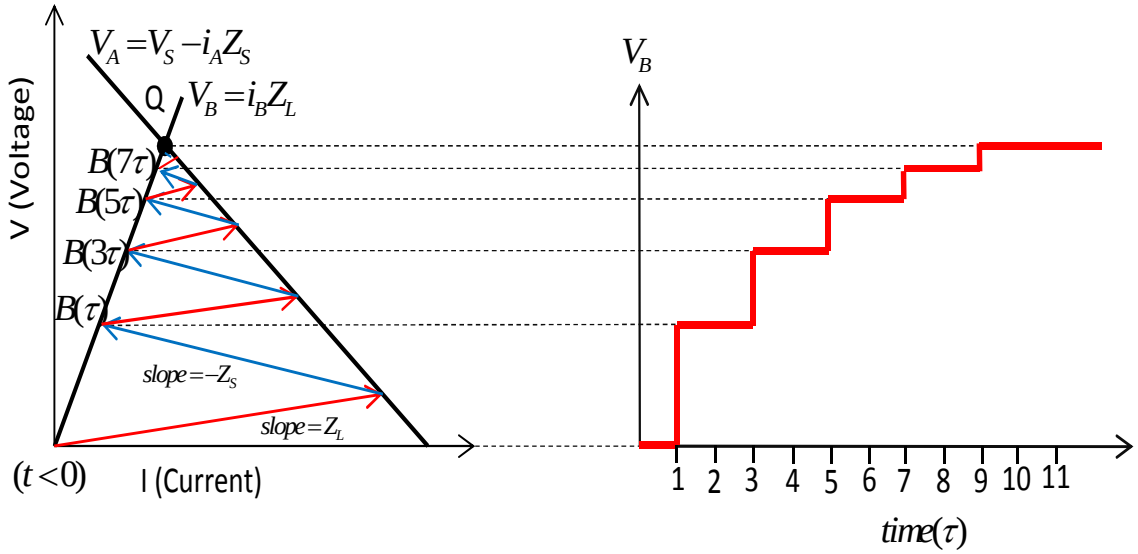

Figure 2.10 Transient voltage at the load (Z_L) using the Bergeron diagram method

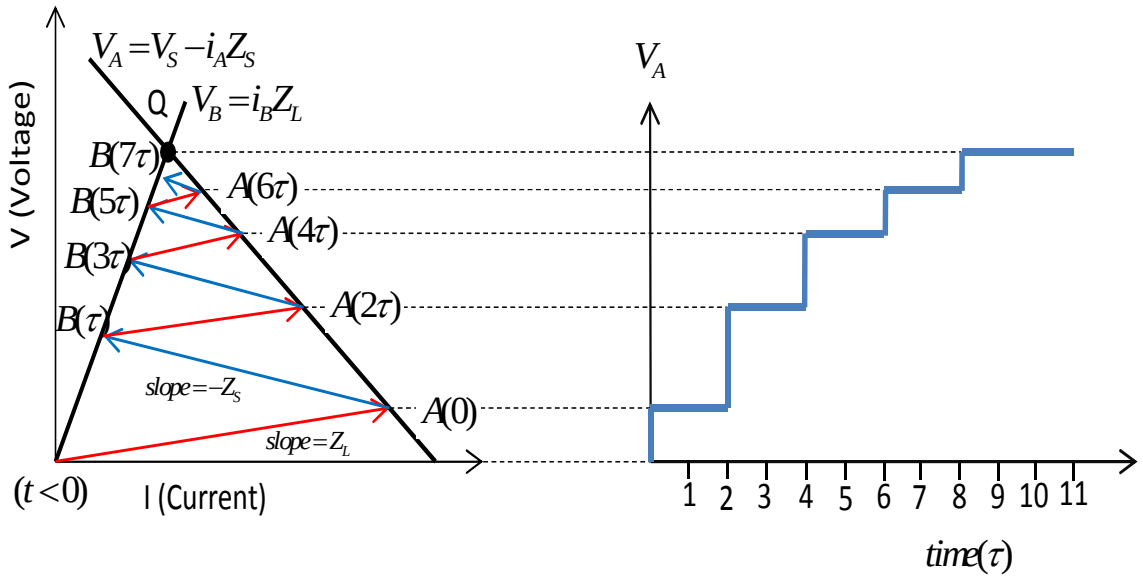

Figure 2.11 Transient voltage at the source (Z_S) using the Bergeron diagram method

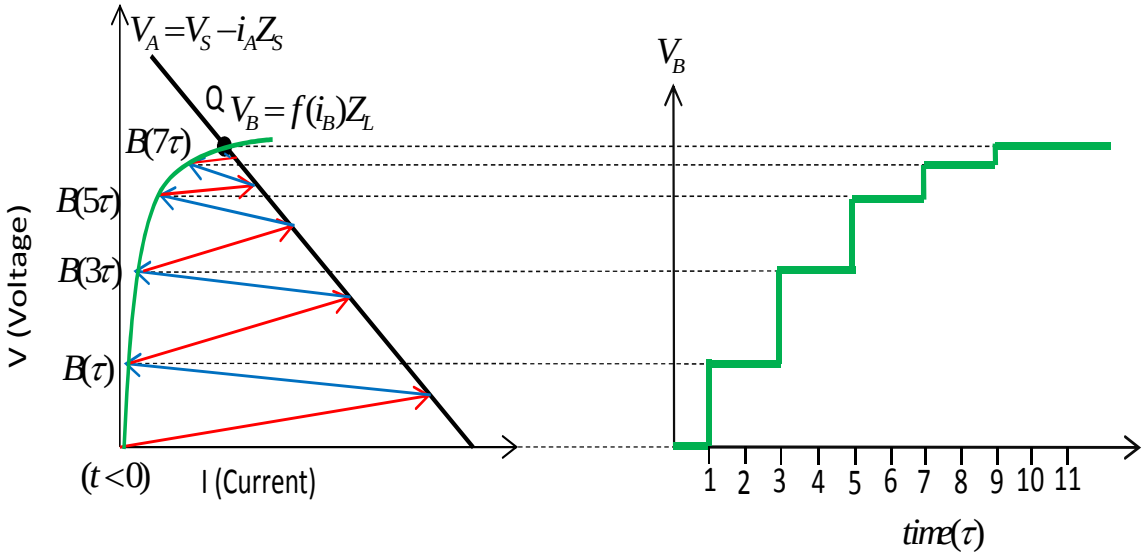

Figure 2.12 Transient voltage at the source (Z_S) with nonlinear load (Z_L) using the Bergeron diagram method.

2.5 Second Generation Forward Methods

First generation forward methods trace the propagation of idealized waveforms graphically. These methods provide conceptual results and intuitive steps in general; however, the waveforms are rather idealized. They are a good approximation to real world situations, but are not sufficiently detailed to provide the forward solutions for locating small faults. Additionally, for more complicated transmission line configuration (e.g., multiple sections), these first generation (graphical) forward methods become impossibly cumbersome to solve. Therefore, some of the better solutions have been developed. This section describes the next generation of methods for predicting reflectometry responses of wires and wiring systems.

2.5.1 Finite Difference Time Domain (FDTD)

The finite difference time domain method has been one of the most popular techniques for computational electrodynamics modeling. The FDTD concept was first introduced by Kane Yee in 1966 [24], but it was not widely used until the 1990s due to the extensive computational resources required. This method solves Maxwell's equations in the time domain by converting the differential equations to difference equations and iteratively resolving these difference equations.

One-dimensional (1D) FDTD can be used to solve any problem that is uniform in two dimensions and the wave propagates in the third dimension. This applies to many/most wiring simulations. Assume a TEM wave propagates in x-direction, the electric field is z-polarized and the magnetic field is y-polarized as shown in Figure 2.13.

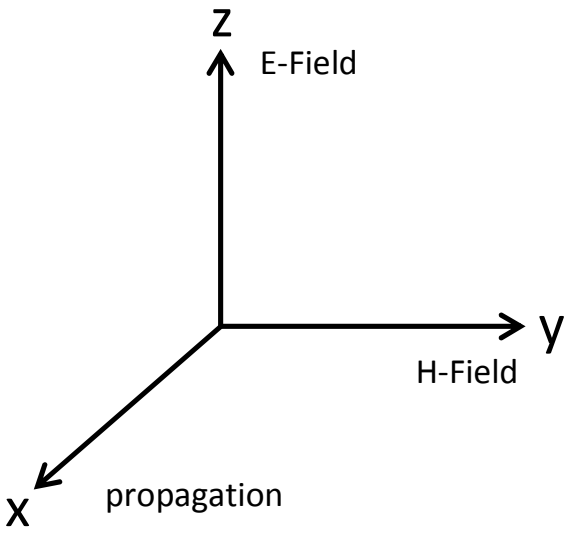

Figure 2.13 Electric and magnetic fields propagating in the x-direction in TEM mode

Maxwell's equations in differential form shown in (2–10) and (2–11) govern the time varying electromagnetic fields in free space. Equation (2–10) is also known as Ampere's law, and (2–11) is Faraday's law [22].

When Maxwell's differential equations (2–10) and (2–11) are examined, it can be seen that the change in the E-field in time (derivative) causes the change of the H-field across the space (curl). On the other hand, the change in H-field in time causes the change of E-field across the space. If only one dimension is considered, equations (2–10) and (2–11) can be written as (2–12) and (2–13).

$$\nabla \times \mathbf{H} = \frac{\partial \mathbf{D}}{\partial t} = \varepsilon \frac{\partial \mathbf{E}}{\partial t} \tag{2–10}$$

$$\nabla \times \mathbf{E} = -\frac{\partial \mathbf{B}}{\partial t} = -\mu \frac{\partial \mathbf{H}}{\partial t} \tag{2–11}$$

$$\varepsilon \frac{\partial \mathbf{E}}{\partial t} = \nabla \times \mathbf{H} = \begin{vmatrix} \hat{a}_x & \hat{a}_y & \hat{a}_z \\ \frac{\partial}{\partial x} & 0 & 0 \\ 0 & H_y & 0 \end{vmatrix} = \hat{a}_z \frac{\partial H_y}{\partial x} \tag{2–12}$$

$$-\mu \frac{\partial \mathbf{H}}{\partial t} = \nabla \times \mathbf{E} = \begin{vmatrix} \hat{a}_x & \hat{a}_y & \hat{a}_z \\ \frac{\partial}{\partial x} & 0 & 0 \\ 0 & 0 & E_z \end{vmatrix} = -\hat{a}_y \frac{\partial E_z}{\partial x} \tag{2–13}$$

Equations (2–12) and (2–13) can further be arranged in the scalar terms as (2–14) and (2–15).

$$\varepsilon \frac{\partial E_z}{\partial t} = -\frac{\partial H_y}{\partial x} \tag{2–14}$$

$$\mu \frac{\partial H_y}{\partial t} = \frac{\partial E_z}{\partial x} \tag{2–15}$$

By applying the central finite difference (CFD) [25] approximation, (2–14) and (2–15) become (2–16) and (2–17)

$$\frac{{E_z}^{n+\frac{1}{2}}(k) - {E_z}^{n-\frac{1}{2}}(k)}{\Delta t} = \frac{1}{\varepsilon} \frac{{H_y}^{n}(k+\tfrac{1}{2}) - {H_y}^{n}(k-\tfrac{1}{2})}{\Delta x} \tag{2–16}$$

$$\frac{H_y^{n+1}(k+\frac{1}{2}) - H_y^{n}(k+\frac{1}{2})}{\Delta t} = \frac{1}{\mu}\frac{E_z^{n+\frac{1}{2}}(k+1) - E_z^{n+\frac{1}{2}}(k)}{\Delta x} \tag{2–17}$$

where Δt is the time step while Δx is the cell size. Finally, (2–22) and (2–23) can be rearranged as (2–18) and (2–19).

$$E_z^{n+\frac{1}{2}}(k) = E_z^{n-\frac{1}{2}}(k) + \frac{\Delta t}{\varepsilon \cdot \Delta x}\left[H_y^{n}(k+\tfrac{1}{2}) - H_y^{n}(k-\tfrac{1}{2})\right] \tag{2–18}$$

$$H_y^{n+1}(k+\tfrac{1}{2}) = H_y^{n}(k+\tfrac{1}{2}) + \frac{\Delta t}{\mu \cdot \Delta x}\left[E_z^{n+\frac{1}{2}}(k+1) - E_z^{n+\frac{1}{2}}(k)\right] \tag{2–19}$$

From (2–18), the future state of the electric field can be obtained from the previous states of electric and magnetic fields. Likewise, (2–19) indicates that the future state of magnetic field can be derived from the previous magnetic and electric fields. This leapfrog style of algorithm goes on continuously until the system reaches steady-state. In the case where the wave hits an impedance discontinuity, it will reflect from the interface and (if applicable) propagate into the media at a different magnitude and velocity of propagation.

With proper discretization of the model, FDTD can be used to trace the complicated electromagnetic wave propagation numerically. FDTD is a grid-based computational electrodynamics modeling technique in the time domain. It simplifies the complex electromagnetic problems by defining the electric field vector and magnetic field vector components in a volume of space

At any point in the spatial volume, the updated E-field and H-field values depend on the previous values stored in the memory. In order to achieve high resolution, a very fine grid structure is typically implemented. This translates to a very large computational resource. Thus, this method is usually not feasible to implement in transmission line systems with fine and detailed fault models, where the structures are typically thin and long.

In general, the FDTD algorithm can be summarized as the flow diagram shown in Figure 2.14. The fact that the FDTD is capable of solving complex electromagnetic differential equations in time domain with gridded cells makes this method highly popular. It is especially true when the high performance computers are made widely available. FDTD records the wave propagation, E-field and H-field during the process. This feature also enables the animated display of electromagnetic wave propagation. Additionally, with resolution high enough, the gridded structure is capable of modeling structures with complex geometric shapes. Such flexibility is another attractive feature among researchers.

FDTD requires to grid or discretize the entire computational model, in which often requires excessive amount of computational resources for the fields to move along these cells. This phenomenon is particularly obvious on models with long and thin features. Unfortunately, most electrical wires belong to this category.

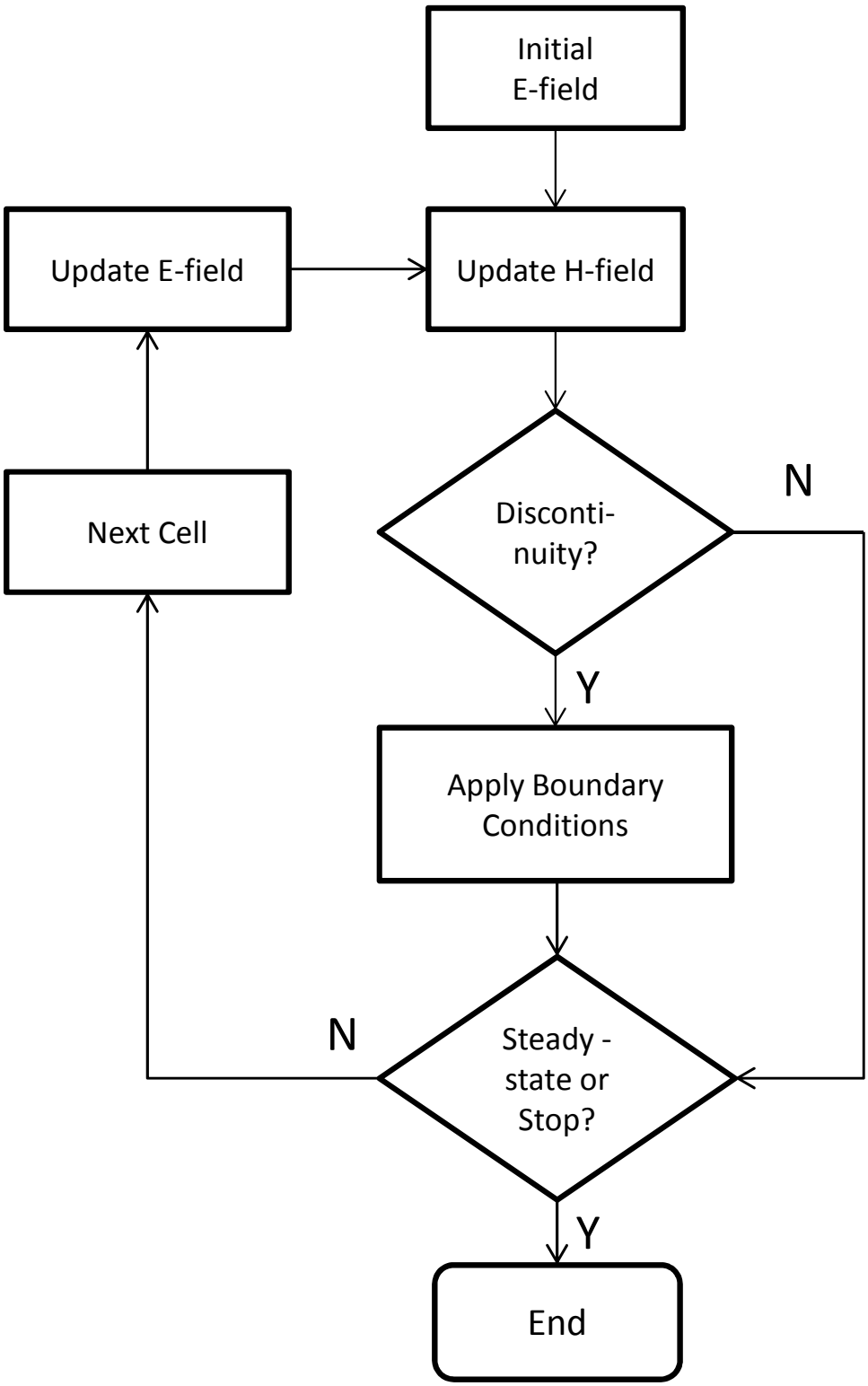

Figure 2.14 A general FDTD algorithm flow chart diagram of FDTD.

2.5.2 The Generalized Bounce Diagram

Although the simple bounce diagram method is hardly ever used for simulation purposes, the generalized bounce diagram may be. This method utilizes a similar concept with blend of a numerical technique that makes this legacy method much more powerful [8]. The generalized bounce diagram (GBD) divides the transmission line into numerous tiny elements and puts them into arrays or matrix form. Figure 2.15 shows a simple branched network with each arm of the network divided into numbers of small elements. Each of these small elements has the same electrical length, that is, the physical lengths of these elements may be different, but it takes the same amount of time for the signal to travel through each small element.

The input signal scatters through the system by passing the signal to the next element during the iteration. At the junctions or locations where impedances do not match perfectly, the boundary condition rules apply. Figure 2.16 demonstrates an impedance mismatch at point P. A portion of the incidental signal reflects back with the magnitude of Γ and transmits through P at the magnitude of T, where Γ and T are the reflection coefficient and transmission coefficient as defined previously. After summing all the signals per element, the total response at the particular time is defined and ready for the next iteration.

The GBD method normally uses an impulse signal and propagates down the wire. Iterating over time and applying the boundary conditions, we are able to obtain the impulse response of the system. From signal and systems theories, we can convolute the input signal with the system impulse response in order to obtain the reflectometry output of the system. This result is often called the signature of the reflectometry.

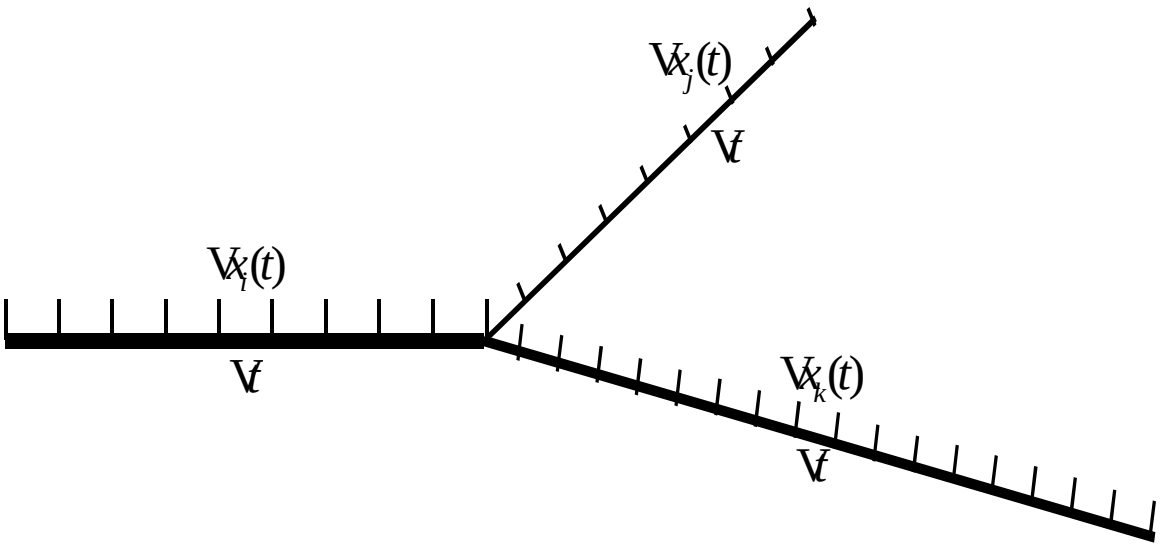

Figure 2.15 An example of a simple branched network using generalized bounce diagram.

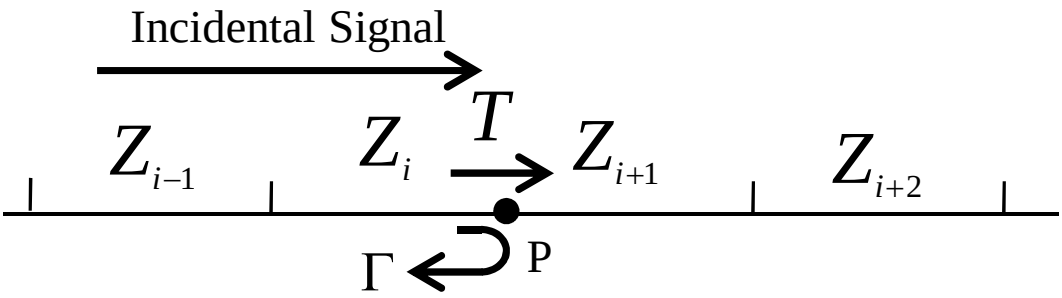

Figure 2.16 Boundary condition of an impedance mismatch in GBD algorithm, where T denotes the transmission coefficient while Γ represents the reflection coefficient.

A step function is frequently used as the signature profile in a TDR system. By convolving this step function with the system impulse response acquired with GBD, the TDR response (signature) can be obtained. Sequence Time Domain Reflectometry (STDR) and Spread Spectrum Time Domain Reflectometry (SSTDR) results can also be achieved with the similar fashion. The signature profile of these systems is convolved with the impulse response result from GBD to obtain the S/SSTDR signatures.

For more rigorous forward solution requirements, the attenuation constants of each transmission line can be distributed evenly into the small elements of the GBD. Additionally, a low pass filtering effect can be applied in order to make the result more realistic.

The GBD technique essentially converts a 3-D problem into 2-D (matrix) or even 1-D (array) problem. Although this method reduces the computational resources dramatically, in applications with long transmission lines that require high resolution, this method can still eat up a lot of computer time.

2.6 Third Generation Forward Method

As we have seen in the previous sections, the graphical first generation methods do not provide realistic results, and tracking the wave propagation in complex structures with these legacy methods can be a daunting task. The second generation methods have improved capabilities by using numerical techniques. With proper setups and fine resolutions, the results from these second generation methods have much better fidelity than the earlier methods. However, these second generation methods often require significant computational resources. This is seen more clearly for configurations with long wires requiring high resolutions such as small faults (high fidelity) on long wires. Moreover, the frequency dependent parameters are not properly accounted for in these methods unless the results are converted between the time and frequency domains where filtering can be applied. In order to accommodate the high efficient and frequency dependent properties that are needed for high fidelity inverse solutions, new methods have been used. Most of the newer methods are based on the scattering parameters (S-

parameters), which offer excellent fidelity and computational efficiency. This dissertation expands upon some of these methods.

Scattering parameters (S-parameters) have been widely used in microwave applications [26] - [28]. Scattering analysis is a very powerful tool that provides the system parameters of an N-port network. The S-parameters relate the incidental voltage waves to the reflected voltage waves. This provides the reflectometry wire fault information, which is carried by the reflected waves. However, without simplification S-parameters may be too cumbersome to apply directly to large scale reflectometry applications. S-parameters are defined as (2–20) [26]

$$S_{ij} = \left. \frac{V_i^-}{V_j^+} \right|_{v_k^+ = 0 \; for \; k \neq j} \tag{2–20}$$

where the "+" sign indicates the incidental voltage signal and the "-" sign represents the reflected voltage signal.

Although a simple transmission line can be represented as a two-port network, for reflectometry, we need only single-port information at the input end where the reflected signal is acquired. Thus, in (2–20) when i=j=1, the S-parameter becomes (2–21).

$$S_{11} = \left. \frac{V_1^-}{V_1^+} \right|_{v_2^+ = 0} \tag{2–21}$$

Equation (2–21) fully describes the relation between the reflected signal (V_1^-) and the incidental signal (V_1^+). This is sufficient for reflectometry purposes.

Figure 2.17 shows a simple single-section setup terminated with a load Z_L and input impedance Z_{in} at the beginning of the wire with length l. From [22], the equivalent input characteristic impedance (Z_{in}) of such a configuration with lossless transmission lines can be calculated as (2–22).

$$Z_{in}(l) = Z_0\left(\frac{Z_L + jZ_0 \tan \beta l}{Z_0 + jZ_L \tan \beta l}\right) \tag{2–22}$$

In the case where the transmission line is lossy, (2–22) can be rewritten as (2–23)

$$Z_{in}(l) = Z_0\left(\frac{Z_L + jZ_0 \tanh \gamma l}{Z_0 + jZ_L \tanh \gamma l}\right), \tag{2–23}$$

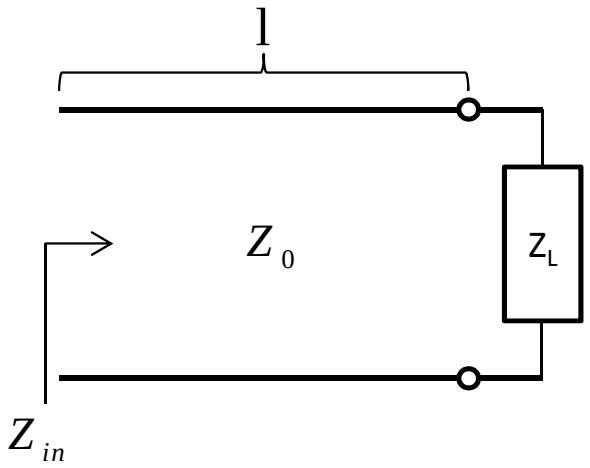

Figure 2.17 The equivalent input characteristic impedance observed from a distance l away from the load Z_L.

where γ is the complex propagation coefficient that includes both attenuation constant and phase constant.

This concept can be extended to multisection configurations. As shown in Figure 2.18, an n-section cascaded TDR setup is terminated with a load Z_L. Each section has an arbitrary length of $l_1, l_2, \ldots, l_n$. Likewise, the characteristic impedance of each section can also be arbitrary as $Z_0(1), Z_0(2), \ldots, Z_0(n)$. The input characteristic impedances $Z_{in}(1), Z_{in}(2), \ldots, Z_{in}(n)$, are defined as the look-in impedance at the beginning of the section, which includes all the cascaded characteristic impedances up to the end of line (the load).

From (2–22) and (2–23), the equivalent input impedance at section n can be calculated as (2–24) [10]:

$$Z_{in}(n) = Z_0(n) \cdot \left(\frac{Z_L + jZ_0(n) \tanh \gamma_n l_n}{Z_0(n) + jZ_L \tanh \gamma_n l_n} \right) \tag{2–24}$$

Likewise, substituting (2–24) as the load impedance of section (n-1), $Z_{in}(n-1)$ can be calculated as (2–25).

$$Z_{in}(n-1) = Z_0(n-1) \cdot \left(\frac{Z_{in}(n) + jZ_0(n-1) \tanh \gamma_{n-1} l_{n-1}}{Z_0(n-1) + jZ_{in}(n) \tanh \gamma_{n-1} l_{n-1}} \right) \tag{2–25}$$

Thus, at the beginning of the transmission line, the input characteristic impedance $Z_{in}(1)$ can be calculated as (2–26).

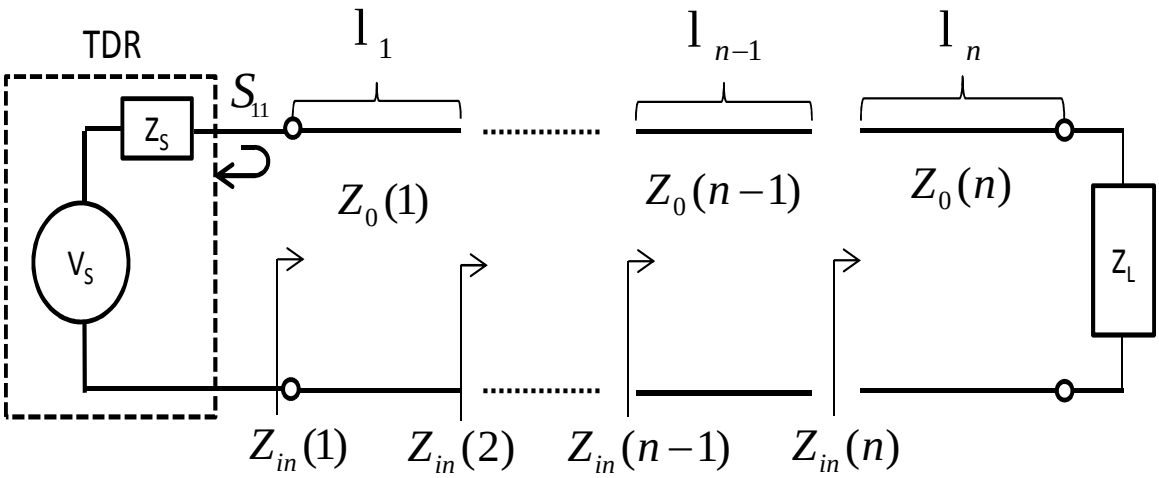

Figure 2.18 An n-section cascaded configuration with load impedance of Z_L and source impedance of Z_S.

$$Z_{in}(1) = Z_0(1) \cdot \left(\frac{Z_{in}(2) + jZ_0(1)\tanh\gamma_1 l_1}{Z_0(1) + jZ_{in}(2)\tanh\gamma_1 l_1} \right) \tag{2–26}$$

Therefore, the reflection coefficient S_{11} right after the TDR tester can be calculated as (2–27).

$$S_{11} = \Gamma = \frac{Z_{in}(1) - Z_S}{Z_{in}(1) + Z_S} \tag{2–27}$$

Note that the equations above are defined in the frequency domain. Therefore, they cannot be used directly to obtain the time domain reflectometry result. As a standard practice, the time domain result can be calculated as (2–28)

$$f(t) = iFFT\left\{S(f) \cdot H_{TDR}(f)\right\}, \tag{2–28}$$

where *S(f)* is the incidental signal in frequency domain. For TDR, most systems use a sharp rise step function, pulse or impulse signal as the input.

With proper modification of S-parameters, this method can be flexible and efficient to obtain the reflectometry forward method. Yet, there is a simpler way of handing the cascaded configurations.

2.7 Summary of Existing Forward Modeling Methods

This chapter summarizes some of the most frequently used forward transmission line modeling techniques. The bounce diagram, the Bergeron diagram, the generalized bounce diagram, the finite difference time domain method and the S-parameter methods were discussed. Each of these methods has its advantages and limitations.

The bounce diagram method provides graphical procedures to trace the propagation of electromagnetic waves on transmission lines. The Bergeron diagram expands the nonlinear transmission line modeling capability while retain the graphical features. These first generation methods help new learners to understand the transients intuitively, but they cannot be used for inversion due to lack of fidelity.

The FDTD method opens new possibilities by modeling electromagnetic waves numerically, but the inflexibility of building wire sections makes this method less attractive. The GBD method simplifies the FDTD by using strictly the time and space of the wave propagation. Without having to calculate the electric field and magnetic field, GBD outperforms the FDTD in speed. However, it loses the critical frequency dependent parameters.

The popular S-parameter has a proven history of being used in inversion for geophysical applications. This frequency domain method offers high fidelity without sacrificing efficiency. Different from geophysical applications, transmission line modeling often requires flexible multisection cascading features. Therefore, the next chapter will introduce a new method that allows such features to be implemented conveniently.

CHAPTER 3

MODULARIZED FORWARD MODELING TECHNIQUES

3.1 Overview

Chapter 2 reviewed methods that are commonly used for today's forward transmission line modeling. All of these methods may be effective, but none are ideal for modeling small faults with high fidelity on long transmission lines. In this chapter, we will introduce some newer forward modeling techniques that are better suited to small faults on long wires.

One of the problems with existing modeling techniques is flexibility. For each different wiring configuration, traditional techniques require significant overhaul or even reprogram of the entire model. A method that enables the user to configure model setups like building LEGO® blocks is greatly needed. Therefore, this chapter discusses these newer modularized methods that provide the ease of modeling construction without sacrificing performance and accuracy.

Each element in the wiring configuration (the good wire, the fault, connectors, branches, etc.) will be either measured or simulated independent of the rest of the system. These independent modules will be combined to obtain the response of the total system using any combination of measured or simulated results for each module.

The first generation forward modeling techniques are essentially tracing propagating waves on the wire graphically. It becomes very complicated and difficult to trace all the forward and reflected propagating waves on configurations that are more than just a few sections. Therefore, several improved methods have been proposed to solve this problem.

In the second generation methods, the transmission line is logically dissected into numerous small sections. Instead of tracking the wave propagation analogously over the entire transmission line system, these newer methods monitor the condition only on each of the small sections and then combine them into the larger system. Thus, the analysis is simpler at this microscopic level point of view. At each of the time step, or clock, the signals on the wire pass along forward or reversely. Therefore, the total system response can be obtained at a preset simulation time.

It is also important to include the frequency dependent parameters into the simulation model. Parameters such as characteristic impedances, attenuation constants and phase constants are all functions of frequency. Without these critical features, the model cannot retain its fidelity for realistic simulation. Most second generation methods; however, solve problems at time domain one single frequency each time.

A remedy to this problem is to simulate the transmission line model multiple times at broad frequencies of interest. Unfortunately, this approach makes it even more inefficient for most of the second generation methods. Therefore, third generation methods were created to provide further remedies by modeling the transmission line directly in the frequency domain. Therefore, inefficient time domain processes can be eliminated.

3.2 Signal Flow Graph

One method of calculating the response of a transmission line with modular components is to utilize the signal flow graph (SFG). This method is commonly used to evaluate a feedback control system. In fact, the signal propagating on a transmission line is a great example of a feedback system where the output is a function of the input and reflected signal. As shown in Figure 3.1, a single section TDR functional block diagram is demonstrated. The equivalent signal flow graph for this system is shown in Figure 3.2, where Γ_0 is the initial reflection coefficient at the TDR. T_{01} is the transmission coefficient from TDR to the line. T_{10} is the transmission coefficient from the line to TDR. Γ_{10} is the reflection coefficient that describes the signal reflection back to the line at the junction of the TDR and Γ_{12} is the reflection coefficient at the end (load) of the transmission line. The signal propagation time delays in the forward and reverse directions are assumed to be identical. Finally, the input and output terminals are both physically located at the beginning of the transmission line.

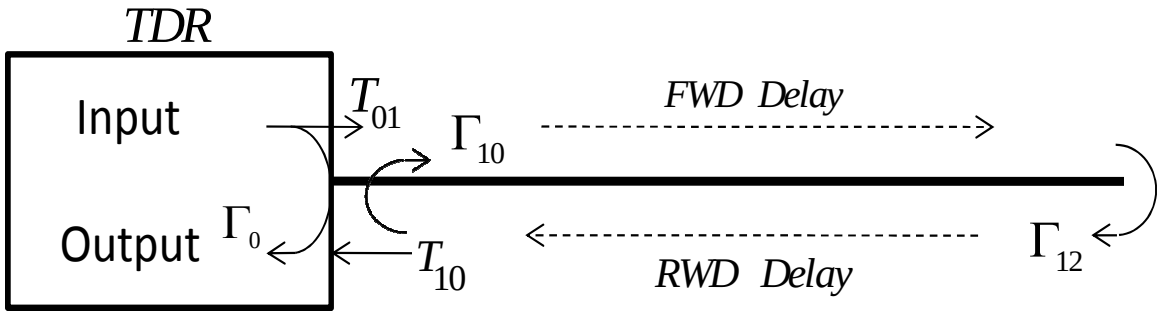

Figure 3.1 A single section TDR representation showing the feedback system on a transmission line

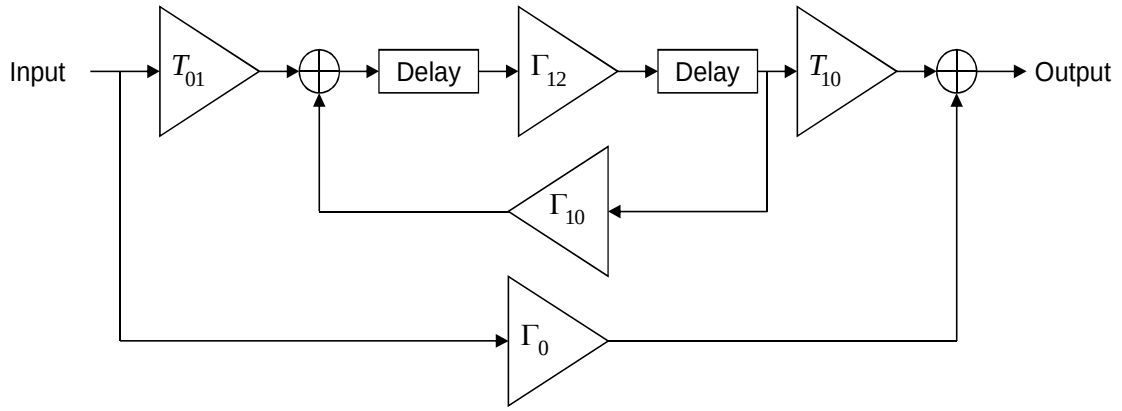

Figure 3.2 The equivalent signal flow graph of a single-section transmission line.

The reflection and transmission coefficients are defined as (3–1) and (3–2).

$$\Gamma = \frac{Z_L - Z_0}{Z_L + Z_0} \tag{3–1}$$

$$T = 1 + \Gamma \tag{3–2}$$

Assume a lossless transmission line is to be modeled. A sharp rising step function is generated inside the time domain reflectometer (TDR). Due to the impedance mismatch, if it exists, between the source and the transmission line, a portion of the signal is reflected back at the magnitude of Γ_0 and the rest transmits down the line with the magnitude of T_{01}. After a time delay, which depends on the wire length, the incidental wave reaches the end of the wire. The signal reflects back with an amplitude of Γ_{12}. In this example, $\Gamma_{12} = 1$ since the end of wire is an open. After another delay of the same length, the wave reaches the TDR tester and, again, a portion of the energy is transmitted back into the TDR system at the magnitude of T_{10} and the rest reflects back on the

transmission line at the magnitude of Γ_{10}. The complete wave propagation steps are shown in the signal flow diagram in Figure 3.2.

Once the signal flow graph is obtained, the block diagram can be simplified algebraically using Mason's gain rule [29], [30], a legacy formula that describes the relationship between any two nodes of a linear network. It is often used to solve the system transfer function, which is the relationship between the output and input. However, with the modern graphical programming languages such as Matlab's Simulink ® or National Instrument's LabVIEW ®, this simplification process can be replaced by making the transmission line signal flow graph into a logical block.

3.3 Extended Signal Flow Diagram

The complicity of the SFG can grow almost exponentially if components and blocks are not carefully placed. This section demonstrates a systematic way of organizing the SFG blocks. Figure 3.3 shows an example of a two-section transmission line setup. The equivalent SFG can be represented as shown in Figure 3.4 where each dashed box represents the individual transmission line.

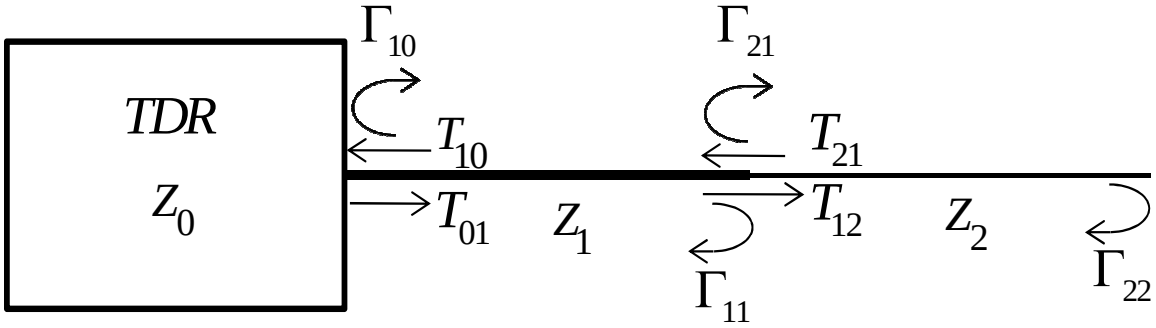

Figure 3.3 An example of a cascaded two-section transmission line system

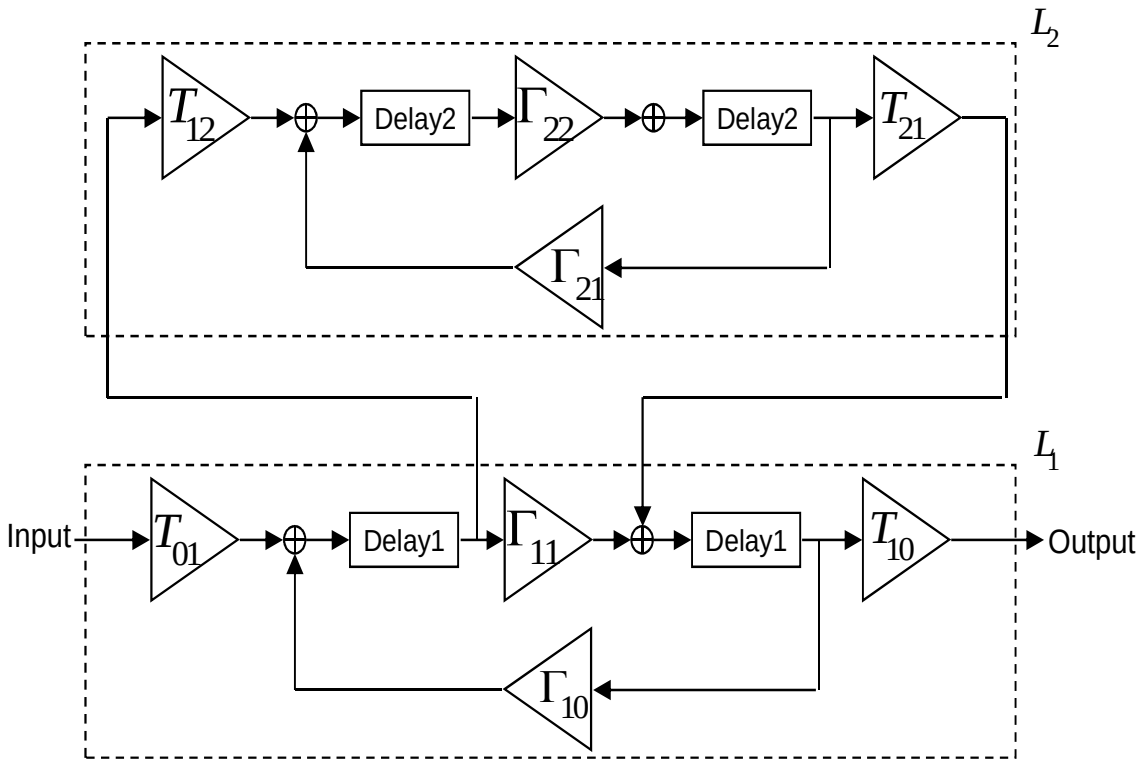

Figure 3.4 The equivalent signal flow graph of a two-section transmission line.

If the elements in the dashed boxes are consolidated as blocks, the SFG demonstrated in Figure 3.4 can by simplified as shown in Figure 3.5, where the upper box represents the second section of wire and the lower box is the first section of the transmission line. Thus, by rotating the blocks by 90^o clockwise, a cascaded N-section configuration SFG is displayed in Figure 3.6.

This extended SFG concept can further be applied on a Y-junction setup depicted in Figure 3.7 and the equivalent block diagram is shown in Figure 3.8. Figure 3.9 shows a more complicated branched network example and the simulation result is demonstrated in Figure 3.10. As we can see, the simulated result matches with the measured data very closely.

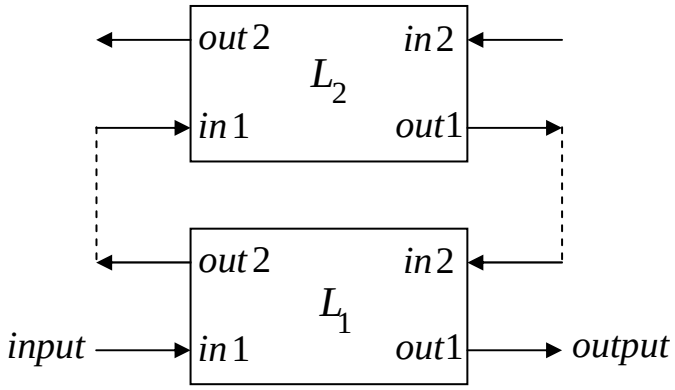

Figure 3.5 The block diagram representing a cascaded two-section setup.

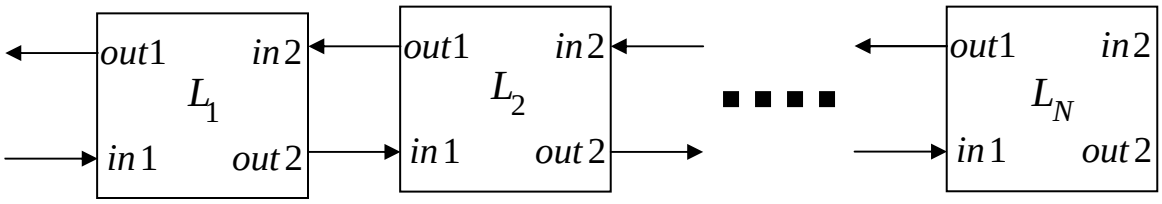

Figure 3.6 The block diagram of an n-section transmission line setup.

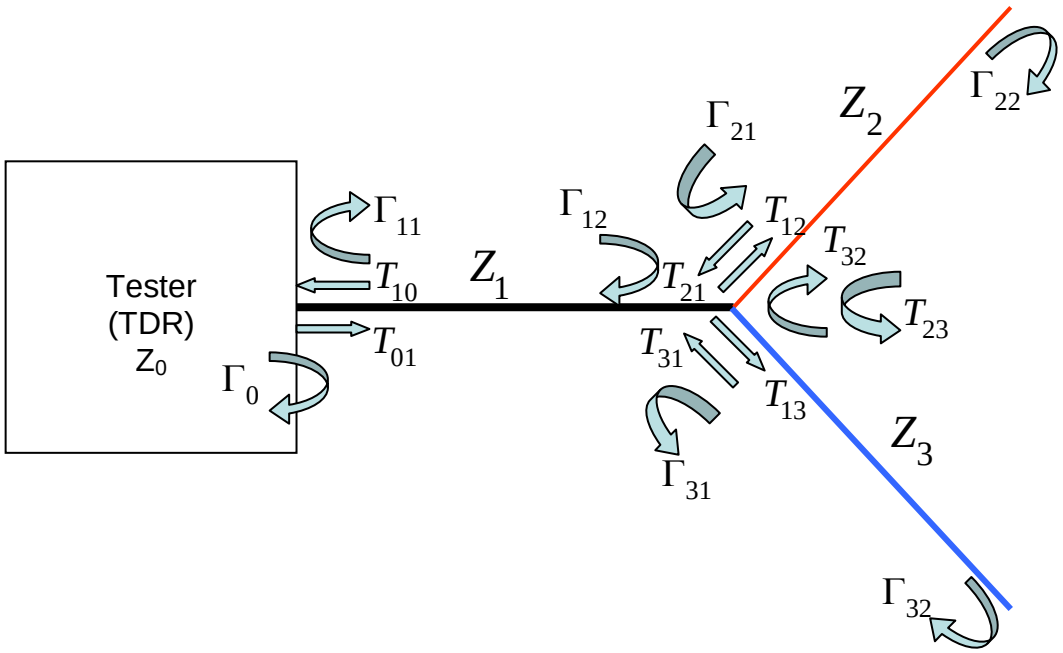

Figure 3.7 An example of a Y-junction transmission line setup.

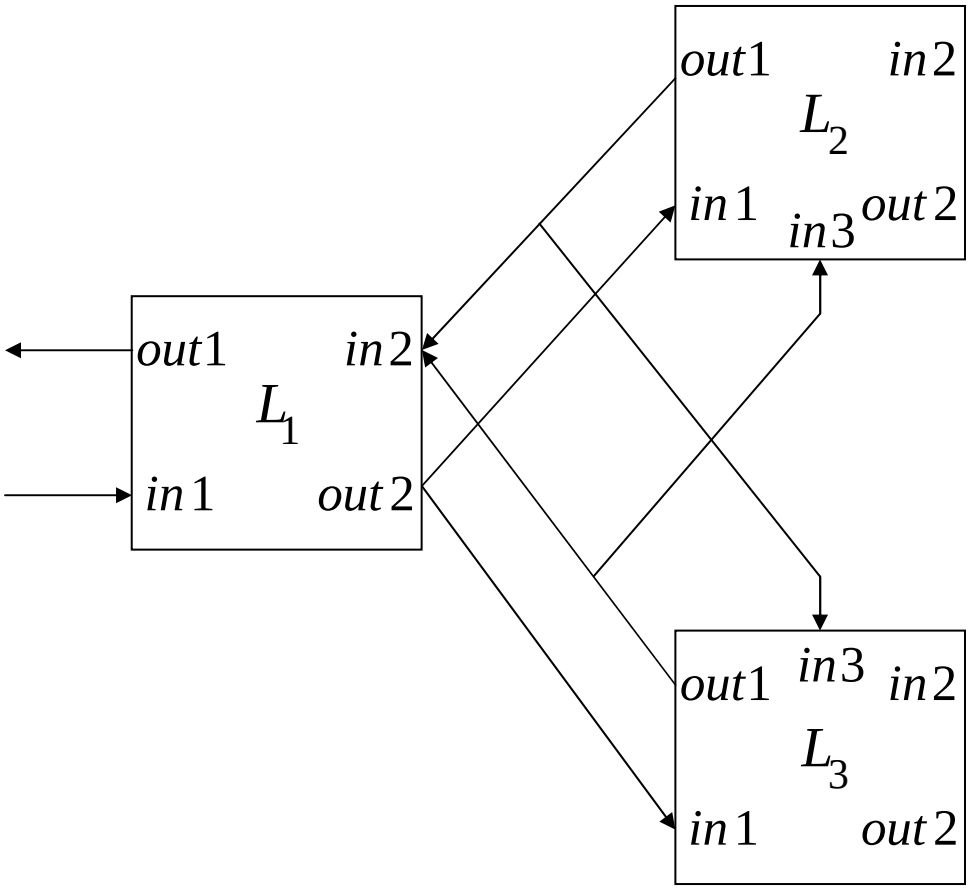

Figure 3.8 The block diagram representation of a Y-junction transmission line setup.

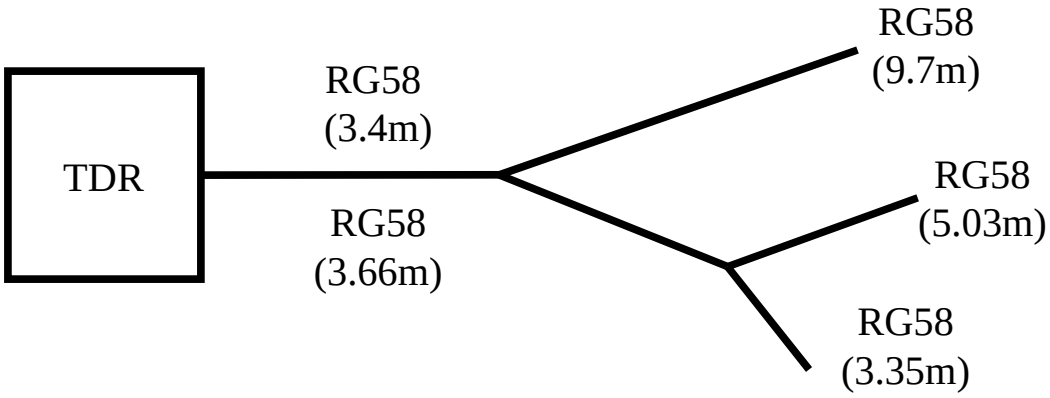

Figure 3.9 An example of a complex RG58 branched network configuration consists different wire lengths.

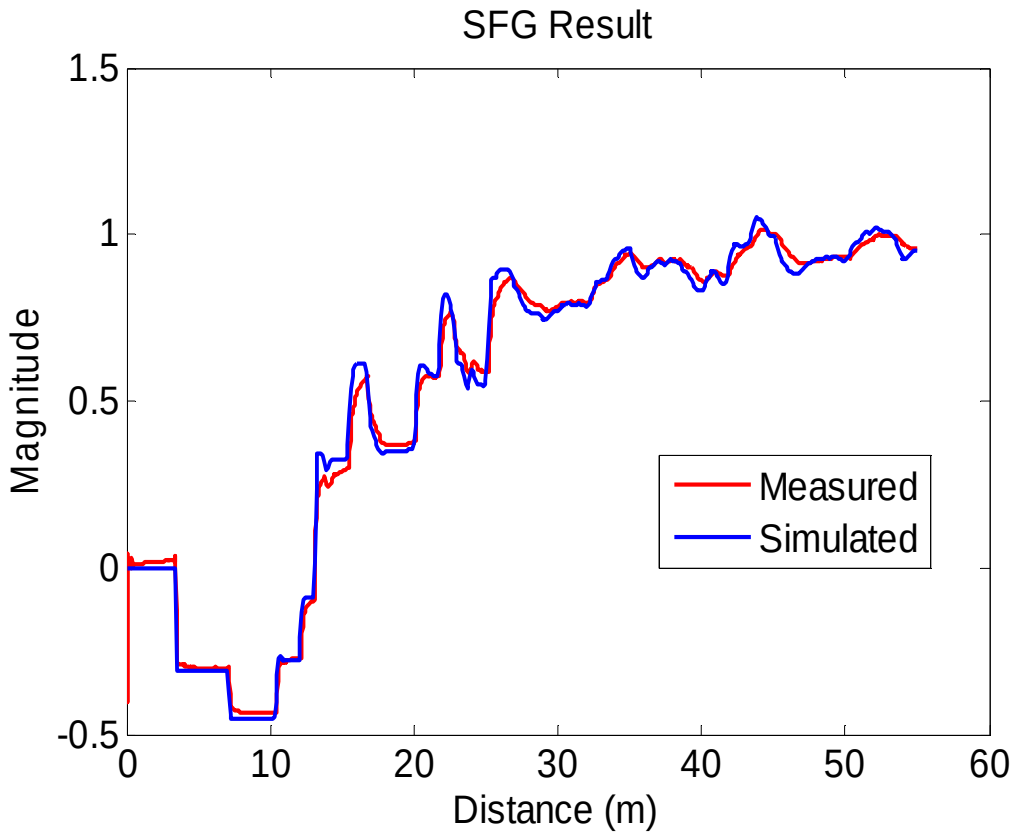

Figure 3.10 The simulated and measured results of the complex branched network configuration

3.4 ABCD Parameters

3.4.1 ABCD Matrix Review

This section describes the ABCD method, which is commonly used to evaluate serial sections of RF devices. The ABCD method provides a transmission matrix which is often called the ABCD matrix [26]. Figure 3.11 shows a two-port network **M** with I_1 is defined as the current flowing into the network while I_2 is defined as the current flowing out from the network. V_1 at port 1 is defined as the input voltage while V_2 at port 2 is defined as the output voltage.

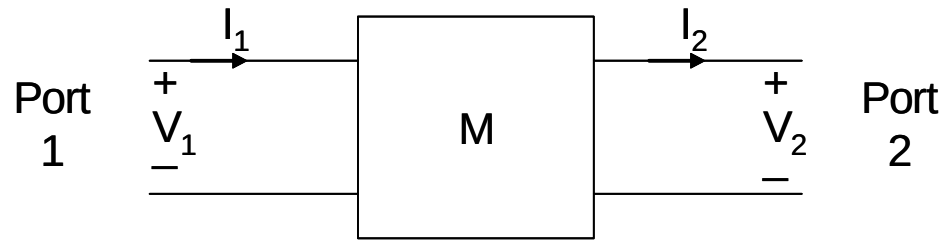

Figure 3.11 A two-port network representing by M.

The two-port network **M** shown in Figure 3.11 can be represented with an ABCD matrix defined as (3–3):

$$\begin{bmatrix} V_1 \\ I_1 \end{bmatrix} = \begin{bmatrix} A & B \\ C & D \end{bmatrix} \begin{bmatrix} V_2 \\ I_2 \end{bmatrix} \tag{3–3}$$

Figure 3.12 shows an n-section cascading two-port network expressed with ABCD matrices $\mathbf{M_1}$, $\mathbf{M_2}$, $\mathbf{M_3}$…$\mathbf{M_n}$. The consolidated transmission parameter is represented by multiplying their ABCD matrices sequentially from the right to the left as shown in (3–4).

$$\begin{bmatrix} A & B \\ C & D \end{bmatrix} = \begin{bmatrix} A_1 & B_1 \\ C_1 & D_1 \end{bmatrix} \cdot \begin{bmatrix} A_2 & B_2 \\ C_2 & D_2 \end{bmatrix} \mathrm{K} \begin{bmatrix} A_n & B_n \\ C_n & D_n \end{bmatrix} \tag{3–4}$$

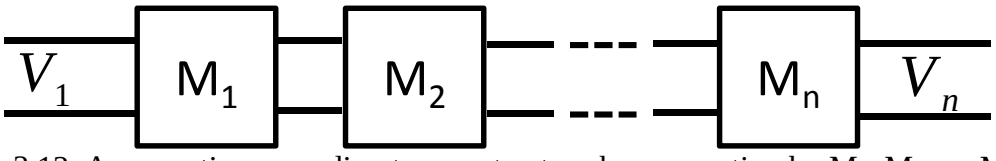

Figure 3.12 An n-section cascading two-port network representing by M_1, M_2,…, M_n.

Therefore, a system of n-section two-port network can be written as (3–5).

$$\begin{bmatrix} V_1 \\ I_1 \end{bmatrix} = \begin{bmatrix} A & B \\ C & D \end{bmatrix} \begin{bmatrix} V_n \\ I_n \end{bmatrix}, \tag{3–5}$$

where V_n and I_n represent the output voltage and current at the end of the n-section two-port network while V_1 and I_1 are the incident voltage and current at the beginning of the n-section two-port network. For reflectometry purposes, we are particularly interested in the voltages at either end of the network. From (3–5), we know that for an n-section two-port network, the incident voltage is (3–6),

$$V_1 = AV_n + BI_n = AV_n \mid_{In=0} \tag{3–6}$$

in which the element-***A*** of the consolidated ABCD matrix fully describes the relationship between the incidental voltage (V_1) and the output voltage (Vn) at the end of the network where I_n=0. This stands true regardless of the number of sections in the two-port network. Therefore, element-***A*** of the consolidated ABCD matrix is the only parameter of interest. Computing only this parameter saves about ¾ of the calculation time, and makes the ABCD approach particularly nice for transmission line reflectometry analysis. The term $I_n=0$ in (3–6) will always hold since the final section of a two-port network can be treated as a shunt in air with zero length, which has a unity matrix. Therefore, this term is satisfied both physically and mathematically.

3.4.2 Using ABCD Method in Reflectometry

Figure 3.13 shows a TDR tester connected to a transmission line as a signal source while a load with a characteristic impedance of Z_L is connected at the end of wire. The TDR has an internal source impedance of Z_S in series with the signal source V_1. The transmission line has a characteristic impedance of Z_T, length l and complex propagation constant of γ. This configuration can also be represented as an equivalent circuit shown in Figure 3.14, where V_1 is the incidental voltage while V_2 is the output voltage measured at the load. The source, transmission line and the load can be represented as M_1, M_2 and M_3 respectively.

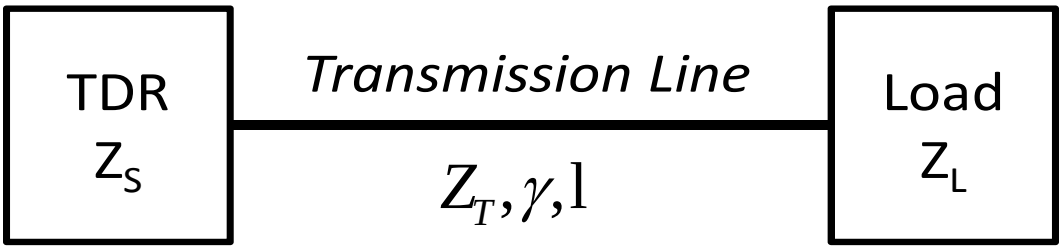

Figure 3.13 A single-section transmission line with characteristic impedance of Z_T, length of l and the complex propagation coefficient of γ. The load is represented as Z_L and the source impedance is Z_S.

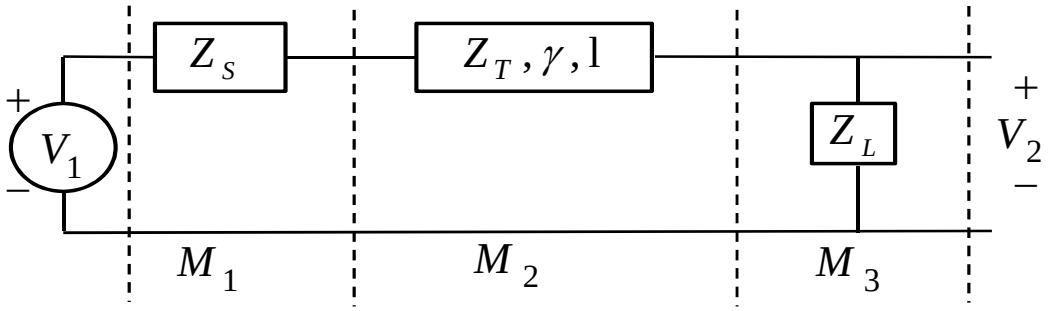

Figure 3.14 – The equivalent circuit representation of a single section transmission line. The source, transmission line and load are represented as M_1, M_2 and M_3 respectively.

There are several possible two-port network parameters that can be used to describe the system. However, the ABCD method is best known for its convenience in cascaded two-port structures. From [26] and [31], the source (M_1), the transmission line (M_2) and the load (M_3) can be represented as ABCD matrices as shown in (3–7) through (3–9).

$$M_1 = \begin{bmatrix} 1 & Z_S \\ 0 & 1 \end{bmatrix} \tag{3–7}$$

$$M_2 = \begin{bmatrix} \cosh \gamma \mathrm{l} & Z_T \sinh \gamma \mathrm{l} \\ Y_T \sinh \gamma \mathrm{l} & \cosh \gamma \mathrm{l} \end{bmatrix} \tag{3–8}$$

$$M_3 = \begin{bmatrix} 1 & 0 \\ 1/Z_L & 1 \end{bmatrix} = \begin{bmatrix} 1 & 0 \\ Y_L & 1 \end{bmatrix} \tag{3–9}$$

The consolidated matrix can be written as (3–10)

$$M = \begin{bmatrix} (1 + Y_L Z_S) \cosh \gamma \mathrm{l} + (Y_L Z_T + Y_T Z_S) \sinh \gamma \mathrm{l} & \chi \\ \xi & \psi \end{bmatrix}, \tag{3–10}$$

where χ, ξ and ψ denote the elements that are not of interest for reflectometry purposes. For the lossless case, (3–8) can be replaced as (3–11).

$$M_2 = \begin{bmatrix} \cos\beta l & jZ_T \sin\beta l \\ jY_T \sin\beta l & \cos\beta l \end{bmatrix} \tag{3–11}$$

and the consolidated ABCD matrix is (3–12).

$$M = M_1 \cdot M_2 \cdot M_3 = \begin{bmatrix} \cos\beta l + jZ_S Y_T \sin\beta l & ? \\ ? & ? \end{bmatrix} \tag{3–12}$$

The transfer function, which is defined as the ratio between the output (V_2) and input (V_1), is actually the so-called TDT (Time Domain Transmission). To use the ABCD method in TDR, we need to consider the wave propagation of the reflective path.

As shown in (3–12), element-***A*** of the consolidated matrix is the only parameter we are interested in. Therefore, we do not need to derive elements **B**, **C** and **D** and they can be ignored. The matrix leads us to (3–13) and (3–14).

$$V_1 = (\cos\beta l + jZ_S Y_T \sin\beta l)V_2 \tag{3–13}$$

$$V_2 = \frac{V_1}{\cos\beta l + jZ_S Y_T \sin\beta l} \tag{3–14}$$

The usefulness of (3–13) and (3–14) may not be realized at first glance since they are in the frequency domain. However, with the following example, we will find that it provides the so-called TDT (Time Domain Transmission) response. Figure 3.15 shows a TDT example with four cascaded sections. The lengths of the transmission lines are

2.2m (RG62), 3.7m (RG58), 2.77m (RG59) and 17.2m (RG58), respectively. A scope with one mega ohms probe is connected at the end of the wire in which the high impedance acts as an open load and has little effect on the transmission line system. A one volt step source with an impedance of 50 ohms is connected to the beginning of the wire as the signal source. The measured data versus simulated result are displayed in Figure 3.16. The result demonstrates that the ABCD method can precisely model the TDT transmission line effects on this multisection configuration.

The difference between TDT and TDR is that the TDR measures the reflected signal at the beginning of the wire while TDT measures the transmitted signal at the end of wire. Therefore, the reflected signal has to travel "almost" twice as far. In most cases, we measure the reflected TDR signal right at the test equipment.

Figure 3.17 shows an n-section configuration with M_1 being the TDR source while M_n represents the load. The TDR signal is typically acquired between the internal impedance (M_1) and the beginning of a transmission line (M_2). In this example, it would be V_2. The TDR algorithm, or the transfer function, is the relationship between the source V_1 and the data captured at V_2, which is the signal reflected from the very end of the line.

The forward path (TDT) from V_1 to V_n can be described as (3–15) and the reverse path from V_n to V_2 is written as (3–16)

$$V_1 = \left[\prod_{x=1}^{n} M_x\right]_A \cdot V_n \quad \text{or} \quad \frac{V_n}{V_1} = \left[\prod_{x=1}^{n} M_x\right]_A^{-1} \tag{3–15}$$

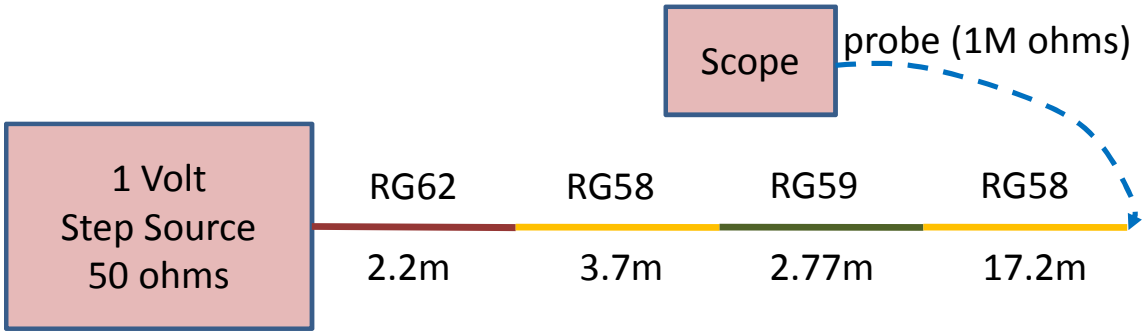

Figure 3.15 A four cascaded sections TDT example

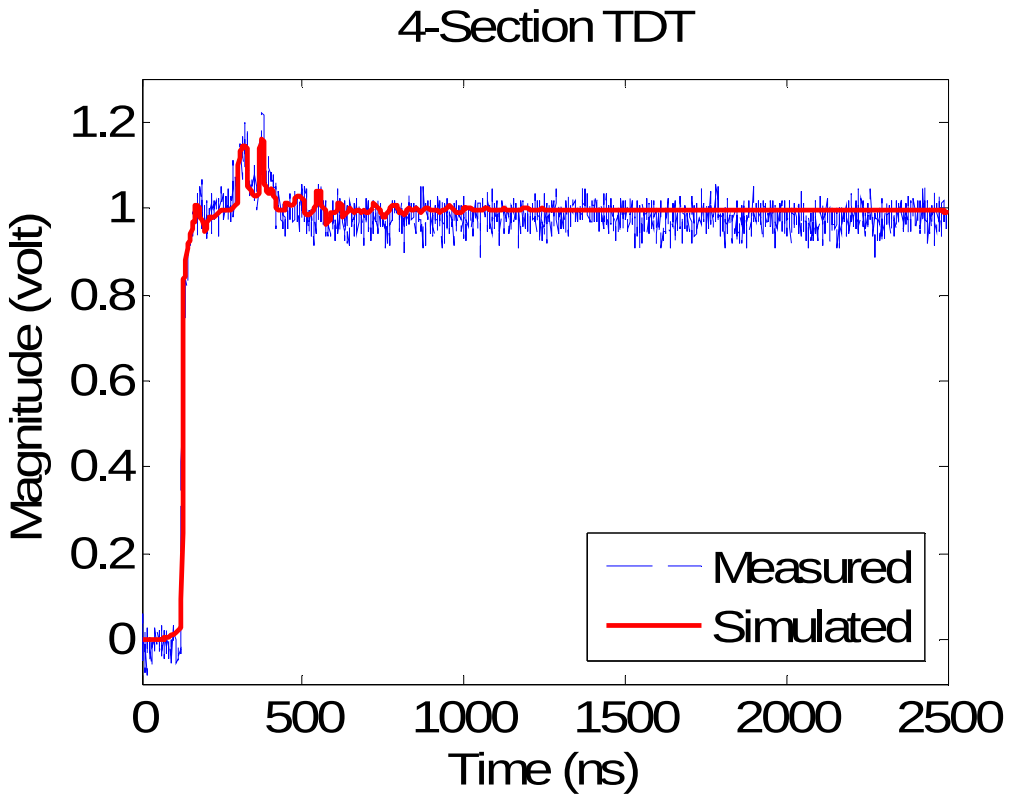

Figure 3.16 The result of the four cascaded sections TDT example

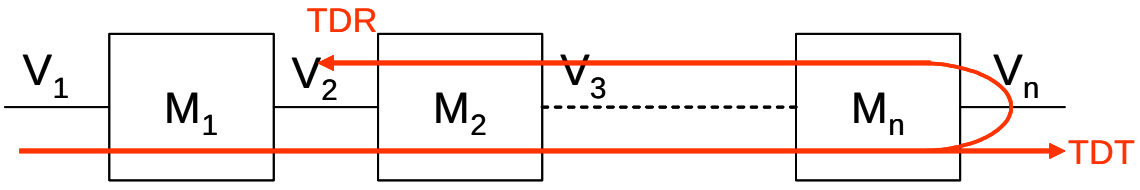

Figure 3.17 n-section TDT and TDR paths

$$V_2 = \left[\prod_{x=2}^{n} M_x\right]_A \cdot V_n \quad \text{or} \quad \frac{V_2}{V_n} = \left[\prod_{x=2}^{n} M_x\right]_A, \tag{3–16}$$

where $[\mathbf{M}]_{\mathbf{A}}$ denotes the element-**A** of the ABCD matrix **M**. Therefore, the TDR transfer function can be calculated as (3–17) , or an easier to understand term shown in (3–18).

$$H_{TDR} = \frac{V_2}{V_1} = \frac{V_n}{V_1} \cdot \frac{V_2}{V_n} = \left[\prod_{x=2}^{n} M_x\right]_A \Bigg/ \left[\prod_{x=1}^{n} M_x\right]_A \tag{3–17}$$

$$H_{TDR} = \frac{[\text{Reverse Path}]_A}{[\text{Forward Path}]_A} \tag{3–18}$$

The time domain expression is simply the inverse Fourier transform of the product of the transfer function and input signal *S* (typically a step function) in frequency domain as displayed in (3–19).

$$f(t) = \mathrm{F}^{-1}\left[H(\omega) \cdot S(\omega)\right] \tag{3–19}$$

Figure 3.18 shows a complex configuration with multiple sections of transmission lines and a load consisting of a 1nH inductor and a 47pF capacitor. The configuration also includes an internal impedance of 50 ohms and o.1 uF coupling capacitor within the TDR tester.

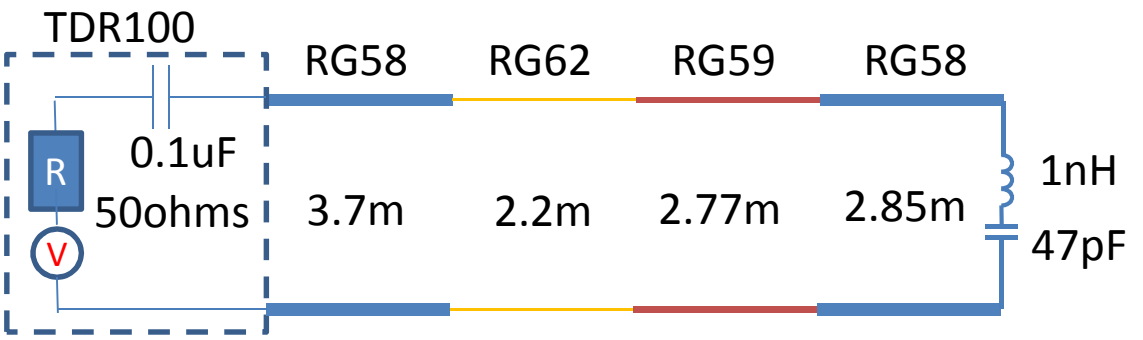

Figure 3.18 A TDR example of multisection transmission lines with reactive load of 1nH and 47pF.

This configuration can be very difficult to model with legacy methods. By using the ABCD method in the frequency domain, and converting the data to the time domain, the result demonstrated in Figure 3.19 can be obtained within a fraction of a second using a standard home PC.

The result of ABCD method clearly shows its capability in modeling complex transmission line configurations. In the above example, there are multiple section transmission lines along with a reactive load. The ABCD method simplifies the transmission line structures by representing each line section, whether it is a transmission line, fault, source impedance or a load, with a single ABCD matrix. Thus, modeling a cascaded transmission line is easily done by connecting the modularized blocks. It is demonstrated that this frequency domain method is accurate, computationally efficient and therefore superior to the earlier techniques presented.

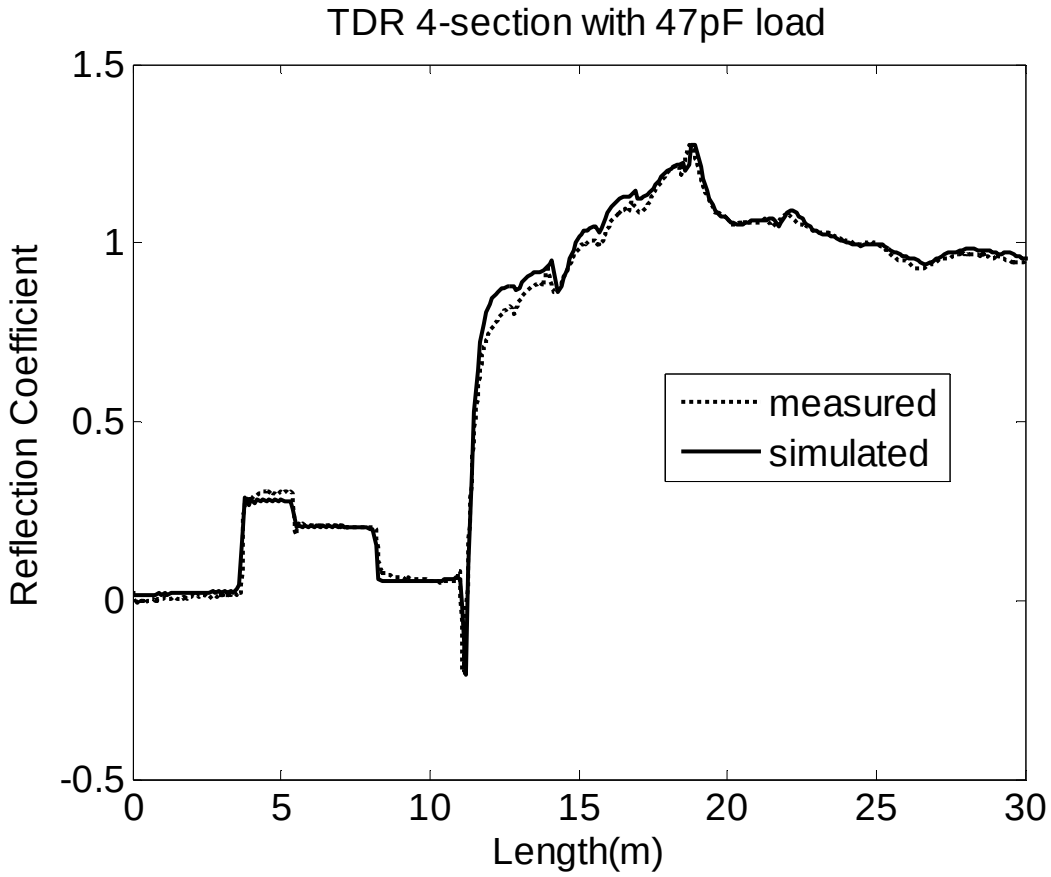

Figure 3.19 The TDR result of multisection transmission line with reactive load.

CHAPTER 4

AN INTERPOLATION APPROACH OF BUILDING CHAFED WIRE PROFILES AND PREDICTING WIRE FAULT SIGNATURES

4.1 Overview

A method of building a chafed wire profile and predicting fault signature is presented in this chapter. For simplicity, an RG-58 coaxial cable is demonstrated. This method can also be applied to other transmission lines with different geometries. The demonstrated method constructs a fault profile that covers a wide range of frequencies and fault severities, making a quick assessment of the fault severity possible. This efficient mathematical/numerical expression is important for future inverse solution purposes.

4.2 Approach

Hard wire faults including opens and shorts have been well studied. These faults are easier to find than intermittent faults or less severe faults with minimal impedance change. Most of reflectometry measurements have been demonstrated to be effective on hard faults. However, the partial faults (chafes) are the ones that are more difficult to identify since the system usually does not show any noticeable symptom until the fault is more severe.

Chafes are the result of improper workmanship, abrasion or vibration against other wire or structural members [32]. Chafes expose the conductor, and their severity is likely to worsen over time. Like human health, early detection of aircraft wiring fault typically gives a much better chance of resolving the problem and preventing catastrophic failures. Early detection of chafed wires often results lower repairing and maintenance cost.

Various techniques [33], [18] have been used to model chafes on electrical wires. Signals propagating in a pure TEM mode are typically assumed. However, for shielded wires, once the shield is damaged the signal no longer propagates entirely in the TEM mode and the analysis can be much more difficult due to the higher order modes. Although these higher order modes do not play a significant role when the fault is small and the frequency is low, once the fault is severe or the frequency is high enough, the effect can be negatively noticeable (making it potentially detectable by reflectometry). Analytical electromagnetic modeling does not work effectively on multiple modes with arbitrarily geometric variations. Thus, modern modeling techniques use numerical methods to synthesize the reflectometry results. A common drawback among these numerical techniques is the heavy burden of the computational resources. This is especially true when 3D techniques are employed.

CST Microwave Studio offers a powerful 3D Quasi-TEM mode [34] simulation. This is useful for frayed wires where the electric field or magnetic field has longitudinal components along the direction of propagation. In other words, both TEM and higher modes exist on the frayed wire. Like most iteration-based (e.g., FDTD, FEM) commercial software packages [35], CST is painfully slow at high resolution or where the

point of interest is small but the wire is long. This is because the transmission line is divided into many small cells/grids with equal sizes. Passing the numerical information along through these enormous is computationally extensive. Although these numerical modeling software packages produce precise results, relying entirely on them to generate a wide range of profile is not feasible.

4.3 Analysis

Figure 4.1 shows the electric field and magnetic field inside an RG58 coaxial cable. Based on the definition described in [22], the signal is propagating in the TEM mode since the electric field and magnetic field are perpendicular to the direction of wave propagation.

However, once the shield is damaged, the field lines start to bend and the characteristic impedance calculation is no longer as simple as it is shown in (2–2). Figure 4.2 demonstrates the electrical field and magnetic field with 60-degree, 5 cm cutaway in the shield of an RG58 coaxial cable at 5GHz.

To determine the characteristic impedance of a chafe, a technique proposed in [36] utilizes the 2-D finite difference method (FDM) to estimate the effective capacitance (C_{eff}) of the frayed wire section. The effective characteristic impedance Z_{eff} can be derived as (4–1) and (4–2)

$$Z_{eff} = \frac{1}{V_p C_{eff}} \tag{4–1}$$

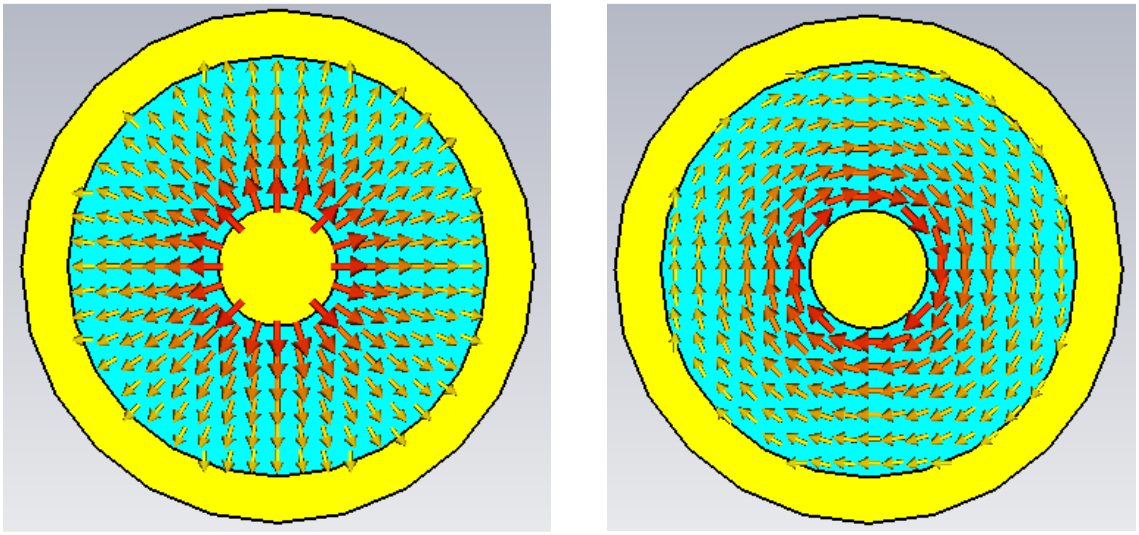

Figure 4.1 (a) Electric field and (b) magnetic field in a coaxial cable

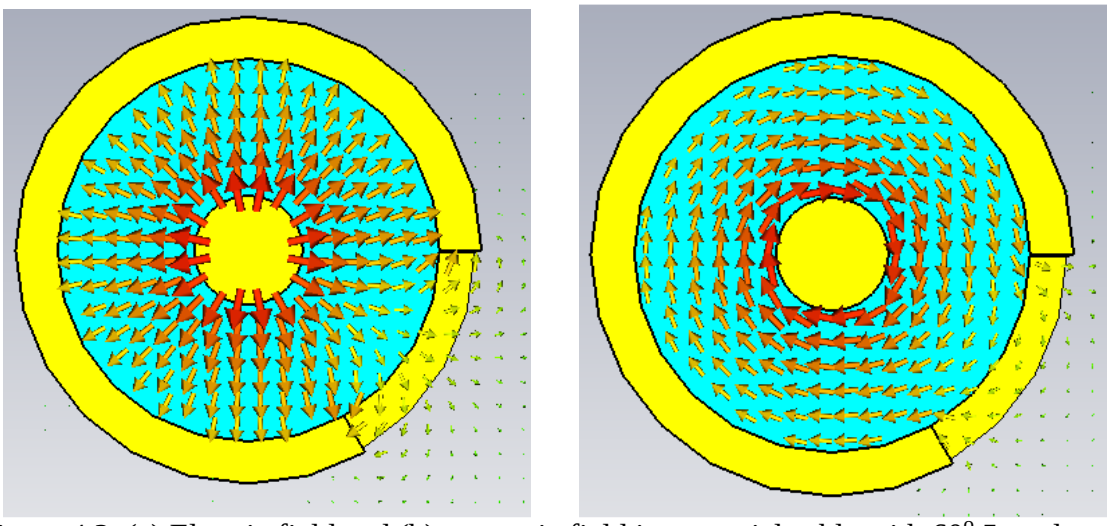

Figure 4.2 (a) Electric field and (b) magnetic field in a coaxial cable with 60^{o} 5 cm long cutaway

$$V_P = \frac{1}{\sqrt{\mu_0 \varepsilon}}, \tag{4–2}$$

where V_P is the velocity of propagation, ε is the dielectric constant of the insulation material and μ_0 is the permeability.

With CST's Quasi-TEM mode simulation, which combines the effects of both TEM and higher order modes, instead of using multistage processes (such FDM to calculate effective capacitance and derive the characteristic impedance), we can obtain the characteristic impedance of the fault directly. As shown in Figure 4.3, 13 different damages to the shield varying from 0 degree to 359 degrees were obtained using CST. By employing the polynomial curve fitting algorithm [37], we can plot the profile that represents the properties of the faulty shield. This profile represents the prediction of the fault severity of the chafed RG58 coaxial cable. A ninth order polynomial expression derived by Matlab® curve fitting toolbox can be written as (4–3)

$$Z(\theta) = p_0 + p_1 \cdot \theta^1 + \mathrm{K} + p_8 \cdot \theta^8 + p_9 \cdot \theta^9 = \sum_{n=0}^{9} p_n \theta^n \tag{4–3}$$

where θ is the cutaway angle in degrees and p_0~p_9 are constant coefficients.

Since the characteristic impedance is frequency dependent, we can generate a few more sets of data at different frequencies of interest and use the similar polynomial surface fitting algorithm to obtain the frequency depended characteristic impedance profile (3D) of the faulty RG58 as shown in Figure 4.4. Similarly, a characteristic impedance function of cutaway angle and frequency can be obtained as (4–4).

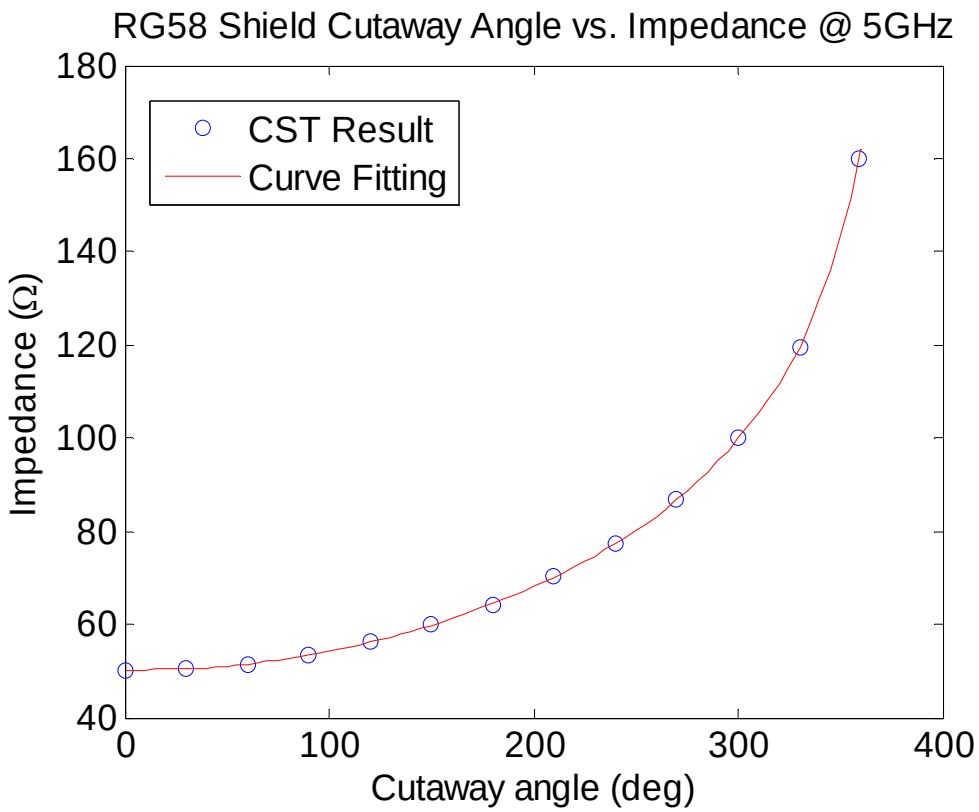

Figure 4.3 2D impedance profile of RG58 coaxial cable at the frequency of 5GHz.

$$Z = func(\theta, f) \tag{4–4}$$

Once this fault profile is defined, it can be reused again and again without further time-consuming simulations or calculations. This type of simple expression is particularly useful in inverse simulations that require hundreds or thousands of forward simulations. Additionally, field technicians can estimate the severity of the fault based on the fault profile equation (or chart) of each type of cable.

After the chafe profile is identified, the fault signature with TDR (or other reflectometries) can be predicted. A simple test setup is shown in Figure 4.5. A Campbell Scientific TDR100 is used as the test source. A shield cutaway 5 cm long and

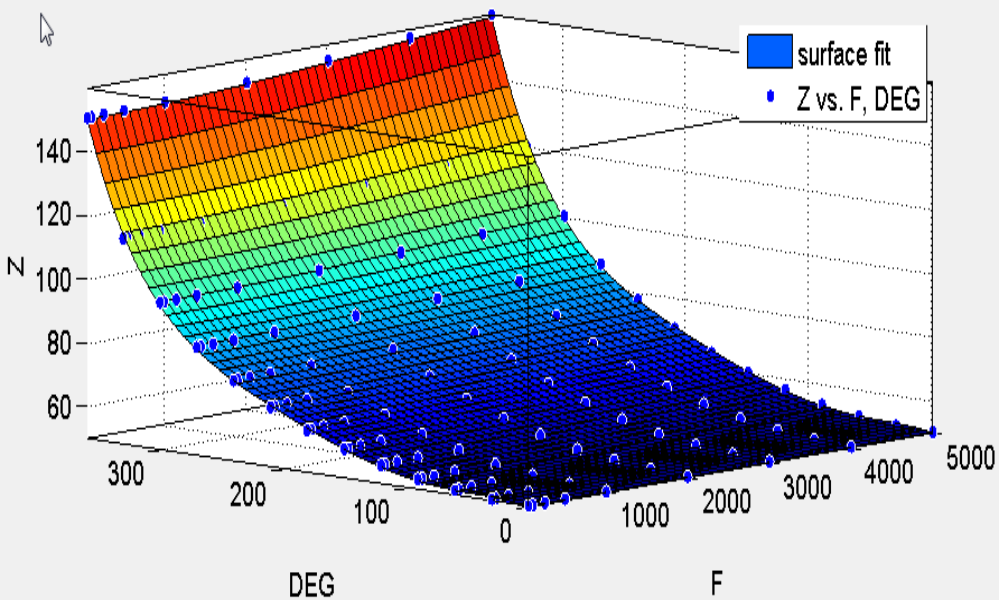

Figure 4.4 3D impedance profile of RG58 coaxial cable with frequency range from 1MHz to 5GHz

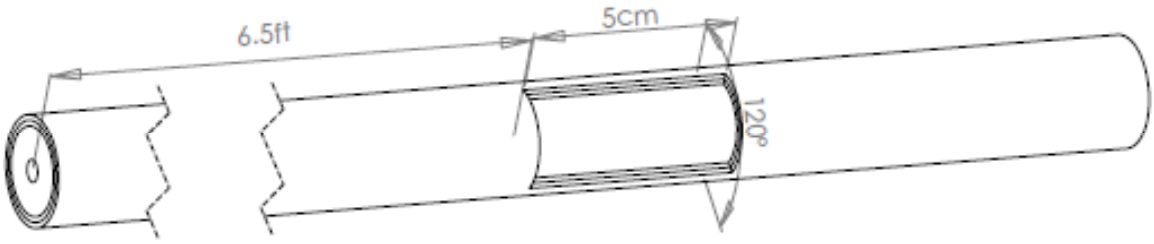

Figure 4.5 5 cm long, 120^{o} cutaway shield damage at 6.5 feet on a 12 feet long RG58

120^{o} wide at 6.5 feet of a 12 feet RG58 coaxial cable is demonstrated. To synthesize the TDR result of a chafed wire, one can launch a full 3D FDTD method for the entire wire. However, a more efficient frequency-domain ABCD method is used for this work. Instead of discretizing the wire into numerous FDTD cells, the ABCD method simply divides the entire structure into three sets of ABCD matrices, the good wire before the chafe, the chafe itself and the good section after the chafe. Other sections such as different types of wires, loads and connectors, could also be included.

4.4 Results

The TDR signature of the chafed wire is presented in Figure 4.6. The agreement between the measured and simulated results is excellent. If this simulation was done entirely in the 3D finite integration technique such as CST or HFSS, it would takes from minutes to hours to complete depending on the resolution and computer performance. With the defined fault profile and the assistance of the frequency domain ABCD method, the polynomial profile building method took less than a second to perform the same task. Additionally, with the defined fault profile, we can easily plot the prediction of 5 cm chafes of various angle cutaways on an RG58 cable at 6.5 feet. This is shown in Figure 4.7.

A simple yet effective wire fault profile building technique has been presented. Although only RG58 coaxial cable was demonstrated, this method can be applied to other types of transmission lines as well. Numerical modeling of multimode chafed transmission lines in 3D is a slow process, but it is one of the most precise techniques available for the quasi TEM mode. Once the simulation has been completed, the results can then be used to efficiently provide the values for inverse solutions.

The demonstrated method provides a quick solution for building a fault or chafe profile that can be used in libraries for forward or inverse solutions. The ABCD method can be combined with this approach to solve wire fault location problems quickly and efficiently Finally, efficient forward modeling is one of the key elements for the success of any inversion technique. With this profile building technique, numerical iterations can be reduced or possibly eliminated, where most of the inversion effort is spent.

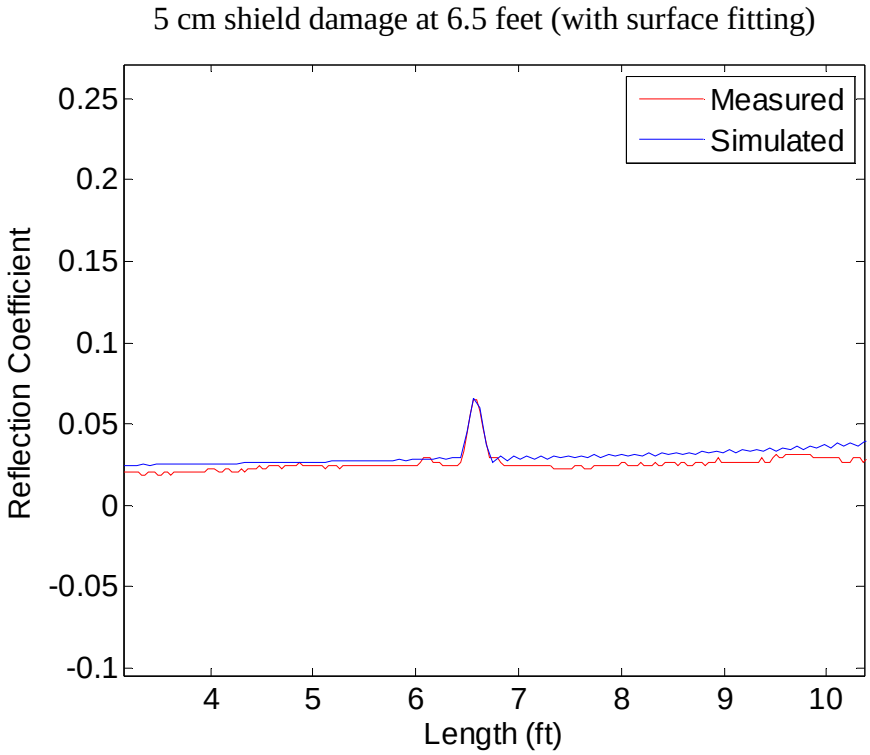

Figure 4.6 5 cm, 120^{o} shield cutaway at 6.5 feet on a 12 feet long RG58 coaxial cable.

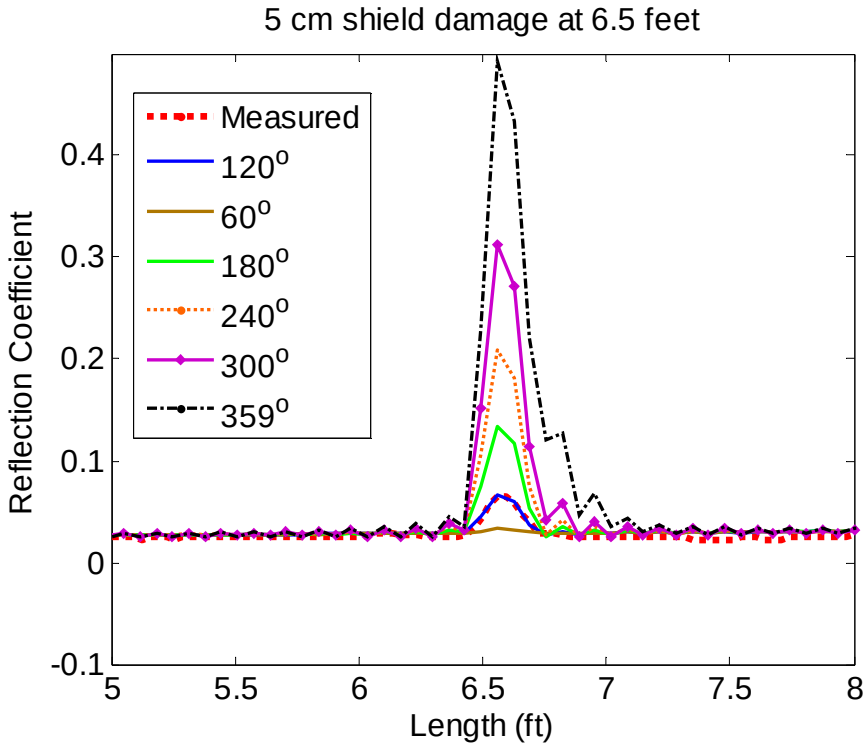

Figure 4.7 Prediction of fault signatures on a chafed RG58 cable with 5 cm long cutaway.

CHAPTER 5

INVERSE SOLUTION

5.1 Overview

Transmission line fault location typically requires an accuracy of a few inches (at most, 2 feet) while the total wire length can be longer than a few hundred feet. On top of these, the fault location and the nature of the fault are often unknown. For live wire applications, the magnitude of test signal is limited and destructive tests are usually not permitted. These requirements make a small fault on a long wire very difficult to detect and identify since the small reflections are often treated as noises.

When reflectometry is used, we need to be able to pull the reflection information from the fault (often small) out of the noise and other signature reflections from the normal wiring system. This requires an algorithm to 'invert' the data, identify the normal signature, and identify and diagnose the fault signature. This chapter is about possible inversion algorithms for wire fault location.

A great deal of work has been published in layer peeling model inversions in geophysical applications [38] - [40]. These algorithms are used to identify properties of an object that is deep in the ground. We will consider some of these techniques for wire fault location inversion algorithm.

A classical inverse problem can be described by an operator equation as (5–1) [41].

$$\boldsymbol{A}\boldsymbol{m} = \boldsymbol{d},\ \boldsymbol{m} \in \boldsymbol{M},\ \boldsymbol{d} \in \boldsymbol{D} \tag{5–1}$$

where $\boldsymbol{D}$ is the space of data, $\boldsymbol{M}$ is the space of model parameters and $\boldsymbol{A}$ is the operator of the forward model that calculates the proper data $\boldsymbol{d} \in \boldsymbol{D}$ for the given model parameter $\boldsymbol{m} \in \boldsymbol{M}$. In transmission line reflectometry, $\boldsymbol{D}$ can be a collection of measured TDR, STDR or SSTDR signature/data. $\boldsymbol{M}$ could be the physical wire/fault properties such as wire length, impedance or wire size. The model operator, in this example, would be the forward modeling technique such as the ABCD method, S-parameters or bounce diagram.

In a forward problem, the goal is to obtain the data $\boldsymbol{d}$ (reflectometry signature) with given model parameter $\boldsymbol{m}$ (the physical properties of a wire system including fault). In contrast, the goal of an inverse problem is to obtain the model parameter $\boldsymbol{m}$ with given data $\boldsymbol{d}$. A well-posed problem defined by Hadamard [42] must meet all three of the following conditions:

1. The solution exists. (We can define a wire system that produces the measured reflectometry signature.)
2. The solution is unique. (There is only one system that could produce this signature and it is not true for symmetrical systems.)
3. The solution depends continuously on the data. (There is no element of the wiring system that does not contribute to the reflectometry response. For

instance, parts of the system that are beyond a break of short circuit will not show up.)

For a well-posed problem that meets all three Hadamard's conditions, the model parameter $\boldsymbol{m}$ can be obtained inversely as displayed in (5–2).

$$\boldsymbol{m} = \boldsymbol{A}^{-1}\{\boldsymbol{d}\}, \tag{5–2}$$

where $\boldsymbol{A}^{-1}$ is the inverse operator of the problem. Although it may not always be trivial, the inverse solution can be found mathematically if Hadamard's well-posed definitions are met. A noiseless single-section TDR inverse problem with only one unknown parameter (length) is usually one of the more trivial well-posed inverse problems and the solution can be found analytically. Unfortunately, most practical inverse problems including those in wire fault location are ill-posed, in which at least one of the Hadamard's conditions is not met. A common solution is to utilize some type of iterative numerical method where highly efficient forward solution is used. This chapter discusses both analytical and numerical inversion techniques and their applications to both well-posed and ill-posed problems found in wire fault location.

5.2 Analytical Inverse Solution

The inverse solution, which takes the measured reflectometry data and determines the location and nature of a wire fault, is much more difficult than a forward problem (a wiring system is given, and the nature and location of the fault is known), where finding the expected reflectometry response is the main task.

In this section, we will use an analytical expression for the expected reflectometry response and solve it directly (analytically) for the transmission line system. This is feasible only for very simple transmission line systems, but it provides a good start for many reflectometry analyses.

Figure 5.1 shows a simple single section open-ended RG59 coaxial cable of length l (2.8 meters). In this simple inversion, we will assume the length (distance to the open circuit, which might be a break in the wire) is unknown and needs to be identified. From (3–17), the TDR transfer function of a single-section configuration can be derived as (5–3)

$$H(\omega) = \frac{\cosh \gamma(\omega) \mathrm{l}}{\cosh \gamma(\omega) \mathrm{l} + \frac{Z_0}{Z_1} \sinh \gamma(\omega) \mathrm{l}} = \frac{e^x + e^{-x}}{C_1 e^x + C_2 e^{-x}} \quad (5\text{–}3)$$

,

where

$$C_1 = (1 + \frac{Z_0}{Z_1}) \quad (5\text{–}4)$$

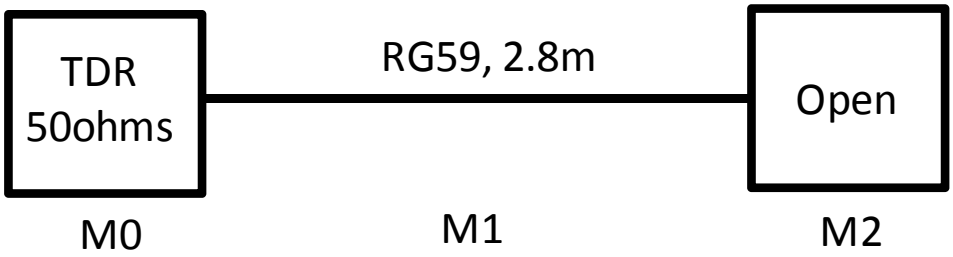

Figure 5.1 A simple single section of 2.8 m long RG59 coaxial cable configuration with an open end

$$C_2 = (1 - \frac{Z_0}{Z_1}) \tag{5–5}$$

$$x = \gamma(\omega)\mathrm{l} \tag{5–6}$$

$$\gamma(\omega) = \sqrt{(R' + j\omega L')(G' + j\omega C')} \tag{5–7}$$

The physical properties of the transmission line are identified; thus R', L', G' and C' can be calculated accordingly. The only unknown parameter in (5–3) is the wire length l, which can be solved analytically as (5–8). Since the transfer function H is a function of frequency, each frequency may produce a slightly different l, this dissertation handles this by taking the average of l produced by all the frequencies.

$$\mathrm{l} = \frac{1}{2\gamma} \ln\left(\frac{1 - HC_2}{HC_1 - 1}\right) \tag{5–8}$$

For a simple single section setup with low or no noise, this inversion problem is well-posed and the analytical inverse solution can be derived mathematically. However, in real world applications, the measured data are noise contaminated. As shown in Figure 5.2, analytical inverse solutions were performed on this single section setup at the signal to noise ratio (SNR) equals to 100dB to 45dB with a step of -5dB. Each solid dot represents the average (mean) for the step, which includes 100 inverse solutions. The upper end of the vertical error bar shows the maximum length revealed during the 100

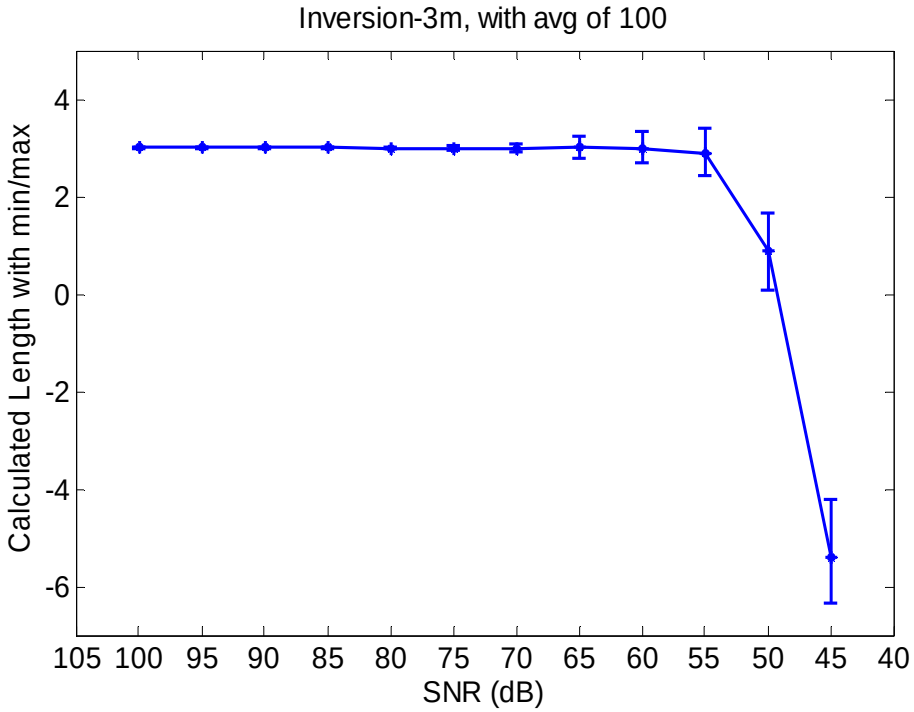

Figure 5.2 The result of single section analytical inversion - noise contaminated. Each step from SNR=100dB to 45dB represents 100 tests. The solid dots represent the mean of each step. The upper end of the vertical error bar indicates the maximum calculated length while the lower end of the error bar show the minimum calculated length.

inverse solutions while the lower end of the vertical error bar indicates the minimum length revealed within the 100 inverse solutions. The fault location can be retrieved precisely up to an SNR equals to about 55dB.

This example shows that the performance of this (and any other) inversion technique depends heavily on the SNR. The noise contributed here can come from the signal source, external interference coupling, variability in the test hardware, or from other normal reflections on the wire. The first three can be reduced by averaging and filtering, but the last one cannot. Therefore, the application of this theoretical method is limited at a low noise environment in simple configurations.

5.3 Scanning Approach

5.3.1 Linear Search Method

Although the analytical inversion method can come in handy for simple configurations, it would not be feasible to calculate the inverse functions analytically for more complicated setups since the mathematical difficulty can grow dramatically. Figure 5.3 shows a two-section setup with both wire lengths unknown. Its transfer function is shown as (5–9).

$$H=\frac{\cosh\gamma_1 l_1\cdot\cosh\gamma_2 l_2+Z_1Y_2\sinh\gamma_1 l_1\cdot\sinh\gamma_2 l_2}{\cosh\gamma_1 l_1\cdot\cosh\gamma_2 l_2+Z_1Y_2\sinh\gamma_1 l_1\cdot\sinh\gamma_2 l_2+50\cdot(Y_1\sinh\gamma_1 l_1\cdot\cosh\gamma_2 l_2+Y_2\cosh\gamma_1 l_1\cdot\sinh\gamma_2 l_2)} \quad (5–9)$$

Solving the inverse function analytically in this example is no longer feasible since there are two unknowns (l_1 and l_2) with only one equation. One way to find the two unknowns with only one equation is to scan the possible values of l_1 and l_2 successively and plug them back into (5–9). With the transfer function and possible l_1 and l_2 values, we can further utilize the ABCD forward method to generate an array of forward solutions. Finally, by comparing the correlation (similarity) between the simulated reflectometry result and measured data, a map of correlation can be generated as shown in Figure 5.4.

This is a 2-D scan showing possible choices of l_1 and l_2 in addition to the correlation between the measured and predicted reflectometry responses. It can be seen that the highest correlation points follow a line. This is not a coincidence as this line represent the total length of the wire ($l_1 + l_2$).

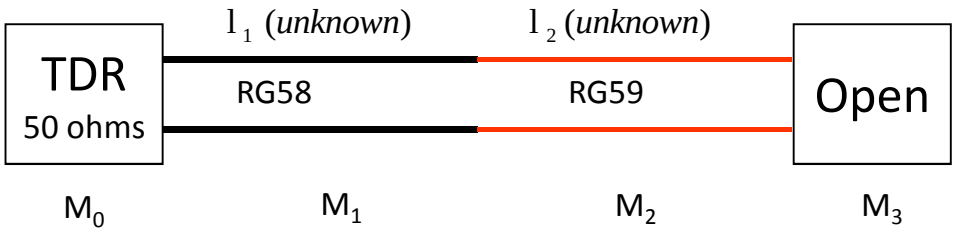

Figure 5.3 Two section configuration with both wire lengths (l_1 and l_2) unknown.

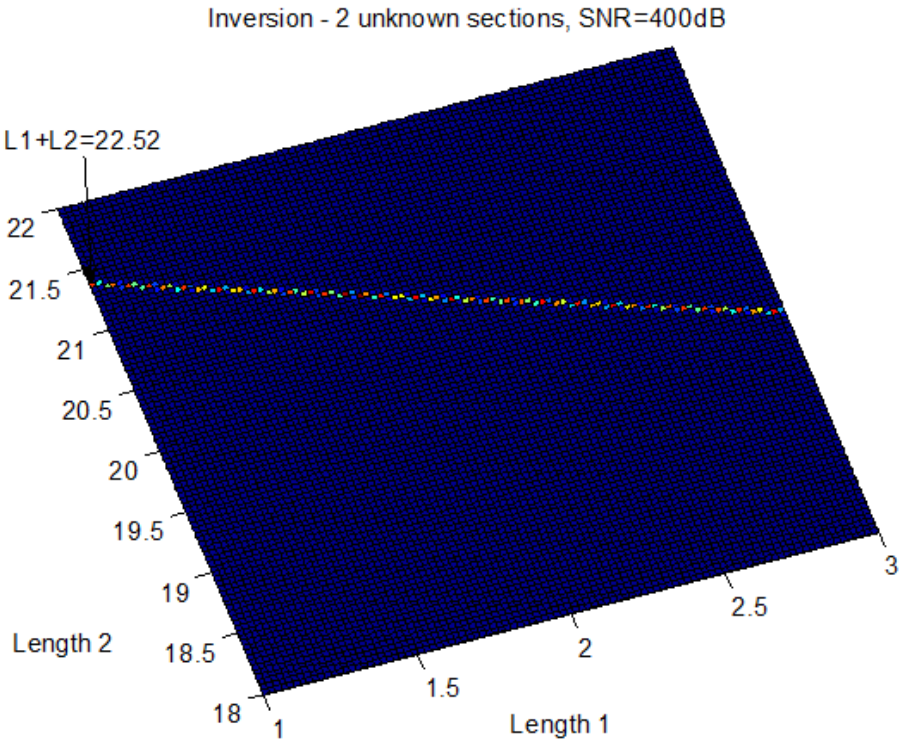

Figure 5.4 Two section inversion result of two-dimensional scanning method.

If we then have a wire with N sections, the total number of scans needed to check every possibility becomes N^2. However, if we scan only the values along the total length of the line (either measure of known priori the total length of the wire), the number of scans and calculations can be reduced to N. This is a linear search inversion method. In cases where noise exists, we can expand the line (search a wider region around this line) and it can still significantly reduce the number of calculations.

This linear search is one of the easiest inversion methods to apply in numerical techniques. Although it is not very efficient, given sufficient resolution, this method is still capable of finding the solution if it exists. This linear search method was tested on a configuration shown in Figure 5.5. There is a single section 12-foot long RG58 cable. A 5 cm long 60^{o} chafe is made in the shield 6.5 feet from the TDR tester (TDR100).

A trivial way to find the fault location is to scan linearly from the beginning to the end of the RG58 coaxial cable. Assuming the fault size (5 cm) is known or estimated, with the resolution of 10 cm per step, a 12 feet (3.68 m) wire would take 368 scans (steps) in order to identify the fault location. At each step, the forward result (predicted reflectometry response for that configuration) is generated and compared with the measured data and the correlation coefficient is recorded. Figure 5.6 shows the correlation coefficient of this linear search approach. The result demonstrates that the correlation coefficient peaks at 6.5 feet.

From the outcome of the linear search, a forward model is created as shown in Figure 5.7. This linear search method seems to work for simple cases. However, in complicated problems (e.g., multisection configuration or long wire with small faults), this method is not very efficient. Therefore, a more efficient method is desired.

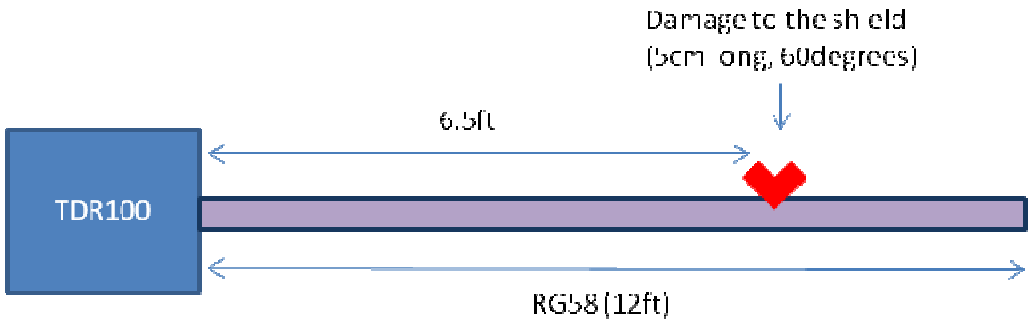

Figure 5.5 A 5 cm long, 60^{o} shield cutaway at 6.5ft on a 12-foot RG58 coaxial cable

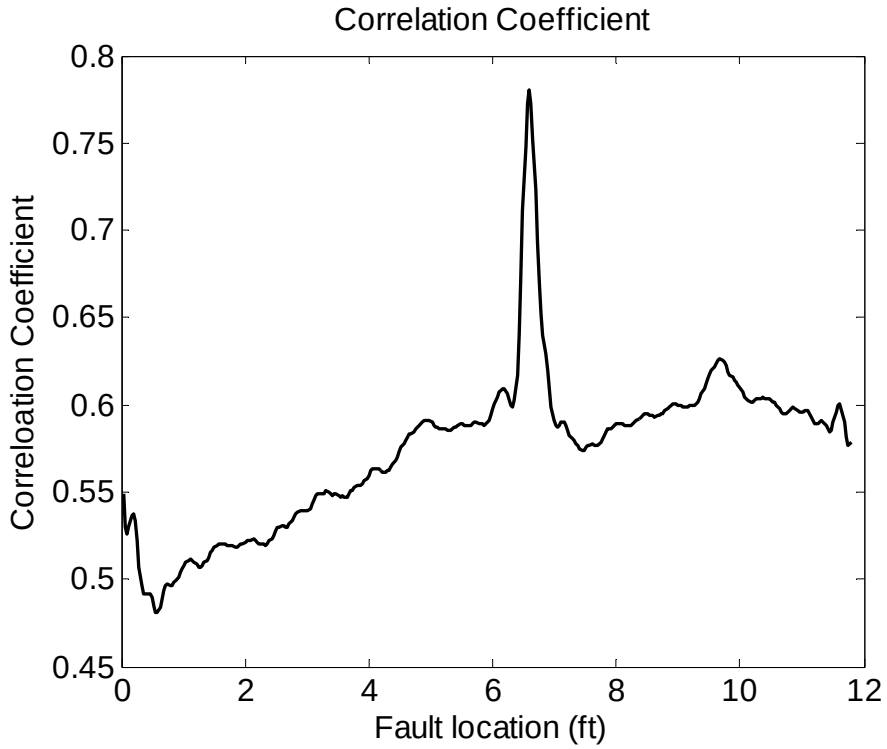

Figure 5.6 The correlation result of the linear scan method on a 5 cm, 60^{o} cutaway at 6.5 feet on a 12-foot-long RG58 coaxial cable.

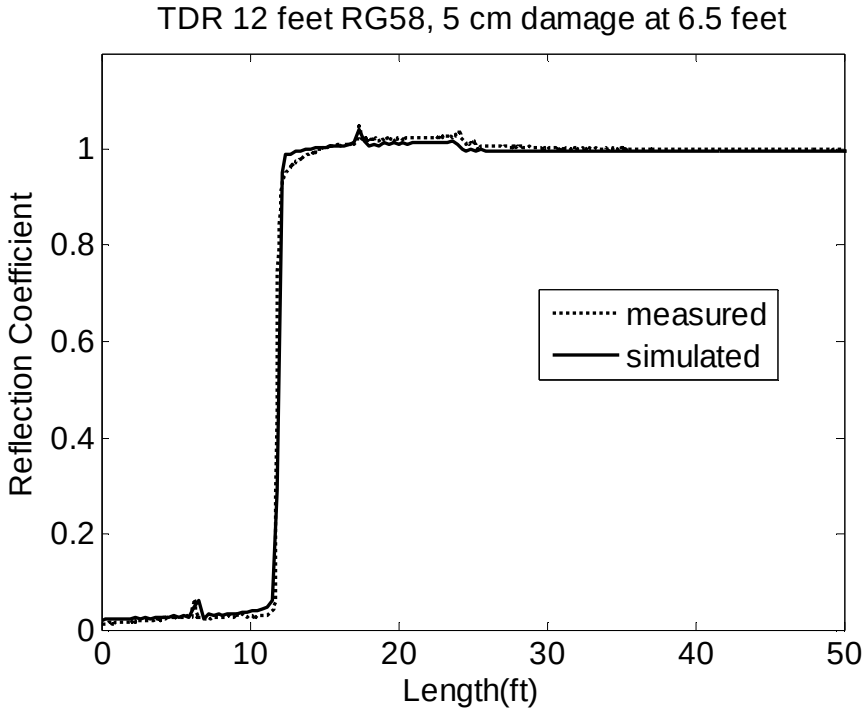

Figure 5.7 The simulated and measured result of a chafe on an RG58 coaxial cable.

5.3.2 Progressive Binary Search Method

To improve the efficiency of the search algorithm, a progressive binary search method is used. It is similar to the binary search in computational data structures [43]. Without knowing the fault size, we can start with a large estimated fault size and coarse resolution. For the same example presented in Figure 5.5, say we start with an estimate fault size to be 2 feet long and the scanning resolution to be 1 foot long. The correlation coefficient is shown in Figure 5.8 for various assumed locations of the fault.

Instead of 6.5 feet where the fault is actually located, the peak correlation coefficient is shown at 5 feet. That would be an acceptable error, using a resolution of one foot and the initial (incorrectly) assumed fault length of 2 feet long. With this combination of assumptions and resolutions, we should expect a maximum error of 3 feet. The reconstructed TDR result after the first iteration of the progressive binary search method is shown in Figure 5.9.

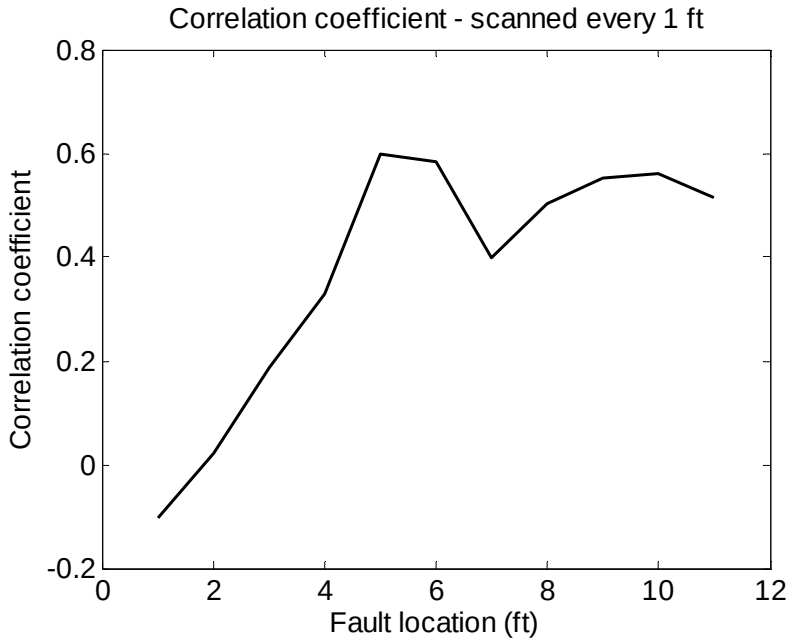

Figure 5.8 First iteration with 2 feet long fault size and 1 foot long step resolution.

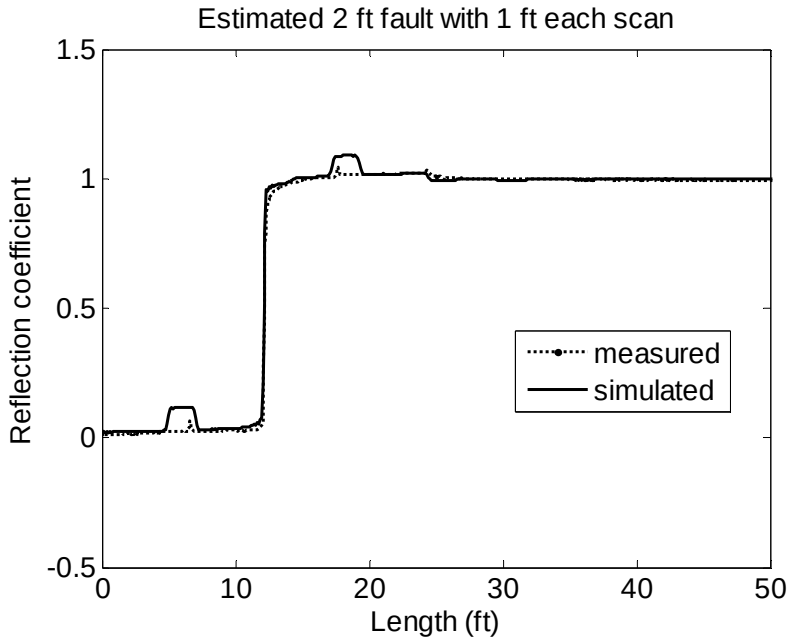

Figure 5.9 The first iteration TDR result of the progressive binary search method.

If the reconstructed result has a greater fault (higher reflection) than the measured data, this is clear from the overestimate of the size of the peaks in the predicted reflectometry response. We then reduce the fault width to half in the next iteration; otherwise, the fault width remains the same. Additionally, by searching the locations with the highest 50% of the correlation coefficient, we can reduce the scanning effort by 50% for the next iteration. The correlation coefficient and reconstructed results after the second, third and fourth iterations are shown in Figure 5.10.

The number of scans required for the progressive binary search is 36 compared to the previous linear search method, which needs 368 scans. This binary search method is significantly more efficient than the linear search method. The flow chart of the progressive binary search method is displayed in Figure 5.11. This method significantly improves the efficiency over the linear scan method. However, for more complicated problems, this method often fails. Therefore, a more robust method is needed.

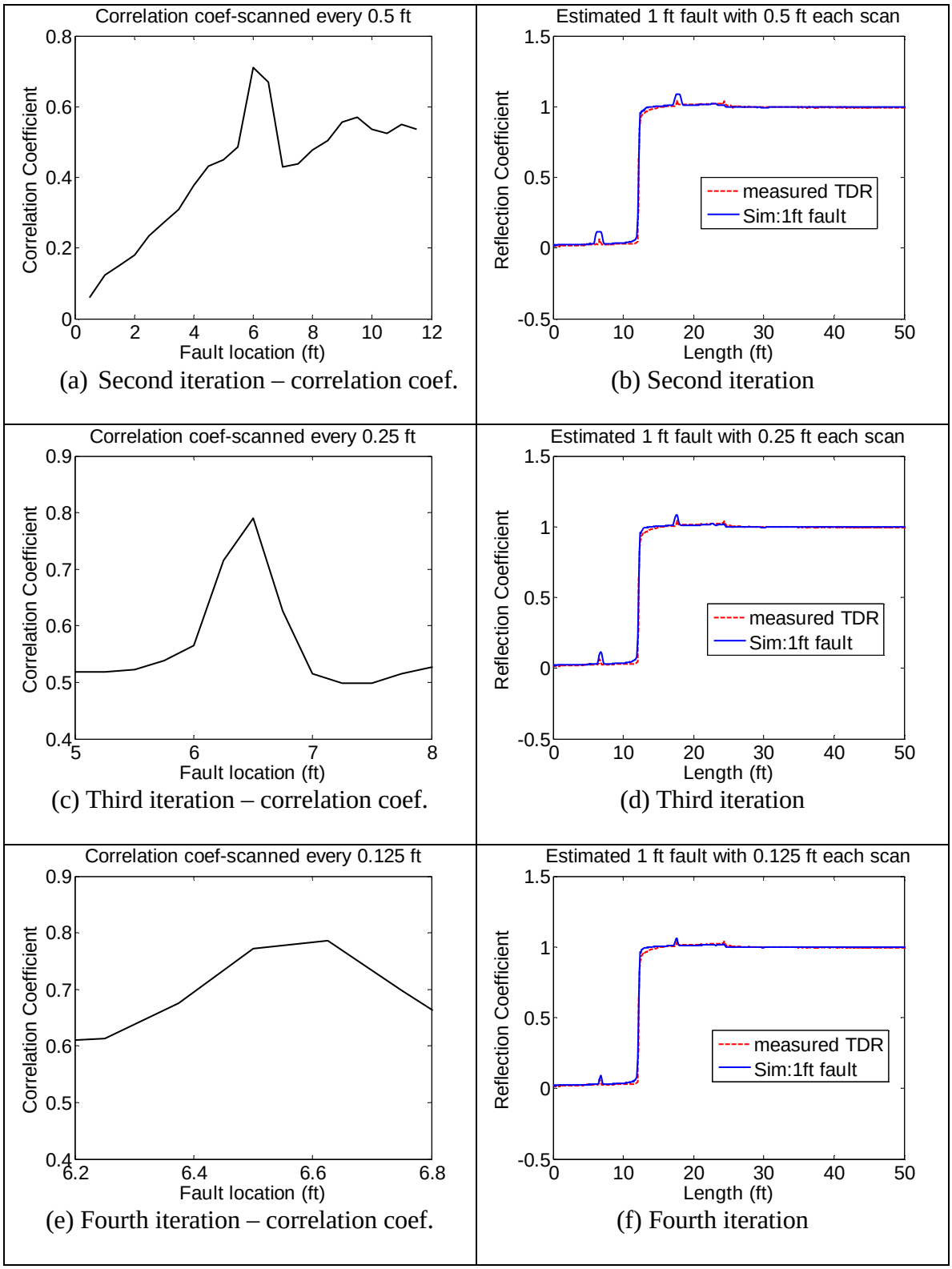

Figure 5.10 Correlation coefficient and reconstructed signal after the second, third, fourth binary search iterations for a 12 feet wire with a 5 cm, 60^{o} chafe at 6.5 feet.

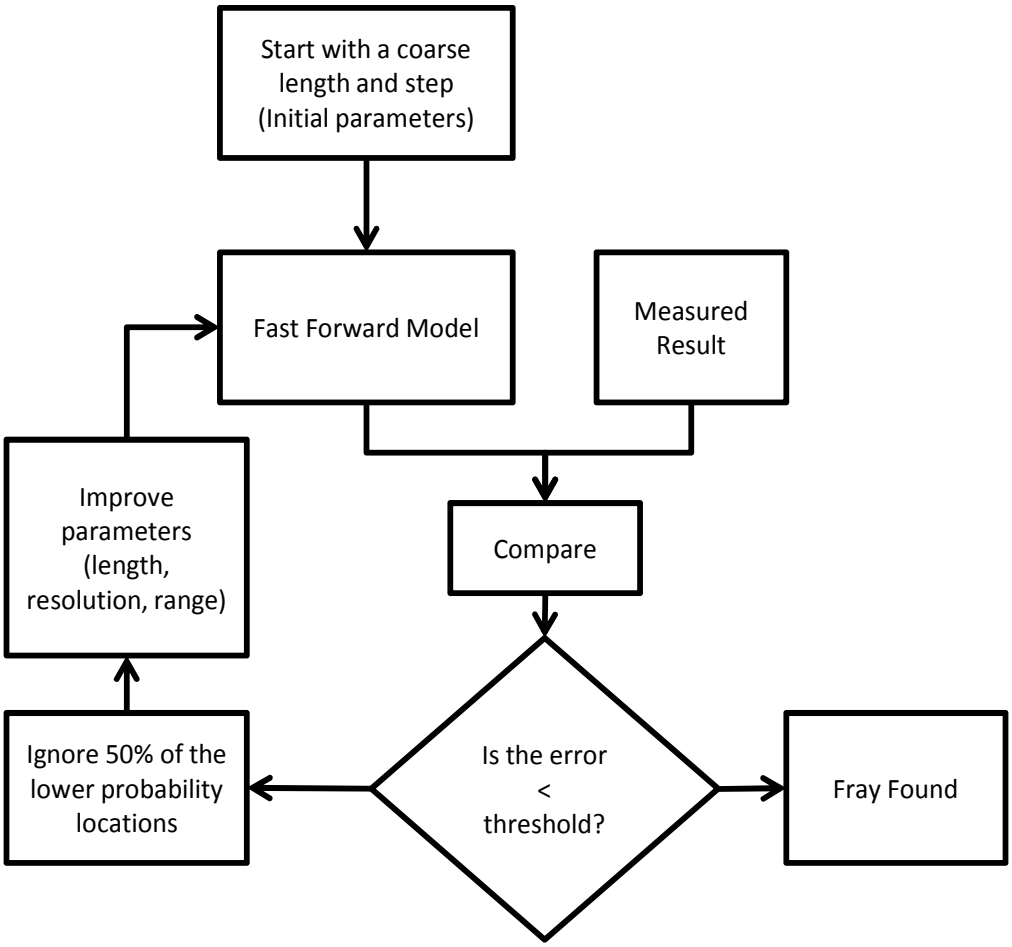

Figure 5.11 Flow chart of the progressive binary search method.

5.4 Iterative Inversion

The iterative inversion and reconstruction algorithm block diagram is shown in Figure 5.12. To an extent, it is similar to some of the other numerical inversion methods described in [44] - [46].

An efficient and accurate forward solver that can produce high fidelity forward results is critical for this iterative method (also most other inversion methods). This forward solver simulates the "behavior" of the system. Thus, once we plug in the proper system parameters, the outcome of the forward solver and the measured data should be highly alike. Ideally, with a noise-free measurement and perfect forward model, they

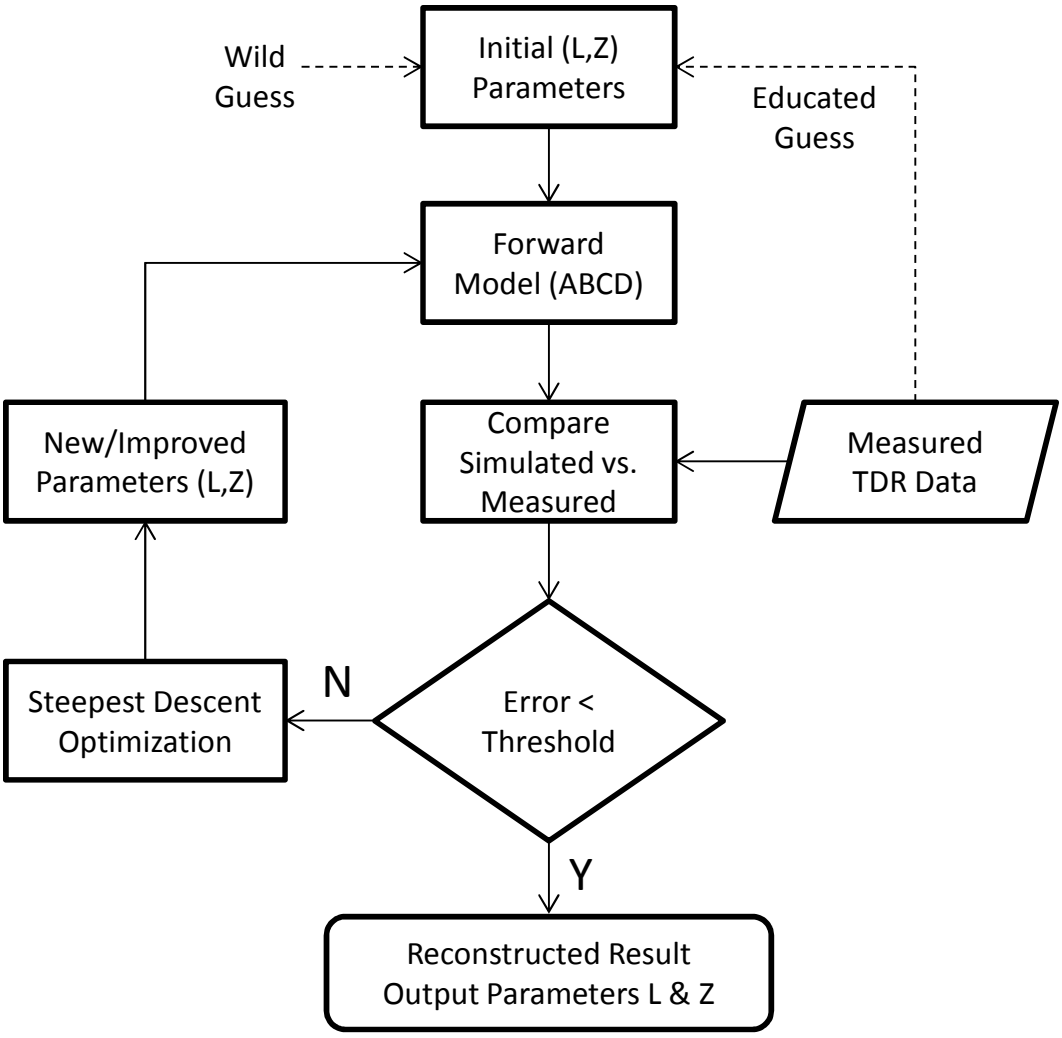

Figure 5.12 Iterative inversion and reconstruction algorithm block diagram

would be identical. From the previous chapters, the ABCD forward modeling method has proven to be efficient and accurate, and it will be used in this section of the dissertation.

The velocity of propagation (VoP) is the traveling speed of electromagnetic waves in a transmission medium. The VoP in free space (vacuum) is the speed of light as shown in (5–10), where μ_0 is the permeability in the vacuum and ε_0 is the permittivity in the vacuum.

$$VoP = \frac{1}{\sqrt{\mu_0 \varepsilon_0}} = c \approx 3 \times 10^8 \ \ m / s \tag{5–10}$$

The electromagnetic waves also propagate at different speeds in different mediums. Most of the transmission line materials have the same permeability as in the vacuum. (5–10) can be rewritten as (5–11) where ε_r is the relative permittivity (dielectric constant) of the transmission line material.

$$VoP = \frac{c}{\sqrt{\varepsilon_r}} \tag{5–11}$$

RG58 coaxial cables typically use polyethylene (PE) as the dielectric insulator. The dielectric constant of the polyethylene is 2.25 [47]. That makes the velocity of propagation on an RG58 coaxial cable to be 66% of the speed of light (0.66*c). In this chapter, we shall use the VoP on an RG58 as the basis, or normalization factor for all wire sections.

Consider a multisection transmission line setup with a total “normalized length” of 10.9 m as shown in Figure 5.13. Note the normalized length does not always equal the physical length of the wire since wires may have different velocities of propagation. In this case, the velocity of propagation is assumed to be 0.66*c, where c is the speed of light.

The number of sections, length of each section and characteristic impedances are all initially assumed to be unknown. Only the load (open) and total length are known.

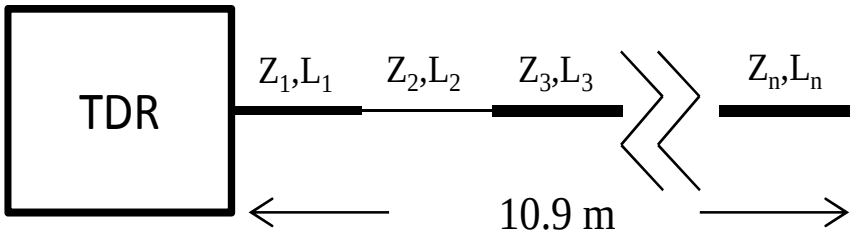

Figure 5.13 A multisection configuration. From left to right: RG58 (3m), RG62 (1.9m), RG59 (2.4m) and RG58 (4m) respectively – All lengths and characteristic impedances are assumed to be unknown.

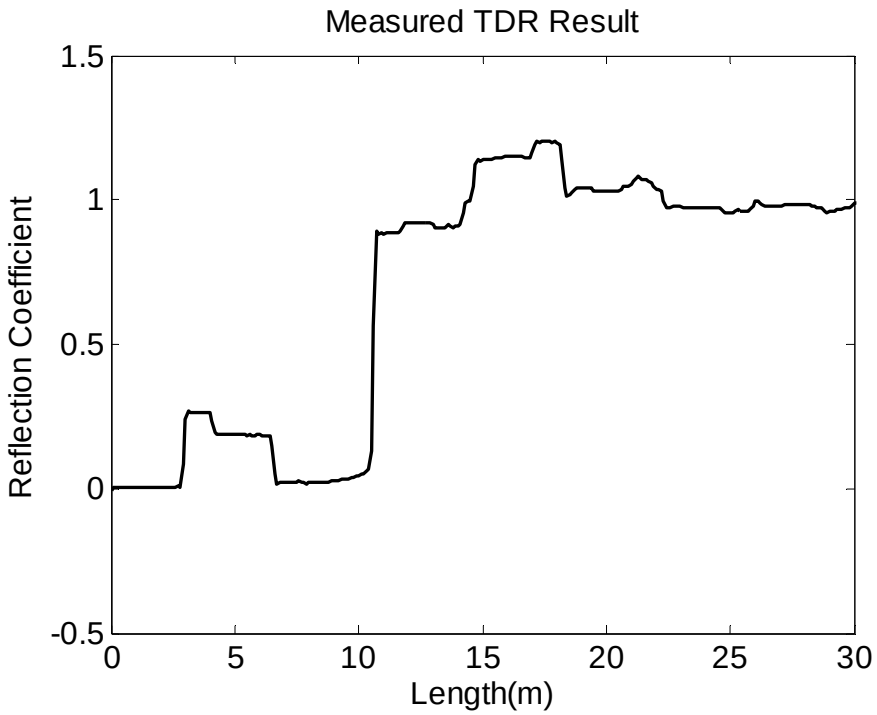

Figure 5.14 Measured TDR result on the multisection configuration.

These parameters can either be previously determined or estimated from the measured TDR data.

A 50-ohm TDR tester (Campbell Scientific TDR100) that generates a sharp rising edge step signal is used as the signal source and the measured result is displayed in Figure 5.14. The objective is to identify the number of sections, length and characteristic impedance of each section of the cable based on the measured data.

The inversion process starts off by dividing the transmission line into numbers of small segments as shown in Figure 5.15. For simplicity, the 10.9 m long wire is divided into 109 10-cm long segments. This number can be further increased if higher resolution is needed.

Next, we assume each of the 109 segments has uniform characteristic impedance, say 60 ohms. Although the initial characteristic impedance can be any reasonable positive real number, an educated guess would improve the convergence performance.

Ideally, instead of assuming a blanket value of characteristic impedances across all the frequencies on all wire segments, it would be the best if we can specify the characteristic impedances as functions of frequency. This is due to the characteristic impedances of electrical wires are frequency dependent. However, since the physical and electrical properties of the wire segments and the size of the fault are all unknown, it would not be possible to produce such frequency dependent functions. Therefore, the best approach is to assume the characteristic impedances are constant across the frequency band of interest.

The initial estimation of length L and characteristic impedance Z profile is shown in Figure 5.16, and the reconstructed signal (using ABCD forward method) versus measured result is shown in Figure 5.17. Not surprisingly, the initial reconstructed signal has little similarity to the measured result.

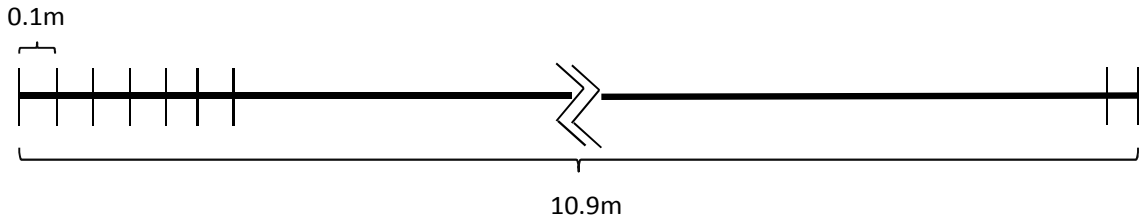

Figure 5.15 Dividing the wire into numerous small sections.

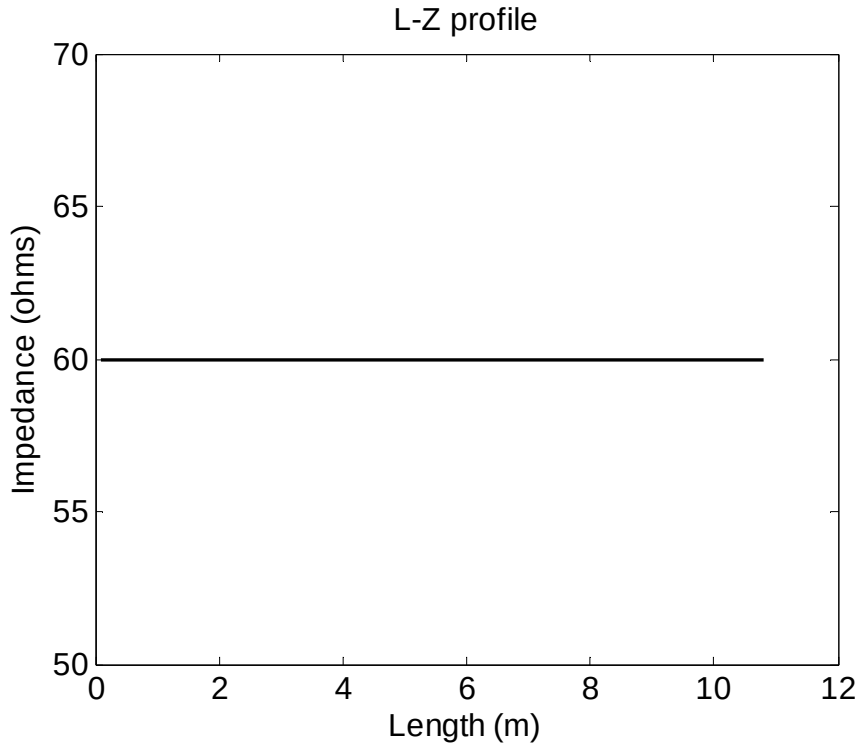

Figure 5.16 L (length) and Z (characteristic impedance) profile of the initial estimation

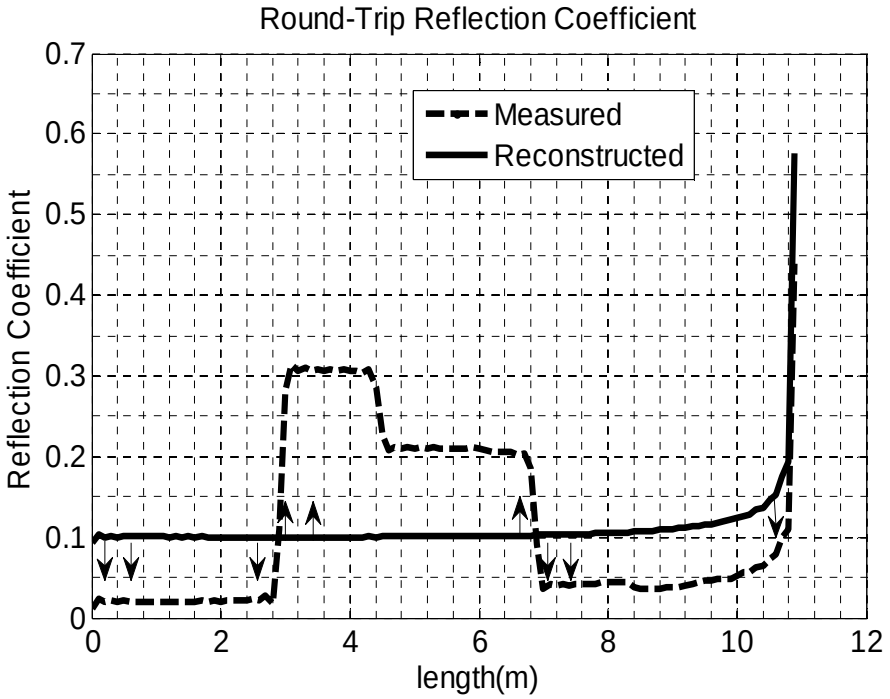

Figure 5.17 Measured result (dashed line) versus first iteration result (solid line) with Z=60 ohms assumed for sections.

For each of the 109 individual small segments, we compare the reconstructed signal (dashed) against the measured result (solid). If the reflection coefficient of the reconstructed signal is smaller than the measured result, it indicates that the characteristic impedance of such section was under estimated. Thus, we need to increase the characteristic by a certain amount, say one ohm, for that segment in the next iteration. In contrast, if the reflection coefficient of the reconstructed signal is greater than the measured data, it shows that the characteristic impedance was over estimated. Therefore, we have to decrease the characteristic impedance in the next iteration. If the difference between the reconstructed signal and measured data is within a preset error, the characteristic impedance is kept intact for the next iteration.

After 50 iterations, the length and characteristic (L-Z) profile is shown in Figure 5.18, which has revealed a four-section structure with lengths of L_1=3m, L_2=1.5m, L_3=2.4m and L_4=4m respectively. The characteristic impedances of Z_1=51 ohms, Z_2=92 ohms, Z_3=73 ohms and Z_4=51 ohms are also revealed.

The reconstructed and measured results are shown in Figure 5.19 and very good agreement is obtained. Note that the second section of the reconstructed signal is identified to be 1.5 m instead of 1.9 m, its actual length. This is due to the fact that RG62 used in this section has higher velocity of propagation (VoP) than RG58, which is 66% of the speed of light (c). Instead of VoP=0.66*c in RG58 and RG59 cables, RG62 has a VoP of 0.84*c. The physical length is then found denormalizing the wire length. In this case, by multiplying the calculated length of 1.5 m by 0.84/0.66, the correct physical length of 1.9 m is obtained.

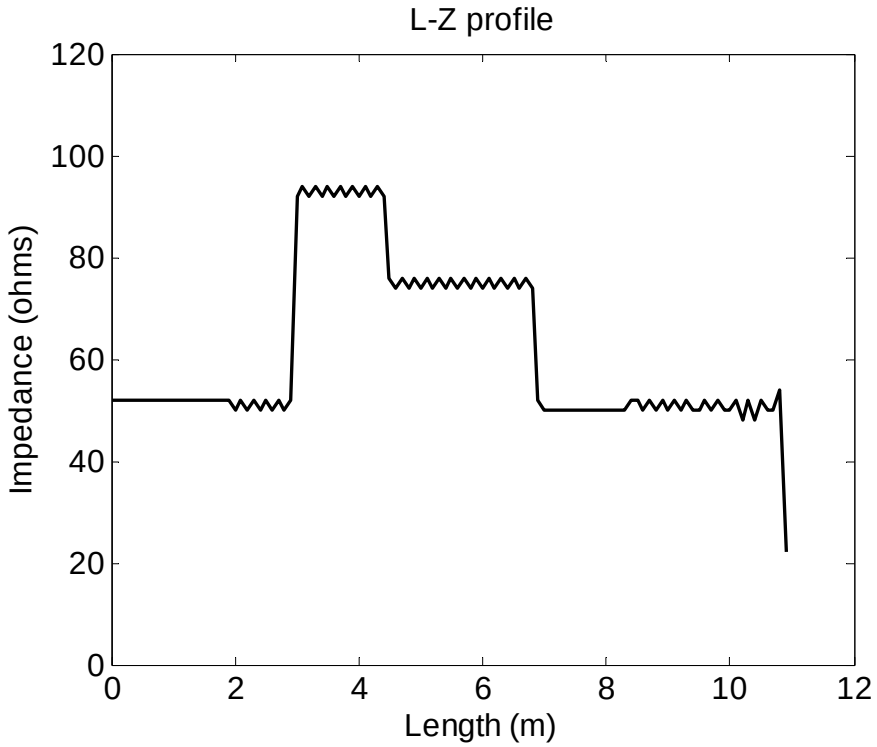

Figure 5.18 The L-Z profile (estimated length and impedance) after 50 iterations with 1 ohm per step.

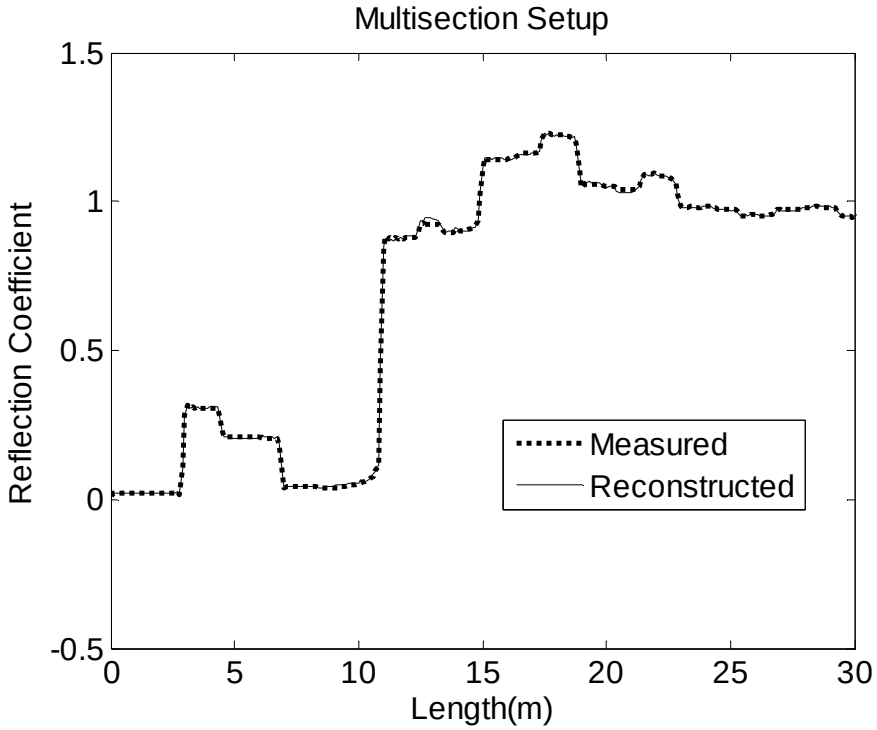

Figure 5.19 The measured result versus reconstructed result after 50 iterations

5.4.1 Applying Steepest Descent Optimization Method

The iterative inversion method described above gives good inversion results with reasonable efficiency as long as we start with a good initial guess. If we start with a poor guess, especially for a complicated system with many sections, this method breaks down. Additionally, the L-Z profile tends to oscillate with this method, especially toward the end of wire. If the impedances in the sections closest tester are not perfectly predicted, this causes incorrect multiple reflections in the later sections.

In addition to the fluctuation, the convergence efficiency of the iterative inversion method is quite low. That is, we can approach our objective linearly only by 1-ohm per iteration. If the initial estimation was way off, it would take a very long time to converge.

A classical, but effective steepest (gradient) descent optimization method [47] can resolve many of these problems. For a defined and real function ***F***, in the neighborhood of a point x in the direction of the negative gradient of $x - \nabla F(x)$, we can find an

$$x_{n+1} = x_n - \gamma_n \nabla F(x_n), \;\; n \geq 0 \qquad (5\text{–}12)$$

where the step size γ is a real number that determines the speed of convergence. If γ is too small (underestimated), this method converges slowly. On the other hand, if γ is too large (overestimated), the convergence may oscillate or may not converge at all. Therefore, choosing a proper γ is critical for optimization. For TDR inversion, our changing variable is the characteristic. The steepest descent function in (5–12) can be rewritten as (5–13).

$$Z_{n+1} = Z_n - \gamma_n \nabla \Gamma(Z_n) \qquad (5\text{–}13)$$

Applying the steepest descent method with the step size γ=110, the convergence efficiency has improved significantly over the iterative inversion discussed in section 5.4. As shown in Figure 5.20, after only 10 iterations, the L and Z profile has achieved the result that is better than the iterative method with 50 iterations shown in Figure 5.18. The reconstructed and measured data also match better, as shown in Figure 5.21 (for steepest descent) compare to Figure 5.19 (for straight iterative method).

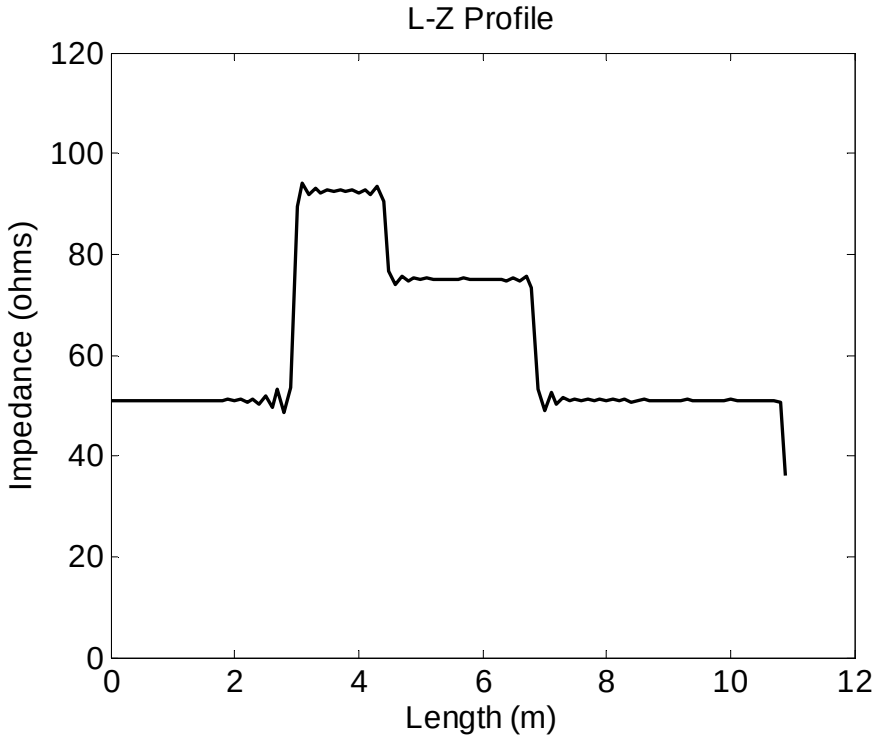

Figure 5.20 L and Z profile after 5 iterations using steepest descent optimization with converging constant γ = 110.

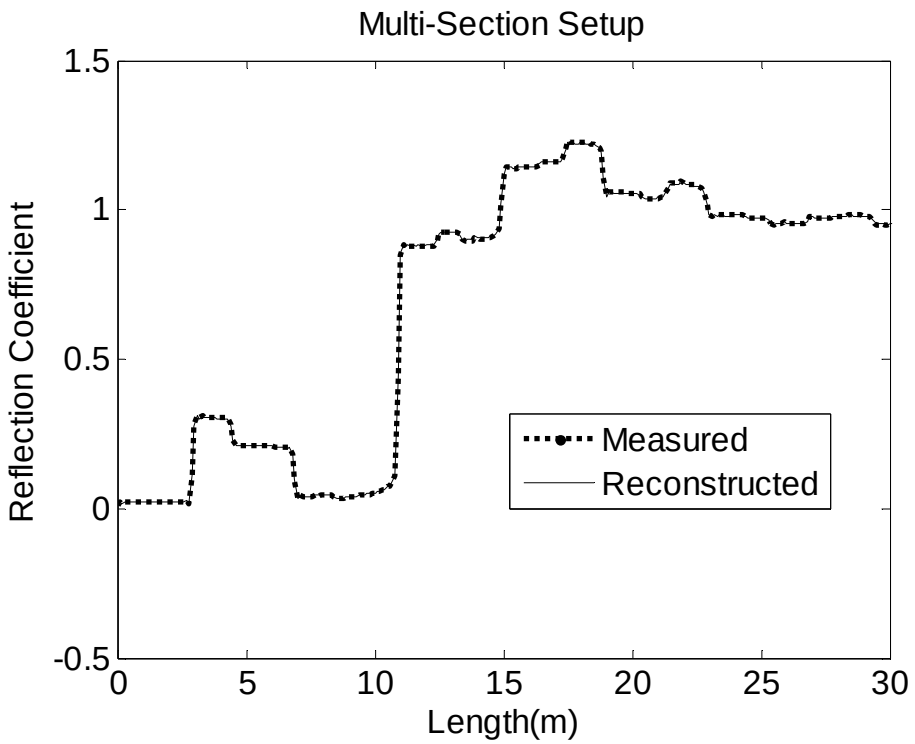

Figure 5.21 The measured versus reconstructed result after 5 iterations using steepest descent with converging constant γ = 110.

5.4.2 Using Iterative Inversion on Frays

Frays on transmission lines are more difficult to identify than the large reflections caused by changes in wire types or significant loads, breaks or short circuits. In addition to their small reflection coefficients that might be buried in measurement noise, the short lengths of most frays also make the detection challenging. A very high frequency TDR would be needed to identify frays. The maximum wire length that could be tested would be reduced, because the high frequencies needed for the fault resolution attenuate quickly on wires, but for now, we will assume a good match between TDR frequency, fault size and distance to fault exists, and concentrate on the algorithm that could be used to locate the fault.

Because the fray is small in size, we must increase the resolution in the search algorithm. Figure 5.22 shows a 3.59 m long RG58 coaxial cable with a chafe that is 1.9 m away from the TDR tester (beginning of the wire). The chafe is 5 cm in length and 120^o cutaway on the shield. The iterative inversion algorithm divides the entire wire into 359 1-cm-long sections. As before, we start with an initial guess of uniform characteristic impedance of 60 ohms for all sections. After 10 iterations, the L and Z profile is shown in Figure 5.23, which identifies a small fault of 5 cm located at 1.9 m from the TDR. The L-Z profile reveals that the characteristic impedance of the fray is roughly 60 ohms. This inversion method shows the characteristic impedance, but not the physical size or the nature of the fault. By evaluating the width of the L-Z profile at length of 1.9 m, a fault size of 5 cm long, 60 ohms impedance is discovered. From [16], we can quickly determine the damage to be 120^o cut on the shield. Figure 5.24 shows the comparison between the measured and reconstructed result. The results are closely matched even with the small reflection coefficient in a noisy measured data.

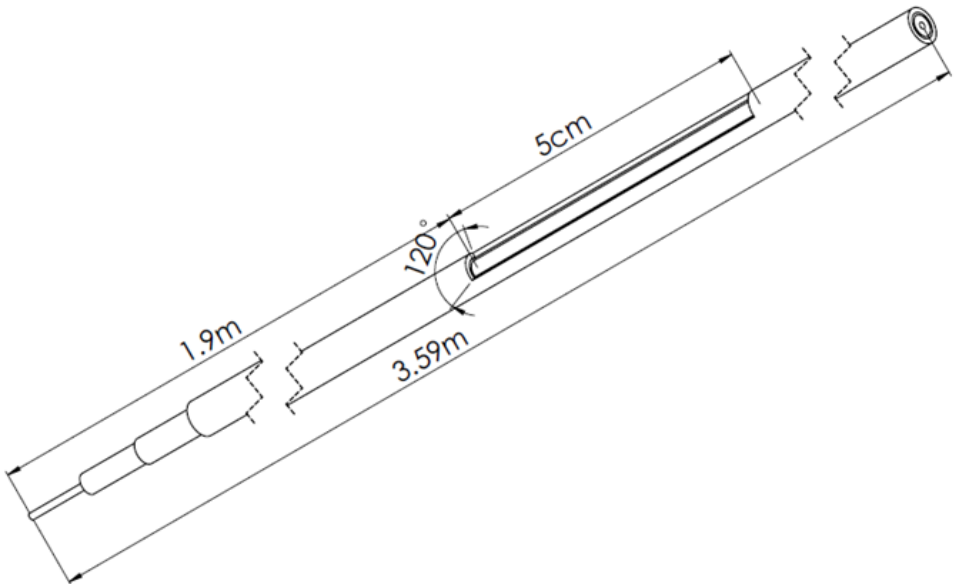

Figure 5.22 A 5 cm long, 120^o shield cutaway at 1.9 m on a 3.59 m long RG58 coaxial

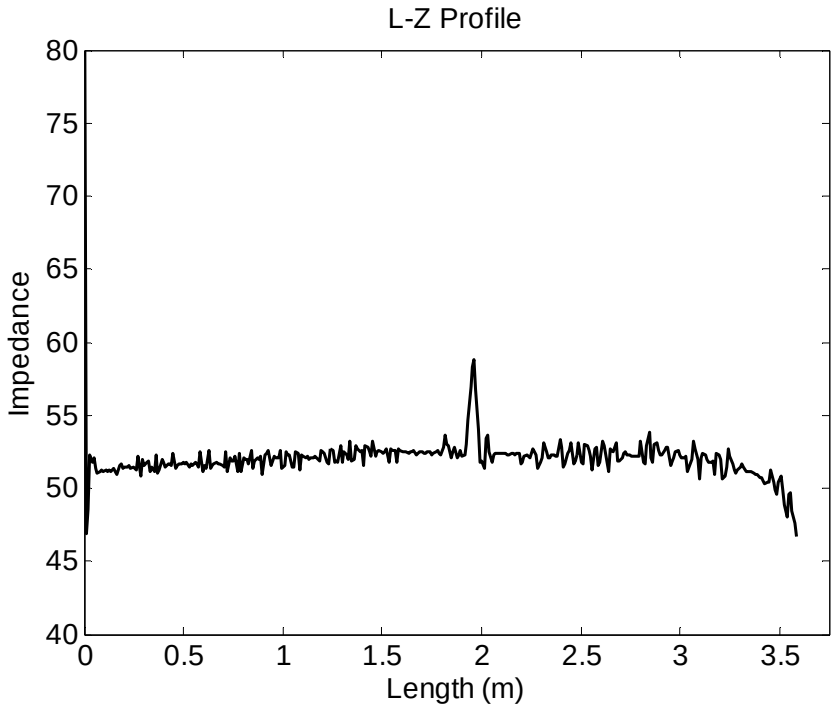

Figure 5.23 L- Z profile after 10 iterations on the frayed RG58 coaxial cable.

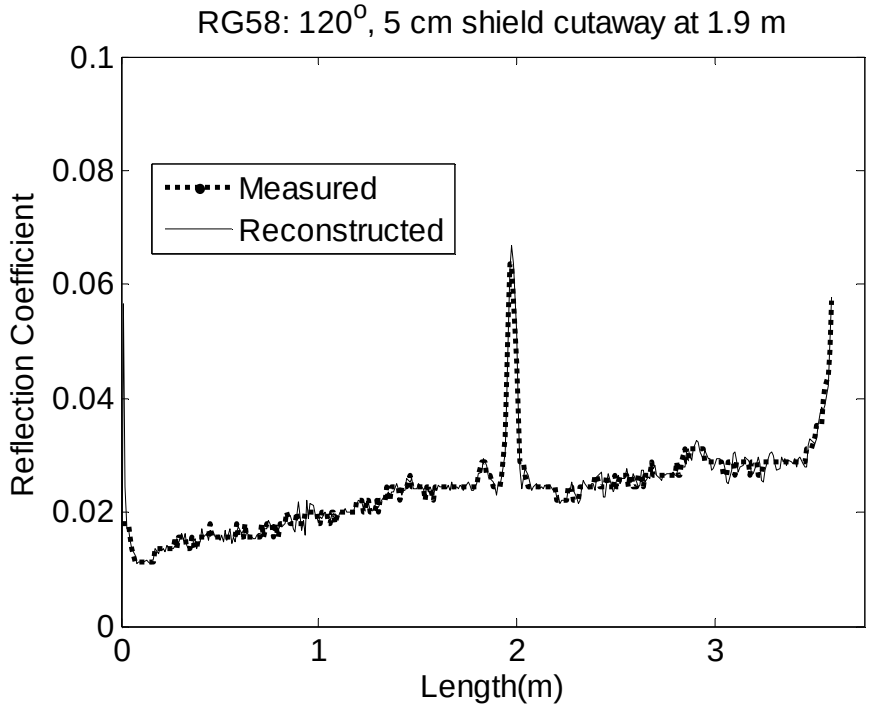

Figure 5.24 The measured vs. reconstructed result on the frayed RG58 coaxial cable.

5.5 Summary of the Inversion Methods

Solving the inverse function analytically shows effective only on simple configurations without noise. In many practical cases, the inverse functions do not exist mathematically. Additionally, the capability of this method is very limited since real world applications are typically more complicated and rarely noiseless.

The linear search method uses correlation coefficient to determine if the maximum likelihood is found between the simulated and simulated result. However, it can be very inefficient in multisection scenarios or long wires with small faults. Progressive binary search method significantly improves the efficiency, but it may not work properly in complex (e.g., multisection) configurations or wires with more than one fault or discontinuities.

Finally the iterative inversion algorithm that employs ABCD method as the forward solver is very accurate and efficient even in multisection and multiple unknown variable scenarios. As the example of 3.59 m RG58 cable shown in section 5.4, this inversion method is capable of determining the location and nature of the fault as small as 5 cm long, 120^{o} fray on the shield that is 1.9 m from the source. The small fault created by the fray only produces a reflection coefficient that is smaller than 0.07. This type of fault is typically difficult to detect especially on a long transmission line where the high-bandwidth rise step signal loses its energy.

Although the performance may vary with different type of transmission lines or in different environment, this iterative inversion method is demonstrated to be effective and capable of providing accurate inverse solution in locating small faults on transmission lines.

CHAPTER 6

CONCLUSIONS

Various existing forward modeling techniques have been presented in this dissertation. In general, the first generation methods use a graphical representation that provides visual aids to monitor the idealized electromagnetic wave propagation on transmission lines. The lack of fidelity makes these methods inappropriate for inversion purposes. The second generation methods employ numerical techniques for wave tracing, but the need of excessive computational resources lowers the inversion algorithm performance. The third generation method, primarily S-parameters, has shown promising performance and results among geophysical applications. Although it can also be used in wire fault location, a more convenient and modularized method is needed.

This dissertation introduced the signal flow graph method that enables modularized solutions by simply connecting the predefined blocks. It is also capable of solving branched network problems using graphical manners. Compared to the previous second generation methods, SFG makes wire fault modeling much easier and more deployable in the field. Instead of having to reprogram each of the different scenarios, field technicians can simply drag and drop the icons that represent different type of transmission lines and the simulation result can be generated accordingly. The modified ABCD method offers very high fidelity with exceptional efficiency. In addition to its

convenience, this frequency domain method is capable of modeling frequency dependent parameters and reactive loads. Therefore, it is suitable for iterative inversion in which the performance of the forward solution directly relates to the inversion outcome.

One of the goals of this research is the inversion algorithm for transmission line fault location. Analytical as well as numerical methods have been presented. Most of these methods can solve only simple configurations. However, the iterative inversion is capable of solving transmission line fault problems with multiple unknown variables (e.g., lengths and characteristic impedances) all together. It is also able to reveal chafes with very small reflections.

6.1 Potential Applications

Some of the contributions of this research include modularized forward modeling algorithms (signal flow graph and ABCD method), the quick profile building technique using commercial software and the iterative inversion method for wire fault location. With this advancement in both forward and inverse modeling techniques, numbers of potential applications that may be benefited including transmission line fault signature generator, high performance transmission line simulation/design tool and enhanced TDR/STDR/SSTDR line tester.

6.1.1 Transmission Line Fault Signature Generator

Radar target generators are often used as an input signal source for radar equipment. This instrument has been used for radar calibration or to train radar operators. It can also be used to generate radar signal signatures for the library. A similar concept

can be applied in transmission line fault location, which is essentially the radar signal that propagates on the wire. The modularized algorithms presented in this dissertation can be a suitable fit in both software or hardware approaches. A common problem with software approach is the performance, where many of unnecessary threads are used by the operating systems. The hardware approach, on the other hand, can generate the simulated data with much better performance. The SFG and extended SFG methods are built with blocks, which can be replaced with physical hardware such operational amplifiers, delay lines and synchronization clocks. Analog to digital converters, digital to analog converters and microcontrollers can also be utilized to improve the flexibility for varies transmission line configurations.

6.1.2 High Performance Transmission Line Simulation and Design Tool

In addition to aircraft and spacecraft applications, many of the high end analog circuit simulators and printed circuit board (PCB) design software packages (e.g., Linear Technology LTspice®, Cadence Allegro and Mentor Graphics Expedition) include limited transmission line effect simulators. These tools provide some simple preliminary predictions on the signal outcome before the products are manufactured. This capability is particularly critical for high speed digital applications where the transient effects can scramble the signal transmission. However, the performance of the existing products is limited and often not capable of providing accurate results without sacrificing computational resources. With the frequency domain modeling techniques introduced in this dissertation, the high performance transmission line simulation can be a great value-added tool that assists in the design of critical circuitry.

6.1.3 Enhanced TDR/STDR/SSTDR Line Tester

Most concurrent wire testers offer graphical display on the test results. However, it is difficult to interpret correctly for inexperienced users. For some complicated setups or faults that are very small, even experienced operators may not identify the faults properly. With the iterative inversion method introduced in this dissertation, the newer equipment would be able to quickly pin-point the location and nature of the fault on the wire. This type of maintenance tool is especially important for technicians of aircraft manufacturers, such as Boeing and Airbus, to reduce the costly grounding of the aircraft. Military aircraft maintenance technicians can also utilize such tools to improve the readiness of the fighter planes. Additionally, aging aircraft wires cannot handle excessive and unnecessary trial and error methods of troubleshooting. Many of the new faults are invoked due to these unintentional activities.

6.2 Future Work

Although the ABCD method discussed in this dissertation shows its excellent fidelity and efficiency in cascaded two-port network structure, like other methods, it does have its limitations. For configurations that are not two-port structure or cannot be simplified into two-port structure, this method fails. Bundle wires and branched networks, for example, are some of the problems that the ABCD method cannot be applied to directly. Therefore, an updated algorithm that can solve these problems is needed.

Most wires do not break or become shorted abruptly. Instead, the insulation and conductors degrade over time due to corrosion or vibration against other wires or

structure members. A known good status, or a baseline data, is critical for detecting very small faults. Without this baseline information, some of the small fault signatures are buried in the environmental noise. Thus, continuing research on the noise effect will improve the determination of the small wire fault location, which is still difficult to find with the techniques available today.

REFERENCES

[1] C. Furse and R. Haupt, "Down to the wire," *Spectrum, IEEE* , vol. 38, no. 2, pp. 34-39, Feb. 2001.

[2] A. J. Herber, "When Aircraft Get Old," *Journal of Air Force Association*, vol. 86, no. 1, Jan. 2003.

[3] M. Kingsley-Jones. (2006, August) Farnborough first news: The race to rewire Airbus A380. [Online]. Available: http://www.flightglobal.com/articles/2006/07/18/207894/farnborough-first-news-the-race-to-rewire-the-airbus.html

[4] N. D. Schwartz. (2007, March) Fortune, CNN Money. [Online]. Available: http://money.cnn.com/magazines/fortune/fortune_archive/2007/03/05/8401277/index.htm

[5] W. Eleazer. (2006, July) The Space Review. [Online]. Available: http://www.thespacereview.com/article/662/1

[6] C. Furse, Y.C. Chung, C. Lo, and P. Pendayala, "A Critical Comparison of Reflectometry Methods for Location of Wiring Faults," *Smart Structures and Systems*, vol. 2, no. 1, pp. 25-46, 2006.

[7] Texas Instruments, "The Bergeron Method - A Graphic Method for Determining Line Reflections in Transient Phenomena," Texas Instruments, Dallas, TX, Oct. 1996.

[8] C. Lo and C. Furse, "Modeling and simulation of branched wiring network," in *Eectromagnetic Compatibility, 17th International Zurich Symposium*, Zurich, 2006, pp. 53-56.

[9] T. Thomas, C. Furse, S. Wu, C. Call, and P. Smith, "Development and Evaluation of a Simulation Model for Wire Harness Reflectometry Assessment," in *12th Joint FAA/DOD/NASA Conference on Aging Aircraft*, Kansas City, 2009.

[10] C.-P Lin, "Analysis of nonuniform and dispersive time domain," *Water Resources Research* p. 1012, 2003.

[11] D. Bänninger, H. Wunderli, M. Nussberger, and H. Flühler, "Inversion of TDR signals—revisited," *Journal of Plant Nutrition and Soil Science*, no. 171, pp. 137-145, 2008.

[12] X. Shuai, O. Wendroth, C. Lu, and C. Ray, "Reducing the Complexity of Inverse Analysis of Time Domain Refl ectometry Waveforms," *Soil Science Society of America Journal*, vol. 73, no. 1, pp. 28-36, Jan.-Feb. 2009.

[13] C.-W. Hsue and T.-W. Pan, "Reconstruction of nonuniform transmission lines from time-domain reflectometry," *IEEE Microwave Theory and Techniques*, vol. 45, no. 1, pp. 32-38, Mar. 1997.

[14] S. Wu, V. Telasula, and C. Furse, "Transmission Line Modeling with ABCD Parameters and Frequency Localization of Signals Based on the Interference Requirements," In preparation, 2011

[15] E. Lundquist, S. Wu, B. Jones, J. Nagel, and C. Furse, "Advanced Forward Methods for Complex Wire," In preparation, 2011.

[16] S. Wu and C. Furse, "A numerical Approach of Building Chafed Wire Profiles and Predicting Wire Fault Signatures," In preparation, 2011.

[17] S. Wu and C. Furse, "An Iterative Inversion for Fault Identification on Transmission Lines Using TDR," In preparation, 2011.

[18] E.Lundquist, S. Wu, C. Furse, and B. Jones, "Aging Wire Fault Diagnosis Using Faster, Higher-Precision Methods," in *The 2011 Aircraft Airworthiness and Sustainment Conference*, San Diego, 2011.

[19] K. M. Fidanboylu, N. Korkmaz, and K. Korkmaz, "A Transmission Line Modeling Technique Using Time Domaing Synthesis," in *Electromagnetic Compatibility - IEEE International Symposium*, vol. 1, Istanbul, May. 2003, pp. 331-334.

[20] C. Christopoulos, *The Transmission-Line Modeling (TLM) Method in Electromagnetics*, 1st ed., Constantine A. Balanis, Ed. San Rafael, CA: Morgan & Claypool, 2006.

[21] S. Kim and D. P. Neikirk, "Time Domain Multiconductor Transmission Line Analysis Using Effective Internal Impedance," in *IEEE 6 Topical Meeting on Electrical Performance of Electronic Package*, San Jose, CA, 1997, pp. 244-258.

[22] F. T. Ulaby, *Fundamentals of Applied Electromagnetics*. Upper Saddle River, New Jersey: Prentice Hall, 1999.

[23] Agilent Technologies. (2006, October) Time Domain Reflectometry Theory. Application Note 1304-2.

[24] R. C. Dorf, Ed., *The electrical engineering handbook*, 2nd ed. Boca Raton, FL: CRC Press, 1997.

[25] R. J. LeVeque, *Finite Difference Methods for Ordinary and Partial Differential Equations - Steady State and Time Dependent Problems*. Philadelphia, PA: Society for Industrial and Applied Mathematics (SIAM), Jul. 2007.

[26] D. M. Pozar, *Microwave Engineering*, 3rd ed. Hoboken, NJ: John wiley & Sons, Inc., 2005.

[27] S. J. Orfanidis. (2010, August) Electromagnetic Waves and Antennas. [Online] Available: http://www.ece.rutgers.edu/~orfanidi/ewa/

[28] M. Steer, *Microwave and RF Design: A Systems Approach*, 1st ed. Raleigh, NC: SciTech Publishing, 2010.

[29] K. K. Parhi and Y. Chen, , Shuvra S. Bhattacharyya et al., Eds. New York, NY: Springer, 2010, ch. Part IV, pp. 791-816.

[30] W. S. Levine, Ed., *The control handbook*, 2nd ed., Boca Raton, FL: CRC Press, 2010.

[31] C. Trask, "The dc isolated 1:1 guanella transmission line transformer," *Sonoran Radio Research*, Aug. 2005.

[32] S. Schuet, K. Wheeler, D. Timucin, M. Kowalski, and P. Wysocki, "Understanding Wire Chafing:Model Development and Optimal Diagnostics Using TDR," in *Aviation Safety Technical Conference*, Denver, 2008.

[33] S. Schuet, K. Wheeler, D. Timucin, M. Kowalski, and P. Wysocki, "Model Based Inference for Wire Chafe Diagnostics," in *Aging Aircraft Conference*, Kansas City, 2009.

[34] P. Russer , *Electromagnetics, Microwave Circuit, And Antenna Design for Communications Engineering*, 2nd ed. Norwood, MA: Artech House Publishers, 2006.

[35] C.i Su, H. Ke, and T. Hubing, "Overview of Electromagnetic Modeling Software," in *25th Annual Review of Progress in Applied Computational Electromagnetics*, Monterey, 2009.

[36] M. Kowalski, "A simple and efficient computational approach to chafed cable time-domain reflectometry signature prediction," in *Annual Review of Progress in Applied Computational Electromagnetics Conference, ACES*, Monterey, 2009.

[37] Mathworks, *Matlab 7 Programming Fundamentals*, 712th ed. Natick, MA: Mathworks, 2011. [Online]. Available: http://www.mathworks.com/help/techdoc /math/brfaisd-17.html

[38] O. Agunloye, "A Numerical Inversion Scheme for Geoelectrical Soundings," *Pure and Applied Geophysics (PAGEOPH)*, vol. 119, pp. 1003-1023, 1981.

[39] P. F. Polatin, K. Sarabandi, and F. T. Ulaby, "An Iterative Inversion Algorithm with Application to the Polarimetric Radar Response of Vegetation Canopies," *IEEE Transaction on Geoscience and Remote Sensing*, vol. 32, no. 1, pp. 62-71, Jan. 1994.

[40] C. P. Lin, "Frequency Domain versus Traveltime analyses of TDR Waveforms for Soil Moisture Measurements," *Soil Science Society of America Journal*, vol. 67, pp. 720-729, 2003.

[41] M. S. Zhdanov, *Geophysical Inverse Theory and Regularization Problems*, 1st ed. Amsterdam, The Netherlands: Elsevier Science, 2002.

[42] J. Hadamard, "Sur les problèmes aux dérivées partielles et leur signification physique," *Princeton University Bulletin*, vol. 13, pp. 49-52, 1902.

[43] N. Dale, C. Weems, and S. Rebelsky, *Object-Oriented Data Structures Using Java*, 3rd ed. Sudbury, MA: Jones & Bartlett Learning, 2011.

[44] S. Schlaeger, "A fast TDR-inversion technique for the reconstruction of spatial soil moisture content," *Hydrology and Earth System Sciences*, no. 2, pp. 971-1009, Jun. 2005.

[45] P. Leidenberger, B. Oswald, and K. Roth, "Efficient reconstruction of dispersive dielectric profiles using time domain reflectometry (TDR)," *Hydrol. Earth Syst. Sci.*, vol. 10, pp. 209-232, 2006.

[46] C. Huebner and K. Kupfer, "Modelling of electromagnetic wave propagation along transmission lines in inhomogeneous media," *MEASUREMENT SCIENCE AND TECHNOLOGY*, vol. 18, pp. 1147–1154, Feb. 2007.

[47] R. Burachik, L.s Mauricio, G. Drummond, A. N. Iusem, and E. D. Castorina, "Full convergence of the steepest descent method with inexact line searches," *Optimization*, vol. 32, pp. 137-146, 1995.

[48] O. Agunloye, "A Numerical Inversion Scheme for Geoelectrical Soundings," *Pure and Applied Geophysics (PAGEOPH)*, vol. 119, pp. 1003-1023, 1981.

[49] C.-P. Lin, "Frequency Domain versus Traveltime analyses of TDR Waveforms for Soil Moisture Measurements," *Soil Science Society of America Journal*, vol. 67, pp. 720-729, 2003.